

**SSC-463**

**INSPECTION TECHNIQUES FOR  
MARINE COMPOSITE  
CONSTRUCTION AND NDE**



This document has been approved  
For public release and sale; its  
Distribution is unlimited

**SHIP STRUCTURE COMMITTEE**  
**2012**

# Ship Structure Committee

RADM P.F. Zukunft  
U. S. Coast Guard Assistant Commandant,  
Assistant Commandant for Marine Safety, Security  
and Stewardship  
Co-Chair, Ship Structure Committee

Mr. H. Paul Cojeen  
Society of Naval Architects and Marine Engineers

Mr. Christopher McMahon  
Director, Office of Ship Construction  
Maritime Administration

Mr. Kevin Baetsen  
Director of Engineering  
Military Sealift Command

Mr. Jeffrey Lantz,  
Commercial Regulations and Standards for the  
Assistant Commandant for Marine Safety, Security  
and Stewardship  
Mr. Jeffery Orner  
Deputy Assistant Commandant for Engineering and  
Logistics

RDML Thomas Eccles  
Chief Engineer and Deputy Commander  
For Naval Systems Engineering (SEA05)  
Co-Chair, Ship Structure Committee

Dr. Roger Basu  
Senior Vice President  
American Bureau of Shipping

Mr. Victor Santos Pedro  
Director Design, Equipment and Boating Safety,  
Marine Safety,  
Transport Canada

Dr. Neil Pegg  
Group Leader - Structural Mechanics  
Defence Research & Development Canada - Atlantic

Mr. Edward Godfrey  
Director, Structural Integrity and Performance Division

Dr. John Pazik  
Director, Ship Systems and Engineering Research  
Division

## SHIP STRUCTURE SUB-COMMITTEE

### AMERICAN BUREAU OF SHIPPING (ABS)

Mr. Craig Bone  
Mr. Phil Rynn  
Mr. Tom Ingram

### MARITIME ADMINISTRATION (MARAD)

Mr. Chao Lin  
Mr. Richard Sonnenschein

### NAVY/ONR / NAVSEA/ NSWCCD

Mr. David Qualley / Dr. Paul Hess  
Mr. Erik Rasmussen / Dr. Roshdy Barsoum  
Mr. Nat Nappi, Jr.  
Mr. Malcolm Witford

### UNITED STATES COAST GUARD

CAPT John Nadeau  
CAPT Paul Roden  
Mr. Jaideep Sirkar  
Mr. Chris Cleary

### DEFENCE RESEARCH & DEVELOPMENT CANADA

#### ATLANTIC

Dr. David Stredulinsky  
Mr. John Porter

### MILITARY SEALIFT COMMAND (MSC)

Mr. Michael W. Touma  
Mr. Jitesh Kerai

### TRANSPORT CANADA

Natasa Kozarski  
Luc Tremblay

### SOCIETY OF NAVAL ARCHITECTS AND MARINE ENGINEERS (SNAME)

Mr. Rick Ashcroft  
Mr. Dave Helgerson  
Mr. Alex Landsburg  
Mr. Paul H. Miller

Member Agencies:

*American Bureau of Shipping  
Defense Research and Development Canada  
Maritime Administration  
Military Sealift Command  
Naval Sea Systems Command  
Office of Naval Research  
Society of Naval Architects & Marine Engineers  
Transport Canada  
United States Coast Guard*



**Ship  
Structure  
Committee**

Address Correspondence to:

COMMANDANT (CG-5212/SSC)  
ATTN (EXECUTIVE DIRECTOR/SHIP  
STRUCTURE COMMITTEE)  
US COAST GUARD  
2100 2ND ST SW STOP 7126  
WASHINGTON DC 20593-7126  
Website: <http://www.shipstructure.org>

**SSC – 463  
SR – 1464**

**NOVEMBER 30, 2011**

**MARINE COMPOSITES NDE, INSPECTION TECHNIQUES FOR MARINE COMPOSITE  
CONSTRUCTION**

With a greater emphasis on fuel economy to reduce operating costs and on improved resistance to environmental degradation, many transportation system elements are investigating greater use of lightweight composite construction. As a result, lighter, more efficient modern composite construction and laminates are constantly being developed. However, these lighter structures offer a wider variety of failure modes that have traditionally been evaluated using visual or destructive inspection techniques.

Sophisticated Non-Destructive Evaluation (NDE) is essential to reliably evaluate fabrication quality and to support lifetime damage inspections. Recently, numerous breakthroughs in NDE equipment and systems have improved NDE performance and reliability and have reduced the amount of destructive evaluations necessary to assess structural strength. This project conducts a state of the art assessment of available NDE techniques for large marine composite structures. In addition, case studies of marine composite NDEs are also included in this report to illustrate the effectiveness of various NDE tools for composite boat and ship surveys.

We thank the authors and Project Technical Committee for their dedication and research toward completing the objectives and tasks detailed throughout this paper and continuing the Ship Structure Committee's mission to enhance the safety of life at sea.

A handwritten signature in black ink, appearing to read 'P. F. ZUKUNFT', written in a cursive style.

P. F. ZUKUNFT  
Rear Admiral, U.S. Coast Guard  
Co-Chairman, Ship Structure Committee

A handwritten signature in black ink, appearing to read 'T. J. ECCLES', written in a cursive style.

T. J. ECCLES  
Rear Admiral, U.S. Navy  
Co-Chairman, Ship Structure Committee

1. Report No. 463	2. Government Accession No.	3. Recipient's Catalog No.	
4. Title and Subtitle Inspection Technique for Marine Composite Construction		5. Report Date 1 June 2011	
		6. Performing Organization Code	
7. Author(s) Eric Greene		8. Performing Organization Report No. SR-1464	
9. Performing Organization Name and Address Eric Greene & Associates		10. Work Unit No. (TRAIS)	
		11. Contract or Grant No.	
12. Sponsoring Agency Name and Address COMMANDANT (CG-5212/SSC) ATTN (SHIP STRUCTURE COMMITTEE) US COAST GUARD 2100 2ND ST SW STOP 7126 WASHINGTON DC 20593-7126		13. Type of Report Final Report	
		14. Sponsoring Agency Code CG - 5	
15. Supplementary Notes The research completed by the above author for the Ship Structure Committee was reviewed by the Project Technical Committee for satisfactory completion of the objectives outlined in the Statement of Work developed and approved for funding by the Principal Members of the Ship Structure Committee. Sponsored by the Ship Structure Committee and its member agencies			
16. Abstract The goal of this project was to conduct an assessment of current Non-Destructive Evaluation (NDE) methods for large, marine composite structures. The assessment surveyed the military, commercial and recreational industries. Informational sources included marine surveyors, NDE equipment manufacturers, shipbuilders, platform owners and academia.  Concurrently, a separate assessment of flaw criticality was conducted to determine the lower limit size of as-built flaws or in-service damage that needs to be detected in order to ensure structural integrity. The critical flaw size for a variety of defects formed the basis for NDE detectability thresholds.  Test panels were assembled or fabricated with imbedded defects to determine the efficacy of various NDE methods.  Case studies of marine composites NDE are also included in this report to illustrate the effectiveness of various NDE tools for boat surveys. Applications included quality assurance NDE used by builders, condition surveys, and NDE used to determine the extent of damage after a known accident.  The initial assessment of NDE technologies revealed laser shearography, thermography, ultrasonic testing and digital tap hammers to be the most promising for marine composite inspection. These technologies were all evaluated during the project's test program.			
17. Key Words		18. Distribution Statement National Technical Information Service U.S. Department of Commerce Springfield, VA 22151 Ph. (703) 487-4650 / www.ntis.gov	
19. Security Classif. (of this report) Unclassified	20. Security Classif. (of this page) Unclassified	21. No. of Pages	22. Price

**CONVERSION FACTORS**  
(Approximate conversions to metric measures)

To convert from	to	Function	Value
<b>LENGTH</b>			
inches	meters	divide	39.3701
inches	millimeters	multiply by	25.4000
feet	meters	divide by	3.2808
<b>VOLUME</b>			
cubic feet	cubic meters	divide by	35.3149
cubic inches	cubic meters	divide by	61,024
<b>SECTION MODULUS</b>			
inches <sup>2</sup> feet <sup>2</sup>	centimeters <sup>2</sup> meters <sup>2</sup>	multiply by	1.9665
inches <sup>2</sup> feet <sup>2</sup>	centimeters <sup>3</sup>	multiply by	196.6448
inches <sup>4</sup>	centimeters <sup>3</sup>	multiply by	16.3871
<b>MOMENT OF INERTIA</b>			
inches <sup>2</sup> feet <sup>2</sup>	centimeters <sup>2</sup> meters	divide by	1.6684
inches <sup>2</sup> feet <sup>2</sup>	centimeters <sup>4</sup>	multiply by	5993.73
inches <sup>4</sup>	centimeters <sup>4</sup>	multiply by	41.623
<b>FORCE OR MASS</b>			
long tons	tonne	multiply by	1.0160
long tons	kilograms	multiply by	1016.047
pounds	tonnes	divide by	2204.62
pounds	kilograms	divide by	2.2046
pounds	Newtons	multiply by	4.4482
<b>PRESSURE OR STRESS</b>			
pounds/inch <sup>2</sup>	Newtons/meter <sup>2</sup> (Pascals)	multiply by	6894.757
kilo pounds/inch <sup>2</sup>	mega Newtons/meter <sup>2</sup> (mega Pascals)	multiply by	6.8947
<b>BENDING OR TORQUE</b>			
foot tons	meter tons	divide by	3.2291
foot pounds	kilogram meters	divide by	7.23285
foot pounds	Newton meters	multiply by	1.35582
<b>ENERGY</b>			
foot pounds	Joules	multiply by	1.355826
<b>STRESS INTENSITY</b>			
kilo pound/inch <sup>2</sup> inch <sup>1/2</sup> (ksi√in)	mega Newton MNm <sup>3/2</sup>	multiply by	1.0998
<b>J-INTEGRAL</b>			
kilo pound/inch	Joules/mm <sup>2</sup>	multiply by	0.1753
kilo pound/inch	kilo Joules/m <sup>2</sup>	multiply by	175.3

1. Introduction.....	1
1.1 Executive Summary .....	1
1.2 Background.....	2
1.3 Acknowledgements.....	3
2. Defects .....	4
2.1 Bonded Joint Failure.....	4
2.2 Air Bubbles.....	6
2.3 Blisters .....	7
2.4 Core Crushing.....	8
2.5 Core Shear Failure .....	10
2.6 Crazeing.....	10
2.7 Delaminations .....	11
2.8 Fiber Failure.....	13
2.9 Kissing Bond.....	14
2.10 Impact Damage .....	15
2.11 Matrix Cracking.....	18
2.12 Moisture Ingress.....	19
2.13 Pit (or pinhole).....	20
2.14 Ply (or Fiber) Waviness .....	20
2.15 Porosity .....	21
2.16 Resin Rich Area .....	21
2.17 Resin Starved Area .....	21
2.18 Skin-to-Core Disbond.....	22
2.19 Surface Cracking.....	24
2.20 Thermal (and Lightning) Damage .....	25
2.21 Voids.....	26
3. NDE Techniques.....	28
3.1 Visual Inspection .....	28
3.2 Tap Testing .....	29
3.3 Ultrasonic Inspection .....	31
3.4 X-Radiography (X-Ray).....	36
3.5 Eddy Current.....	36
3.6 Thermography.....	37
3.7 Moisture Meters .....	39
3.8 Bond Testers .....	39
3.9 Laser Shearography .....	39
3.10 Electron Probe Imaging .....	41
3.11 Modal Methods.....	42
3.12 SIDER.....	44
3.13 Acoustic Emission .....	45
4. Aerospace Damage and Repair Inspection Procedures .....	46
5. Wind Turbine Blades .....	57
5.1 Blade Inspection Program.....	60
5.2 Blade Flaw Characterization.....	61
6. Test Panel Program.....	63
6.1 Previous Composite Laminate Impact Test Programs.....	63

6.2 Project Test Panels .....	67
6.3 Induced Impact Damage .....	78
7. Test Panel NDE.....	81
7.1 Laser Shearography .....	81
7.2 Ultrasonic Inspection .....	85
7.3 Infrared Thermography.....	87
7.4 Digital Tap Hammer .....	90
8. Case Studies .....	92
8.1 Laser Shearography .....	92
8.1.1 RNLI Lifeboats .....	92
8.1.2 Damaged Yacht Hull.....	94
8.2 Infrared Thermography .....	94
8.2.1 Void Detection .....	95
8.2.2 Extent of Damage .....	96
8.2.3 Water Ingress .....	97
8.3 Ultrasonics .....	98
9. Summary .....	101
9.1 Summary of NDE Techniques Examined.....	102
9.2 Flaw Detection in Marine Composites .....	103
10. Conclusion .....	105
11. Recommendations for Future Research .....	106
11.1 Develop Standardized Structural Details .....	106
11.2 Develop Standardized Inspection and Repair Procedures .....	107
11.3 Reduce the Cost of Laser Shearography NDE Equipment .....	107
11.4 Develop a Method to Electronically Code the Location of NDE Equipment.....	107
A-1. Appendix A – Defect Thresholds .....	108
A-2. Appendix B – Effectiveness Summaries .....	111
Glossary .....	116
Text References .....	125

Figures

Figure 1. Bonded joint failure modes .....	4
Figure 2. Cohesive (left) and Adhesive (right) bond failure examples.....	4
Figure 3. Mixed-mode bond failure (light areas) and adhesion failure .....	5
Figure 4. Examples of air bubbles in composite laminates .....	7
Figure 5. Illustration of blisters in boat hulls.....	8
Figure 6. Illustrations of core crushing.....	8
Figure 7. Photographs showing core crushing in Nomex .....	9
Figure 8. Schematic, FE-model and photograph of indentation damage.....	9
Figure 9. Fatigue fracture of PMI 51 S foam core.....	10
Figure 10. Examples of fiberglass crazing in gel coat finishes.....	10
Figure 11. Examples of severe delamination resulting from manufacturing defects .....	11
Figure 12. SEM micrographs of delaminated specimens after interlaminar shear .....	11
Figure 13. Micrograph and X-ray image of an edge delamination.....	12
Figure 14. Delamination of tabbed joint.....	12
Figure 15. Kink band formation with composite laminates are under compression .....	13
Figure 16. Micrograph of fiber fracture and fiber pullout .....	13
Figure 17. Various types of “kissing” bonds .....	14
Figure 18. Mode 1 frequency variation for bonded and disbonded conditions .....	14
Figure 19. The influence of “peel ply” on “kissing” bond formation.....	14
Figure 20. Impact damage types .....	15
Figure 21. Impact damage schematic.....	15
Figure 22. X-ray image of impact delaminations within a CFRP panel.....	16
Figure 23. Photograph of delaminations on Nomex sandwich construction .....	16
Figure 24. Damage types occurring from blunt and sharp object impact.....	17
Figure 25. Foreign object impact damage in honeycomb-cored sandwich laminates .....	17
Figure 26. Sandwich laminate impact damage .....	18
Figure 27. Schematic representation of cracks in laminates.....	18
Figure 28. Micrographs of matrix micro-cracking .....	19
Figure 29. Schematic representation of moisture ingress in sandwich laminates.....	19
Figure 30. Image of pits or pinholes .....	20
Figure 31. Ply waviness morphologies made visible by laminate edge photographs.....	20
Figure 32. FE model geometry, representing one wavy 0° ply.....	20
Figure 33. Composite sample close-up of apex showing extreme fiber-waviness .....	20
Figure 34. Schematic of laminate porosity .....	21
Figure 35. Resin starved areas and micrograph of resin rich areas .....	22
Figure 36. Voids and resin-rich areas shown with backscattered electron imaging.....	22
Figure 37. Schematic of skin-to-core disbond .....	23
Figure 38. Photograph of skin to-core de-bond in a GRP skin, PU foam sandwich .....	23
Figure 39. Crack length measurements showing crack path in PVC foam .....	23
Figure 40. Schematic of surface cracks .....	24
Figure 41. Micrographs of resin burn-off and delaminations from lightning strike.....	25
Figure 42. Lightning damage to wind turbine blades .....	26
Figure 43. Path of lightning strike on sailing yacht with carbon fiber mast.....	26
Figure 44. Micrographs of voids in pre-preg and filament wound materials .....	27

Figure 45. Approximate frequency spectrum for techniques used in NDE.....	28
Figure 46. Picture of a military specification tap hammer.....	29
Figure 47. PoD for Visual and Tap Hammer Inspection Methods.....	30
Figure 48. Typical ultrasonic phased array probe assemblies.....	32
Figure 49. Single-element contact ultrasonic transducer and A-scan image.....	32
Figure 50. Ultrasonic transducer scan movement and linear scan B-scan image.....	33
Figure 51. EPOCH 1000i ultrasonic and phased array flaw detector.....	34
Figure 52. Logarithmic time evolution of surface temperature.....	38
Figure 53. Shearography principal and portable shearography device.....	41
Figure 54. Frequency response plot from vibrometer.....	43
Figure 55. An instrumented hammer is used during SIDER examination.....	44
Figure 56. Aerospace structural design load and damage considerations.....	46
Figure 57. Schematic of a reference standard used for NDE of cored panels.....	47
Figure 58. Reference standard used for NDE of solid laminates.....	48
Figure 59. Probability of Detection (PoD) for composite sandwich panels.....	48
Figure 60. Probability of Detection (PoD) for carbon fiber sandwich panel.....	49
Figure 61. Comparison of advanced inspection techniques with conventional NDE.....	49
Figure 62. Cumulative PoD of all conventional NDE devices.....	50
Figure 63. Cumulative PoD for Woodpecker device.....	50
Figure 64. Some NDE devices evaluated by the FAA.....	51
Figure 65. Ultrasonic backwall echo reduction versus volume porosity.....	52
Figure 66. Phased array inspection of stringer skin bonding.....	53
Figure 67. Entrapped water in a honeycomb panel and a thermographic image.....	54
Figure 68. Various NDE technologies evaluated by Airbus.....	55
Figure 69. Effectiveness of NDE techniques for honeycomb structures by Airbus.....	56
Figure 70. Wind turbine blade damage.....	58
Figure 71. Wind turbine blade damage (continued).....	59
Figure 72. Blade damage formation and growth.....	59
Figure 73. Photographs of wind blade damage.....	60
Figure 74. Classification and quantification of blade defects.....	62
Figure 75. Impact energies used for previous aerospace impact test studies.....	64
Figure 76. Impact damage apparent only with NDE and core crushing process.....	64
Figure 77. Void simulation cavity machining diagram for Pearson 4 test panel.....	68
Figure 78. Void simulation cavity machining diagram for Pearson 5 test panel.....	68
Figure 79. Void simulation cavity machining diagram for Pearson 6 test panel.....	69
Figure 80. Void simulation cavity machining diagram for Pearson 7 test panel.....	69
Figure 81. Description of panels USNA 1 and USNA 2.....	70
Figure 82. Description of panels USNA 3 and USNA 4.....	71
Figure 83. Description of panels USNA 5 and USNA 6.....	71
Figure 84. Description of panels USNA 7 and USNA 8.....	72
Figure 85. Description of panels USNA 9 and USNA 10.....	72
Figure 86. Layout of E-glass and carbon fiber test panels.....	74
Figure 87. Test panel delamination arrangement.....	75
Figure 88. Test panel water ingress arrangement.....	75
Figure 89. Test panel shear defect arrangement.....	76
Figure 90. Test panel construction.....	76

Figure 91. Test panel construction (continued) .....	77
Figure 92. Test panels with 1-inch grid for damage location reference .....	77
Figure 93. Rubber coated barbell is epoxied into PVC tube to form impactor .....	78
Figure 94. Detail of impactor release mechanism .....	79
Figure 95. Impact tester at the US Naval Academy Structures Laboratory.....	79
Figure 96. Vacuum chamber and laser shearography camera .....	81
Figure 97. Panel “Osprey 1” with simulated delaminations and shearograms .....	82
Figure 98. Panel “Osprey 3” with simulated core shear and shearograms .....	82
Figure 99. Panel “Osprey 4” with induced impact damage and shearograms .....	82
Figure 100. Panel “Osprey 6” with simulated water ingress and shearograms .....	83
Figure 101. Panel “Osprey 8” with induced impact damage and shearograms .....	83
Figure 102. Panel “Pearson 4” with machined back-face cavities and shearograms.....	83
Figure 103. Panel “Pearson 6” with machined back-face cavities and shearograms.....	84
Figure 104. Panel “USNA 3” with induced impact damage and shearograms.....	84
Figure 105. Panel “USNA 10” with induced impact damage and shearograms.....	84
Figure 106. Acoustocam i600 used to inspect a project carbon fiber panel .....	85
Figure 107. Impact energies and corresponding ultrasonic NDE data .....	86
Figure 108. Delamination damage and corresponding ultrasonic NDE data.....	86
Figure 109. Machined cavities and corresponding ultrasonic NDE data.....	86
Figure 110. Mark Ashton is shown capturing and analyzing the IR image.....	87
Figure 111. Panel “Osprey 6” with simulated water ingress and thermogram .....	88
Figure 112. Panel “Pearson 6” with machined back-face cavities and thermogram .....	88
Figure 113. Panel “USNA 3” with impact damage and thermogram .....	89
Figure 114. Panel “USNA 6” with impact damage and thermogram .....	89
Figure 115. Digital tap hammer being used to evaluate an Osprey E-glass panel.....	90
Figure 116. Vacuum hood used to test flat panel portions of RNLI lifeboat hulls.....	92
Figure 117. RNLI Severn class topside hull and shearography images .....	93
Figure 118. RNLI Severn class detected hull defects over time.....	93
Figure 119. Full extent of internal damage to hull sandwich construction.....	94
Figure 120. Visible NDE looks defect free but thermal pattern shows anomaly .....	95
Figure 121. Thermographic image of void in gel coat.....	95
Figure 122. Red and white areas indicate anomalies in bondline or skin.....	96
Figure 123. Infrared image above indicates good contact between skin and core .....	96
Figure 124. IR image shows moisture ingress to keel box .....	97
Figure 125. IR anomalies on hull bottom characteristic of moisture ingress .....	97
Figure 126. The dark colored anomaly is characteristic of moisture.....	98
Figure 127. The captured UT waveform of a carbon fiber mast .....	99
Figure 128. UT shows the top reinforcement layer in this area is delaminated.....	100

**Tables**

Table 1. Causes of cohesion failures.....	6
Table 2. Effect of transducer frequency on UT Inspection of composites .....	35
Table 3. Shearography stress method applicability .....	40
Table 4. Laminates studied by Hildebrand .....	65
Table 5. Impact energies studied by Hildebrand .....	65
Table 6. Laminates studied by Marine Materials Laboratory .....	66
Table 7. Impact Energies studied by Marine Materials Laboratory .....	66
Table 8. Solid laminates built by Pearson Yachts.....	67
Table 9. Fabricated test panels.....	73
Table 10. Impact energies used to damage test panels .....	80
Table 11. Effectiveness of digital tap hammer .....	91
Table 12. Summary results from panel testing program.....	102

## **1. Executive Summary**

The goal of this project was to conduct an assessment of current Non-Destructive Evaluation (NDE) methods for large, marine composite structures. The assessment surveyed the military, commercial and recreational industries. Informational sources included marine surveyors, NDE equipment manufacturers, shipbuilders, platform owners and academia.

Concurrently, a separate assessment of flaw criticality was conducted to determine the lower limit size of as-built flaws or in-service damage that needs to be detected in order to ensure structural integrity. The critical flaw size for a variety of defects formed the basis for NDE detectability thresholds.

Test panels were assembled or fabricated with imbedded defects to determine the efficacy of various NDE methods. The panels had the following defects:

Delamination or voids were simulated in solid laminates by machining 1-4 inch diameter cavities from 20% to 80% of panel thickness. Delaminations were simulated in sandwich laminates by placing peel-ply material in between the reinforcement plies. The defects ranged from 0.5 to 4.0 inches in diameter.

Water Ingress was simulated by embedding pockets of water 1-4 inches in diameter into the core just below the top skin.

Core Shear was simulated in sandwich panels by slitting the core prior to lamination and inserting peel ply into the slot during fabrication.

Impact Damage was induced with impact energies between 25 and 250 foot-pounds using a drop weight impactor.

The initial assessment of NDE technologies revealed laser shearography, thermography, ultrasonic testing and digital tap hammers to be the most promising for marine composite inspection. These technologies were all evaluated during the project's test program.

Laser shearography proved to be the most effective NDE technique for discovering the widest variety and smallest defects, perhaps because this is the only NDE method that stresses the part during inspection. It is also the most recently developed technology, and thus the most expensive.

Thermography worked very well to detect water ingress and irregularities in sandwich construction, especially with cores that have kerfs.

Ultrasonic inspection worked well to document the location and depth of delaminations but small survey probes limit the effectiveness to instances where damage sites are known or suspected.

The digital tap hammer proved to be effective only for larger delamination sites.

## **1.2 Background**

An increasing number of marine structures are utilizing composite materials. Major structure and components can be built lighter and corrosion-resistant using composites. The US Navy's DDG-1000 topside structure and LPD-17 advanced enclosed mast are being built with composites. Additionally, the offshore oil industry is starting to build composite risers and habitability modules. Nondestructive Evaluation (NDE) techniques developed for composite aerospace structures are not viable for large marine structures. Therefore, a state-of-the-art assessment of available NDE techniques for marine composite structures is required.

The early years of marine composite construction featured solid laminates that would be considered "overbuilt" by today's standards to compensate for our lack of empirical data. The demand for lighter, more efficient structures led to sandwich construction that utilizes very lightweight cores. These laminates have a wider variety of failure modes, including: core damage, skin-to-core separation, and water ingress. Today's composite vessels also operate at higher speeds, which can dramatically increase structural loads. We also have a greater number of builders building larger composite structures with more combinations of material types and manufacturing processes.

We have thus moved from an age when a marine surveyor could rely on visual detection of delaminations or damaged internal framing to a time when sophisticated NDE tools are required to find damage that is often hidden. Builders also require more sophisticated methods to support quality assurance programs. Fortunately, advances in signal and image processing technology allow us to take advantage of the full electromagnetic spectrum with cost-effective NDE technologies.

The aerospace industry has been the driver in the development of NDE technology for composite structure due to very high platform cost and the criticality of any structural failure. However, the required inspection area for aircraft is much less than ships and the structure is often much more uniform. This means that NDE for ships must be cheaper, faster, and cover a broader range of materials and structural arrangement than systems developed for the aerospace industry.

With a greater emphasis on fuel economy to reduce operating costs and environmental degradation, all transportation systems are investigating greater use of lightweight, composite construction. Sophisticated NDE systems will ensure that these platforms will operate safely and can help foster the economic development associated with domestic fabrication of lightweight ships and ship systems.

### **1.3 Acknowledgements**

We would first like to thank the members of the SSC Project Technical Committee who donated their time and expertise to ensure this project met the standards of the ship research community. PTC members included: Roger Basu, ABS; Stephen Billian, Lockheed Martin; Ron Caputo, USCG; Fai Cheng, Lloyd's Register; Paul Cojeen, SNAME; Pramod Dash, Hindustan Institute of Technology and Science; Robert Dow, Newcastle University; David Howarth, Lloyd's Register; James Huang, National Defense Ottawa; Nicholas Koreisha, Designers & Planners; Raymond Kramer, Raytheon; Elli Lembessis, ABS; Paul Miller, US Naval Academy; Royale Underhill, Defence Research Development Canada; and Daniel Woods, Germanischer Lloyd. A special thanks go to Ms. Lembessis for chairing the PTC and hosting the project meetings.

Dr. Paul Miller of the US Naval Academy was instrumental in our test panel program. He provided test panels from previous investigations and allowed us to conduct the impact testing at the USNA's Structures Laboratory. He also arranged to have the cavities machined into the back of our solid laminates.

Jim Jacobs and Jeff St. John of Osprey Marine Composites worked very closely with us to build the unique test panels with simulated defects.

At Laser Technology, Inc., John Newman worked with us to perform NDE on our test panels using laser shearography and provided valuable case studies for the report. At Imperium, Inc., Bob Lasser and Willard Morris conducted ultrasonic NDE on test panels featured in the report. Mark Ashton of Independent Marine Systems conducted thermographic NDE studies on test panels. Bharat Chaudhry at Thermal Wave Imaging arranged for pulsed thermography analysis of our test panels. The case study on ultrasonic testing was based on survey work done by Bruce Bandos, NSWCCD, Philadelphia. Mr. Ashton also provided case studies of thermography used in the report. Additional thermographic case studies were provided by Bill Trenkle of Todd & Associates and Jack Allinson of J.N. Allinson Associates, Inc. Roby Scalvini of Marine Survey Bureau offered insight into advanced NDE technologies used for yacht inspection.

## 2. Defects

As a precursor to evaluating the efficacy of NDE techniques, this chapter describes the defects that are found in marine composite construction. Included are photographs, illustrations and micrographs to help identify defects of interest. Appendix A is a table of allowable limits and detectability thresholds of defects common to marine composites. Values are provided for conventional (E-glass) and advanced (carbon fiber) laminates.

### 2.1 Bonded Joint Failure

Adhesively bonded joints can suffer from a number of defects, as illustrated in the Figure 1. Particularly of concern are disbonds, which may not be evident from surface examination. This is especially true for kissing bonds, where the bond is intact but there is a lower level of adhesion and little separation of the faces. [NetComposites 2004]

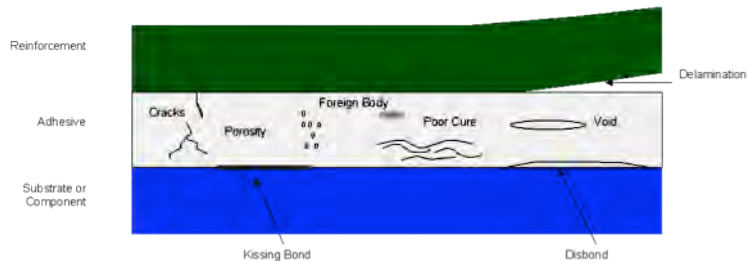


Figure 1. Bonded joint failure modes  
[NetComposites 2004]

### Cohesive Bond Failure

During cohesive failure, the adhesive sticks to both surfaces, but cannot hold them together. With film adhesives used for honeycomb sandwich construction, Cohesive failure usually occurs through the plane of the carrier cloth, which is the weakest plane in an effective bond because of the reduced surface area caused by the presence of the carrier cloth. The surface is rough and often slightly milky in appearance due to matrix cracking formed by the failure (see Figure 2). The causes of cohesive failure include inadequate overlap length and factors causing high peel stress or high thermal stresses. [Davis 2010] Cohesive failure can also occur from the presence of voids or improper bond-line thickness.

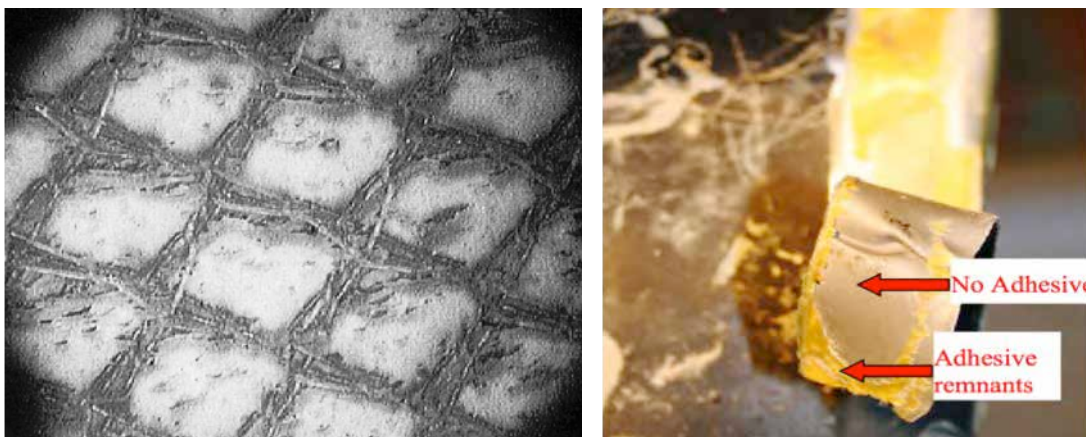


Figure 2. Cohesive (left) and Adhesive (right) bond failure examples  
[Davis 2010]

Adhesive Bond Failure

Adhesive bond failures occur at the interface between the adhesive and the adherent, with residual adhesive remaining at any location on one surface only (see Figure 3). The chemical bonds at the interface are weaker than within the adhesive. The surface of the adhesive is smooth and often replicates surface features from the adherent. Adhesion failures exhibit lower strength than cohesive failures. Causes of adhesive failure include contamination during manufacture, the use of out-of-life adhesive, insufficient surface preparation and inadequate temperature control during production. [Davis 2010]

Mixed-Mode Bond Failure

Mixed-mode failures exhibit both cohesive and adhesive failure, resulting from a partially degraded interface. Mixed-mode failures are essentially a transitional phase between cohesive and adhesive failure. The failure exhibits areas of smooth surface as well as areas, which are rough. The strength of adhesive bonds exhibiting mixed-mode failure is lower than the cohesive failure strength. Figure 3 shows examples of mixed-mode adhesion failures. [Davis 2010]

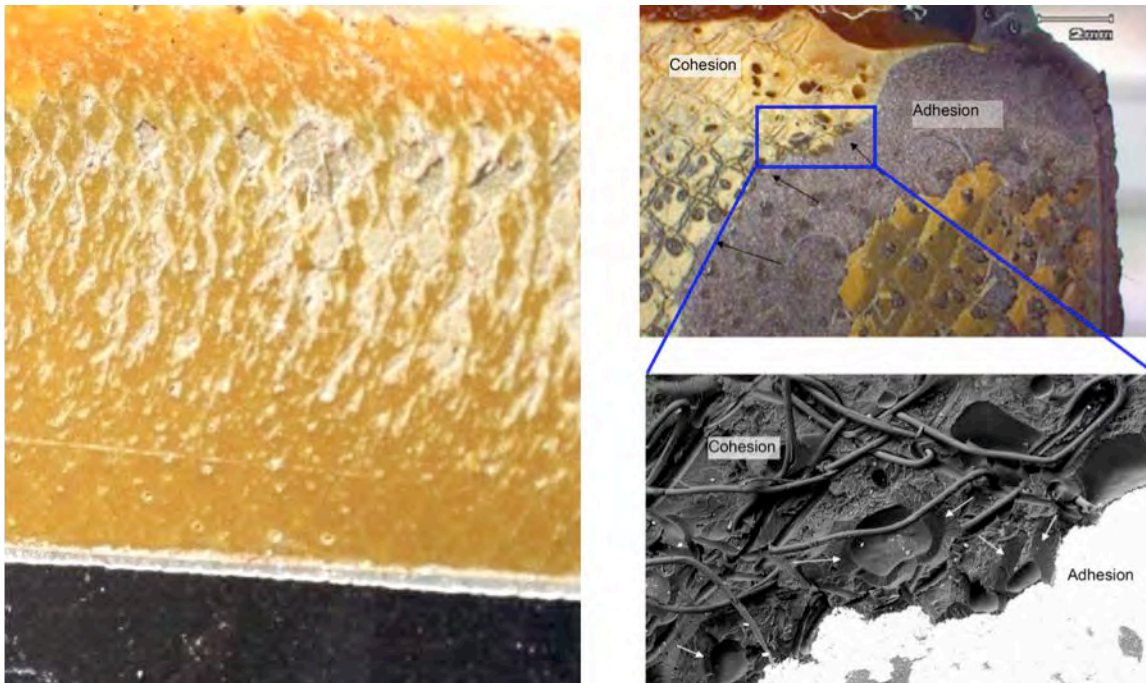


**Figure 3. Mixed-mode bond failure (light areas) and adhesion failure (darker areas) (left) and adhesive bond failure ahead of the disbond front, where the white portion in the lower right of is bare substrate (right). [Davis 2010]**

Adhesive bond failures require closer scrutiny to accurately assess the causes of these failures. Adhesive bonds fail by either cohesion or adhesion failure. Cohesion failures are characterized by the presence of adhesive on both surfaces, the causes of which are summarized in Table 1 along with the related design issues, which should be considered by certification requirements for bonded joints.

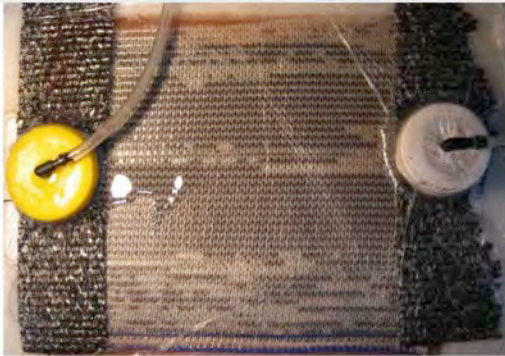
**Table 1. Causes of cohesion failures**

Inadequate overlap length	Poor design
Pell stresses	Poor design or service incidents
Fatigue	Poor design (attempting to bond adherends which are too stiff) (Rare in well designed joints.)
Excessive void content	Moisture contamination or poor pressurization during production
Impact	Service incidents
Skin-to-adhesive failure in sandwich panels	Internal pressure exceeds flatwise tensile strength

Adhesion failures are characterized by the absence of adhesive on one of the adherend surfaces and a replication of the surface from which the bond has separated on the other. Adhesion failures occur because of poorly prepared bonding surfaces, selection of a surface preparation process, which is incapable of producing a durable bond, or due to use of adhesive, which has cured before the bond was formed. These are manufacturing issues, not related to service incidents.” [Davis 2008]

**2.2 Air Bubbles**

Air bubbles in a laminate are defined as air entrapped within and between the plies of reinforcement and are usually spherical in shape. Air bubbles in laminates are always an artifact of the manufacturing process, as illustrated in Figure 4. Ribbed rollers called “bubble busters” are used during hand lay-up to eliminate air bubbles in laminates. Vacuum bag leaks can cause air bubbles in infused laminates.



Air bubbles introduced during infusion manufacturing process due to resin "boiling" [Eddie Matejowsky, Brisbane, Australia, 2006]



Air bubbles trapped during hand layup that were removed by sanding [Boat-Project.com, 2001]



Air bubbles trapped during hand layup before being "rolled out" [Jeff Lilly Restorations, San Antonio, TX]



Using a "bubble buster" to roll out trapped bubbles in hand layup laminate [Greg Murphy, Grand Rapids, MI, 2009]

Figure 4. Examples of air bubbles in composite laminates

### 2.3 Blisters

The blistering of gel-coated, FRP structures has received much attention in recent years. The defect manifests itself as a localized raised swelling of the laminate in an apparently random fashion after a hull has been immersed in water for some period of time. When blisters are ruptured, a viscous acidic liquid is expelled. Studies have indicated that one to three percent of boats surveyed in the Great Lakes and England, respectively, have appreciable blisters. There are two primary causes of blister development. The first involves various defects introduced during fabrication, including defective raw materials. Additionally, blisters can form in service when a part that contains internal voids is heated under environmental conditions. Entrapped liquids are also a source of blister formation. [Greene 1999] Figure 5 shows some examples of blisters in recreational boat hulls.



Blistering like this takes many years to develop, and will not be cured by any amount of heating or de-humidification. Peeling, blasting and thorough fresh water washing remain an essential part of the process.

Unbound fiber behind a yacht's gelcoat. Unbound fiber like this tends to harbor solutes, and will make successful treatment difficult.

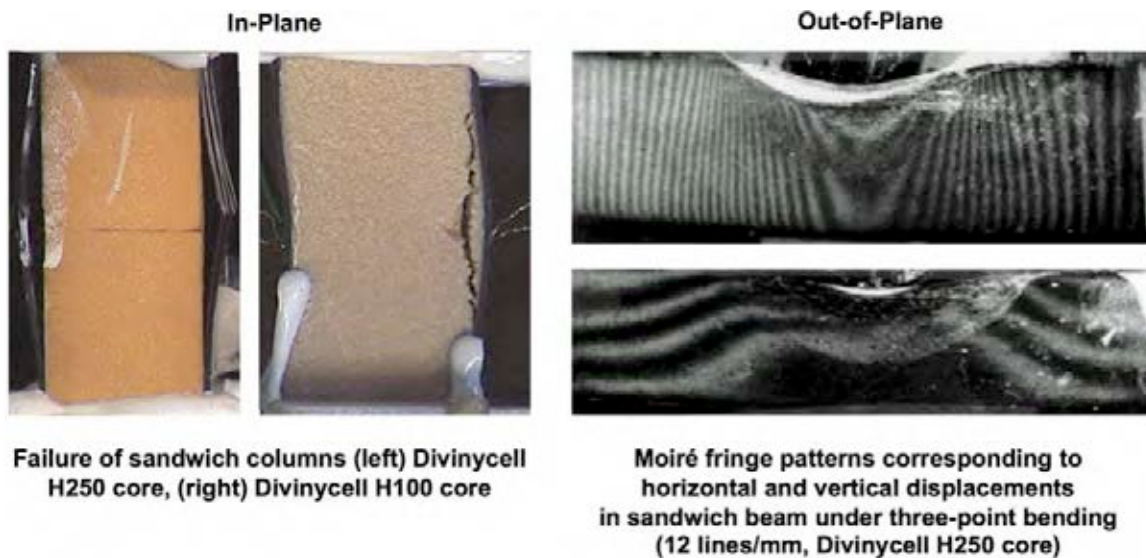
The pock marks seen here were caused by large air inclusions (introduced at newbuild), and not by osmosis.

Figure 5. Illustration of blisters in boat hulls [Clegg 2009]

## 2.4 Core Crushing

Core crushing is caused as a result of impact, local indentation and/or excessive through-thickness loading of a sandwich construction. This type of defect can occur in all types of core material and can result in localized debonding and a lack of support to the sandwich skin laminates, leading to potential failure of the sandwich panel. [Gower 2005]

Examples of core crushing are shown in Figure 6.



Failure of sandwich columns (left) Divinycell H250 core, (right) Divinycell H100 core

Moiré fringe patterns corresponding to horizontal and vertical displacements in sandwich beam under three-point bending (12 lines/mm, Divinycell H250 core)

Figure 6. Illustrations of core crushing [Gdoutos 2004]

Core crushing may not always be evident from the surface. Core crushing is common following collision damage to ship hulls. [NetComposites 2004] Through-bolted hardware attachment can also cause core crushing if high-density inserts or compression tubes around the bolts are not used.

Figure 6 shows examples of in-plane and out-of-plane core crushing. Figure 7 shows examples of honeycomb core crushing. Figure 8 shows a detail of out-of-plane foam core crushing.

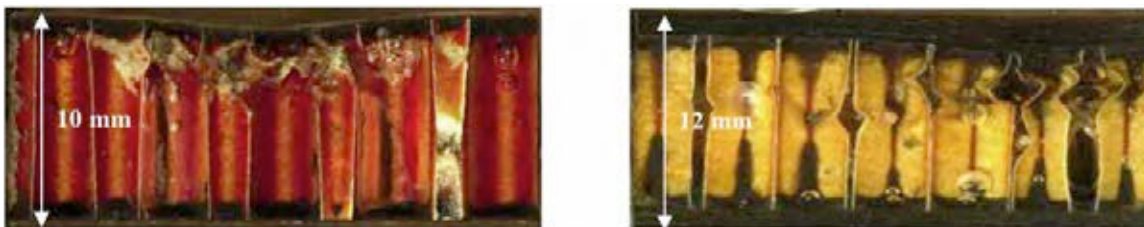


**Figure 7. Photographs showing core crushing in (left) GRP-high density Nomex and (right) CFRP-medium density Nomex sandwich constructions. [Gower 2005]**

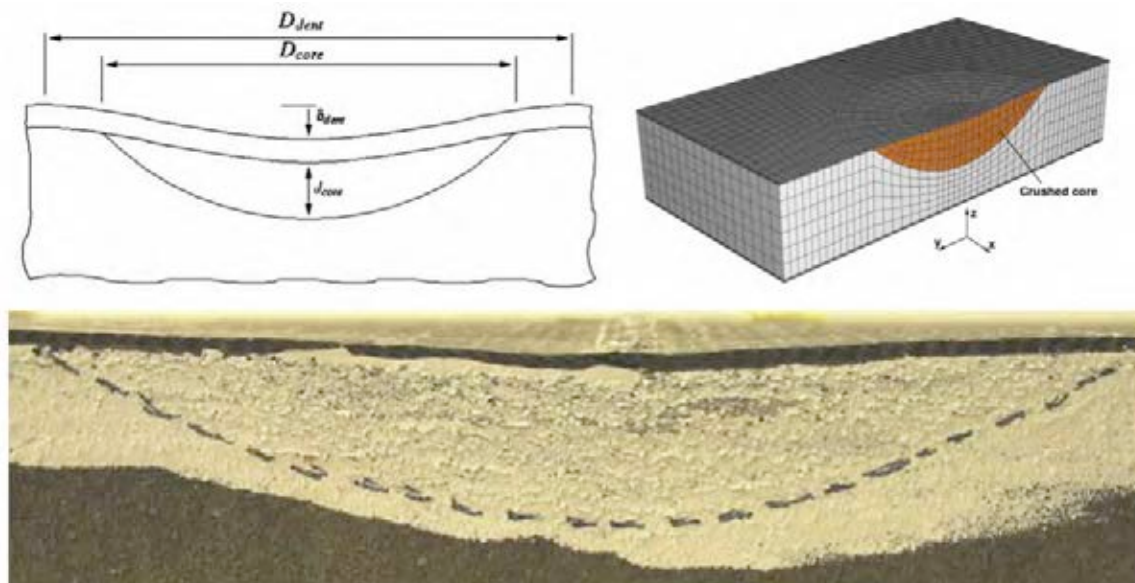


**Figure 8. Schematic of indentation damage (top left), FE-model of a sandwich panel with indentation damage (top right), and a photograph of a cross-section with indentation damage (bottom) [Zenkert 2005]**

### 2.5 Core Shear Failure

In a sandwich laminate, the core resists bending forces via shear loading, which is maximum at the neutral axis. Figure 9 illustrates a classic core shear failure where the crack extends between both face-skins. Note also that the core shear failure is also accompanied by skin-to-core separation.

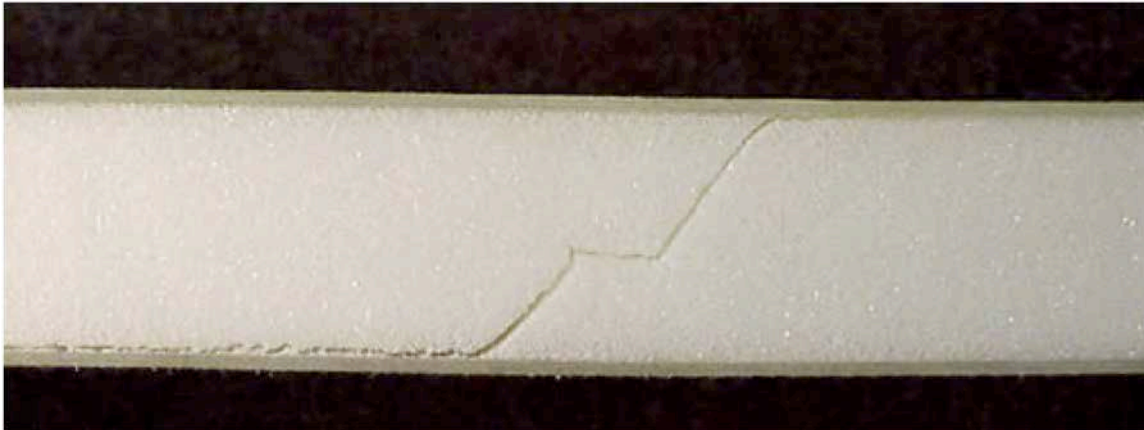


**Figure 9. Fatigue fracture of PMI 51 S foam core,  $P/P_{crit} = 65\%$ ,  $n = 1.1 \times 10^6$  cycles [Roosen 2002]**

### 2.6 Crazeing

Cracks, crazing, and abrasions, are common types of composite laminate damage, which are characterized by a depth typically less than 1/16" (2 mm), where the damage does not extend into the primary reinforcement. This damage has no structural implications by itself. However, if unattended, it can cause further damage by water intrusion and migration. Crazeing may indicate the presence of high stress or laminate damage below the surface. [Greene 1999] Figure 10 shows examples of crazing to fiberglass laminates.

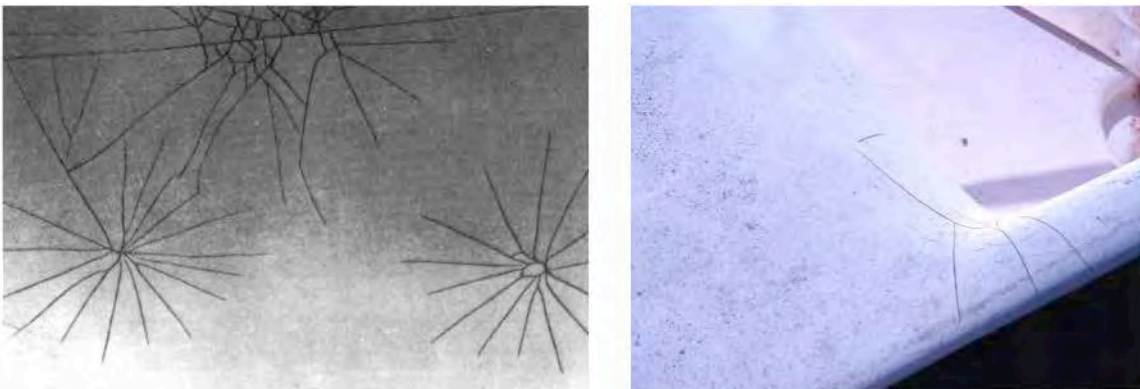


**Figure 10. Examples of fiberglass crazing in gel coat finishes. Note that photo on right shows crazing in area of stress concentration. [Coackley 1991]**

## 2.7 Delaminations

Delaminations occur at the interface between the layers in the laminate, along the bondline between two elements, and between face-sheets and the core of sandwich structures. Delaminations can form due to stress concentrations at laminate-free edges, matrix cracks, or at areas of stress concentrations. Delaminations may also be the result of poor processing or from low-energy impact. Delaminations break the laminate into multiple sub-laminates, which reduces the effective stiffness and ultimate strength of structural assemblies. [Ilcewicz 2009] The terms debond and disbond are often used interchangeably with delamination.

Delaminations are one of the principal defects that can occur in manufacture, machining and in-service. They are caused by contamination at ply interfaces, insufficient cure or expired raw material, inclusions (such as peel ply), and impact loading. This type of defect has a severe detrimental affect on mechanical strength, particularly under compressive loads, and on the life expectancy of composite components. The occurrence of production/handling induced delaminations can be avoided by using best manufacturing processes. [Gower 2005] Figure 11 shows pictures of severe boat hull delamination.



**Figure 11. Examples of severe delamination resulting from manufacturing defects [www.yachtforums.com]**

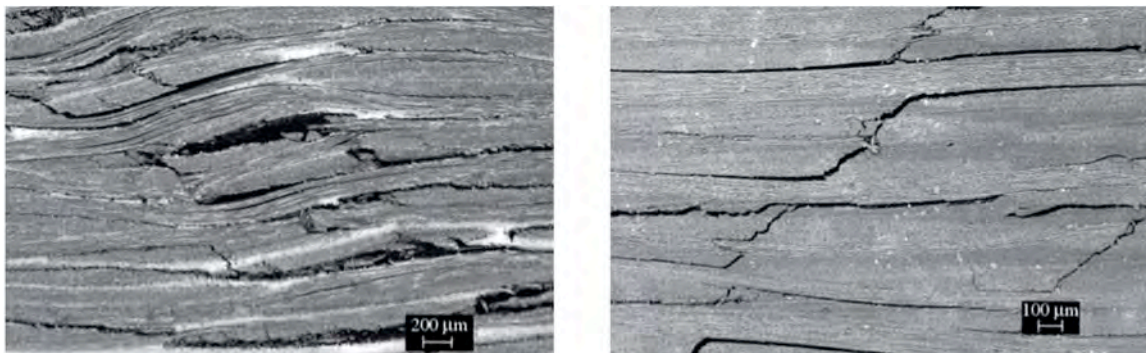


**Figure 12. SEM micrographs of delaminated specimens after interlaminar shear tests of carbon/epoxy laminates [Paiva 2005]**

Environmental ingress can be the basis for formation of sub-surface delaminations. Edge delaminations are quite common due to environmental ingress. [NetComposites 2004] Figure 12 shows scanning electron microscope (SEM) images of delamination in composite laminates. Figure 13 shows edge delamination common to machined composite laminates.

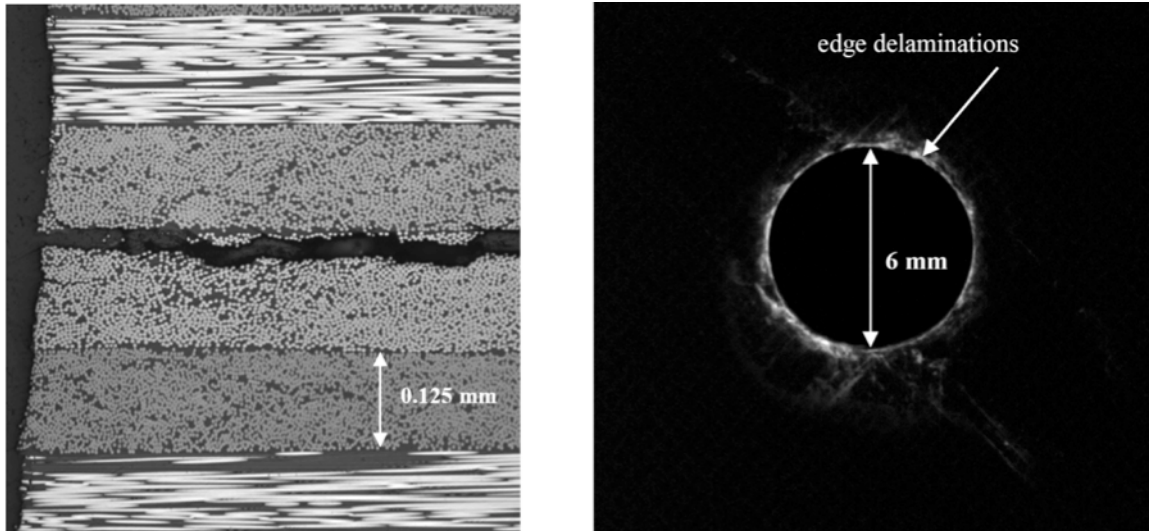


**Figure 13. Micrograph of an edge delamination within a CFRP panel (left) and X-ray image of edge delaminations around a drilled hole in a CFRP panel (right) [Gower 2005]**

Connections such as at bulkheads or hull to deck are accomplished with laminated tabbed joints consisting of successive plies of overlapping glass reinforcement. The tabbed joint forms a secondary bond with the structural components being joined, since the components are usually fully cured when connected. Because the geometry of tabbed joints tends to create stress concentrations, they are susceptible to delaminating and peel, as shown in Figure 14. [Greene 1999]

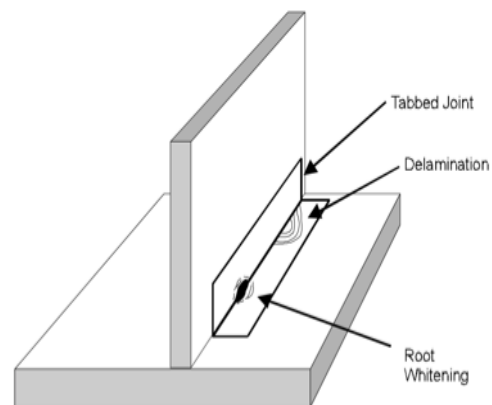


**Figure 14. Delamination of tabbed joint [Greene 1999]**

## 2.8 Fiber Failure

Broken fibers can be critical because loads in composite structures are typically designed to be carried by the fibers. Unlike cracking in metallic structures, fiber failure is usually limited to the zone of impact contact. The resulting loss in residual strength is controlled by a relatively small damage size. One exception can be a high-energy, blunt impact over a large area, which breaks internal structural elements such as stiffeners, ribs, or spars, but leaves the exterior composite laminate skin relatively intact. [Ilcewicz 2009] Figure 15 shows an SEM image of compressive fiber failure and Figure 16 shows an instance of fiber fracture and pullout.



**Figure 15. Formation of kink bands when composite laminates are under compression (marked with arrows) [Rakow 2006]**

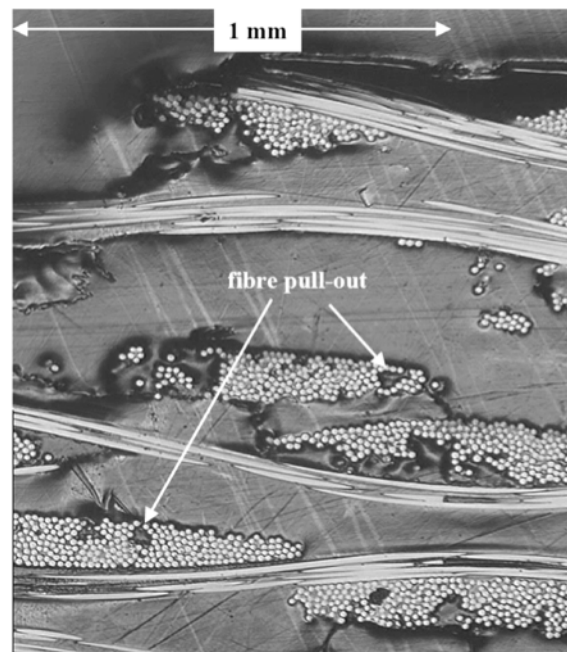
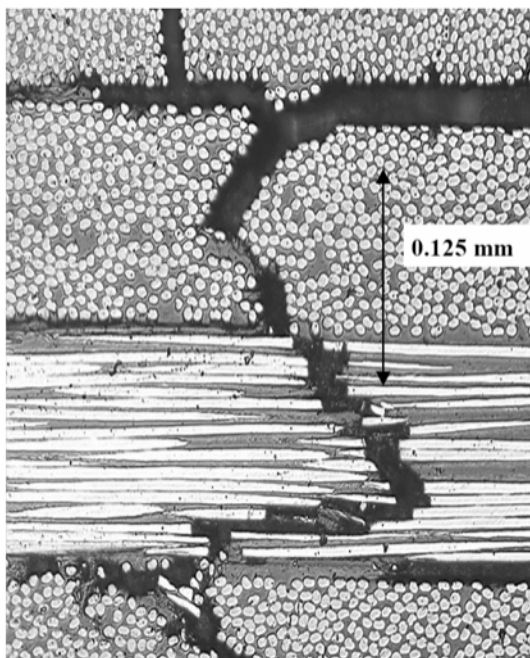


**Figure 16. Micrograph of fiber fracture in a multidirectional CFRP laminate (left) and Micrograph showing fiber pullout in a woven GRP material (right) [Gower 2005]**

Fiber fracture can occur due to manufacturing operations as well as from damage sustained in-service. During manufacture, fiber fracture can be present at the inner radii of corners. Poor machining practice can result in fiber breakage and fraying at the edges of holes or cut-outs. This is to be avoided as such areas of damaged material can act as failure initiation sites and potential channels for moisture ingress. [Gower 2005]

### 2.9 Kissing Bond

A kissing bond refers to the situation where two surfaces have been only partially bonded or are disbonded but touching or in very close proximity. This may be the consequence of poor adhesion, in-service loading or impact damage. The disbond may not be visible externally and because of its tightness may be more difficult to detect using NDE methods than a conventional disbond.

Kissing bonds can potentially occur anywhere in a composite component where there is adhesive bonding, including end-fittings, core bonding and with repair patches, as shown in Figure 17. Detectability by NDE will depend on the size, location and tightness of the kissing bond.

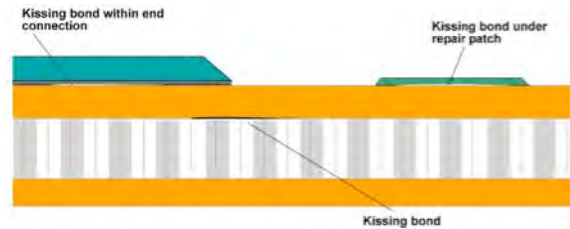


Figure 17. Various types of “kissing” bonds [NetComposites 2004]

The integrity of adhesively bonded composite structures is strongly dependent on good integrity of the bonds. Care and cleanliness in bond preparation is paramount. Any disbonding is likely to exacerbate under in-service loading or with environmental ingress leading to kissing bonds and eventually partial separation of the composite layers that can result in failure of the component. [NetComposites 2004]

Figure 18 shows the change in natural frequency of bonded, partially-bonded and disbonded laminates. Figure 19 shows how the use of “peel ply” material can create a kissing bond condition.

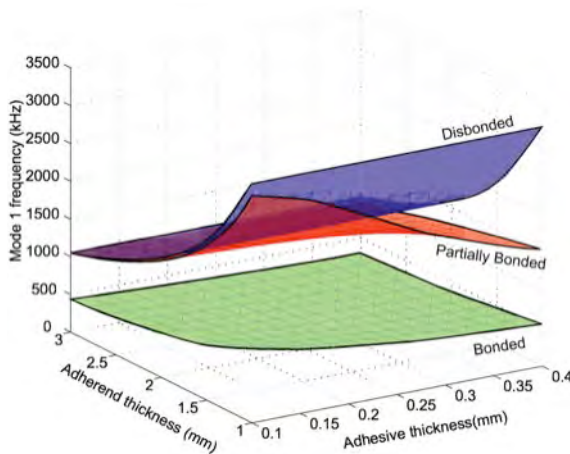


Figure 18. Mode 1 frequency variation with adhesive thickness for bonded, partially bonded and disbonded conditions [Allin 2002]

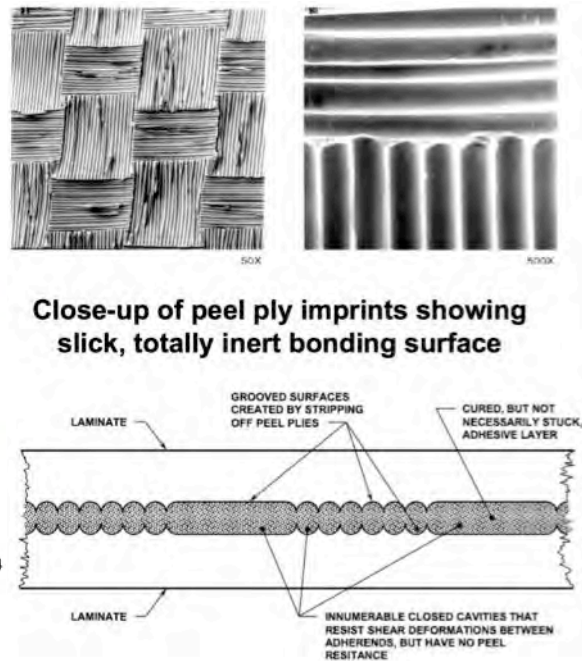
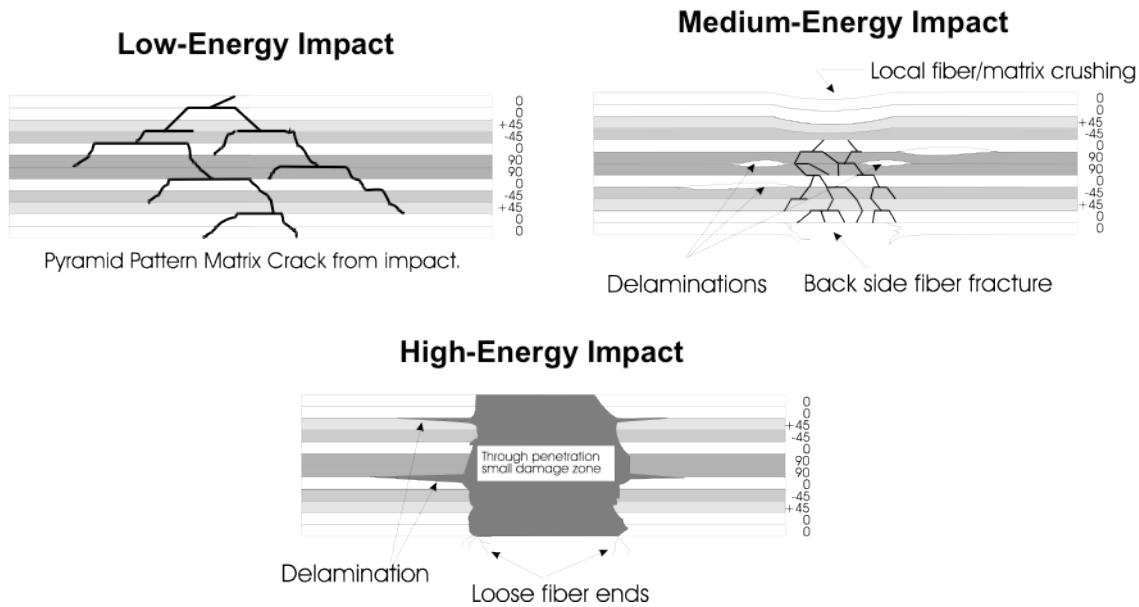


Figure 19. The influence of “peel ply” on “kissing” bond formation [Hart-Smith 2004]

### 2.10 Impact Damage

The diagrams shown in Figure 20 illustrate potential types of damage from various types of impact events. What is not shown in the diagrams is the additional effect of velocity associated with impacts. For example, low-speed, high-energy impacts can leave large-area delaminations and substructure damage without much exterior damage. On the other hand, high-speed impacts (such as bullets) penetrate without leaving wide-area delaminations and potential substructure damage. [Ilcewicz 2009] It is also possible for sandwich laminates to exhibit damage on the inside skin without any noticeable damage on the impacted side. [Miller 2011]



**Figure 20. Impact damage types [Abaris Training Resources Incorporated]**

Impact damage is an important damage mechanism in composite materials that can occur in-service or as a result of handling during or following manufacture. This can give rise to surface indentations and other damage below the surface, such as cracking, delamination or disbonding.

Typically, impact loads will create a conical area of damage below the surface that contain small microcracks and delaminations, as shown in Figure 21. Damage is usually most extensive sub-surface and may be difficult to ascertain on visual examination of the surface itself.

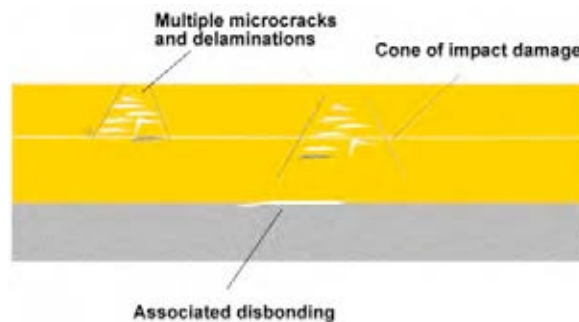


**Figure 21. Impact damage [NetComposites 2004]**

Service-induced damage such as that due to local impacts may occur at many points on the structure. Regions around hatches and attachment points are particularly prone to low-velocity impacts. [NetComposites 2004] High speed hull structure and naval combatants are more likely to receive high-velocity impact damage.

Figure 23 and Figure 24 show the surface of laminates subjected to impact damage. Figures 25 and 26 show sandwich panels with impact damage. It is instructive to note the wide variation in damage depending upon impact energy, impactor geometry and laminate construction.

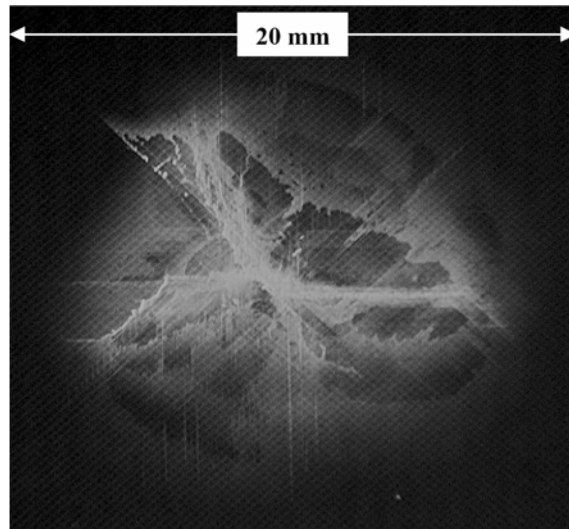


**Figure 22. X-ray image of impact delaminations within a CFRP panel [Gower 2005]**

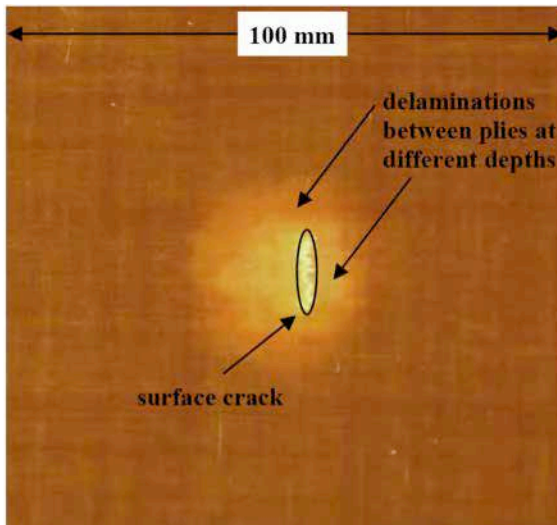


**Figure 23. Digital photograph of centrally located delaminations on the impact surface of a GRP skin on a Nomex sandwich construction (left) and digital photograph of back surface impact damage showing delamination and fiber fracture in a CFRP panel [Gower 2005]**

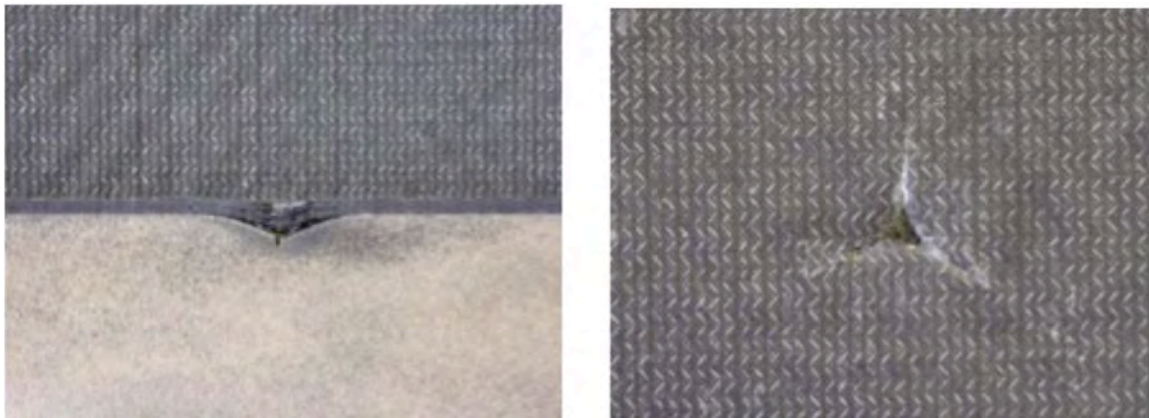


Figure 24. Damage types occurring from blunt object impact (left) and sharp object impact (right) [Zenkert 2005]

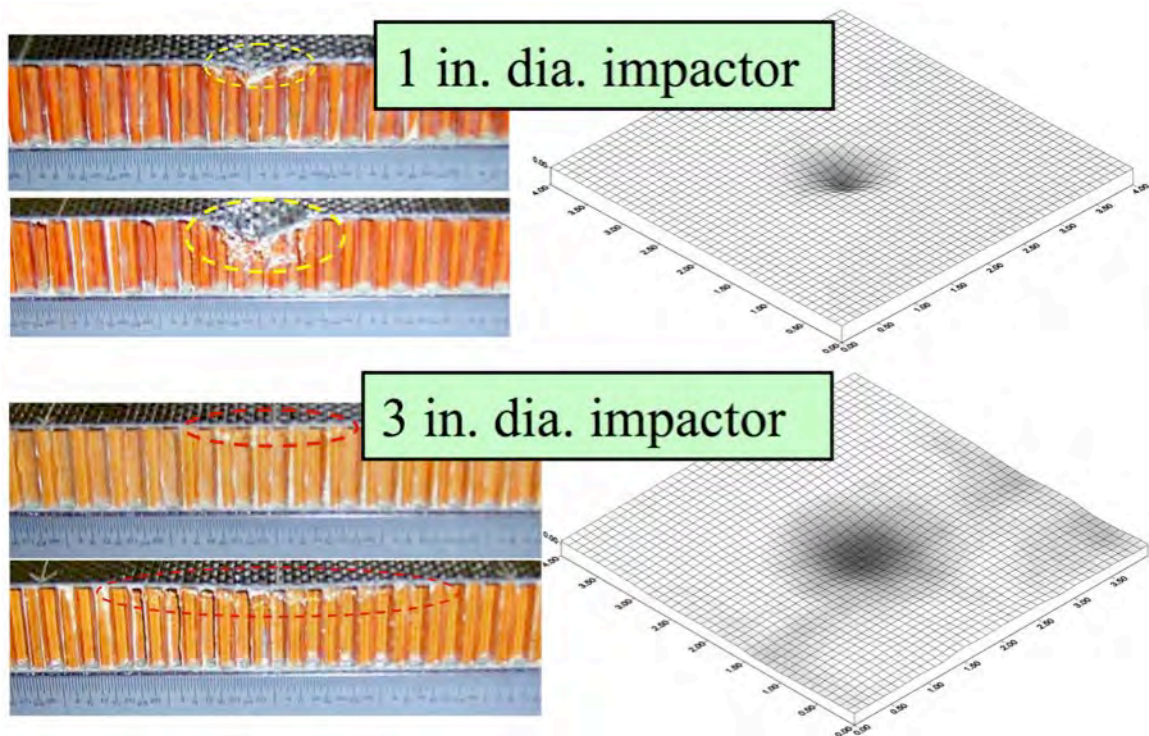


Figure 25. Foreign object impact damage in honeycomb-cored sandwich laminates [Ilcewicz 2006]

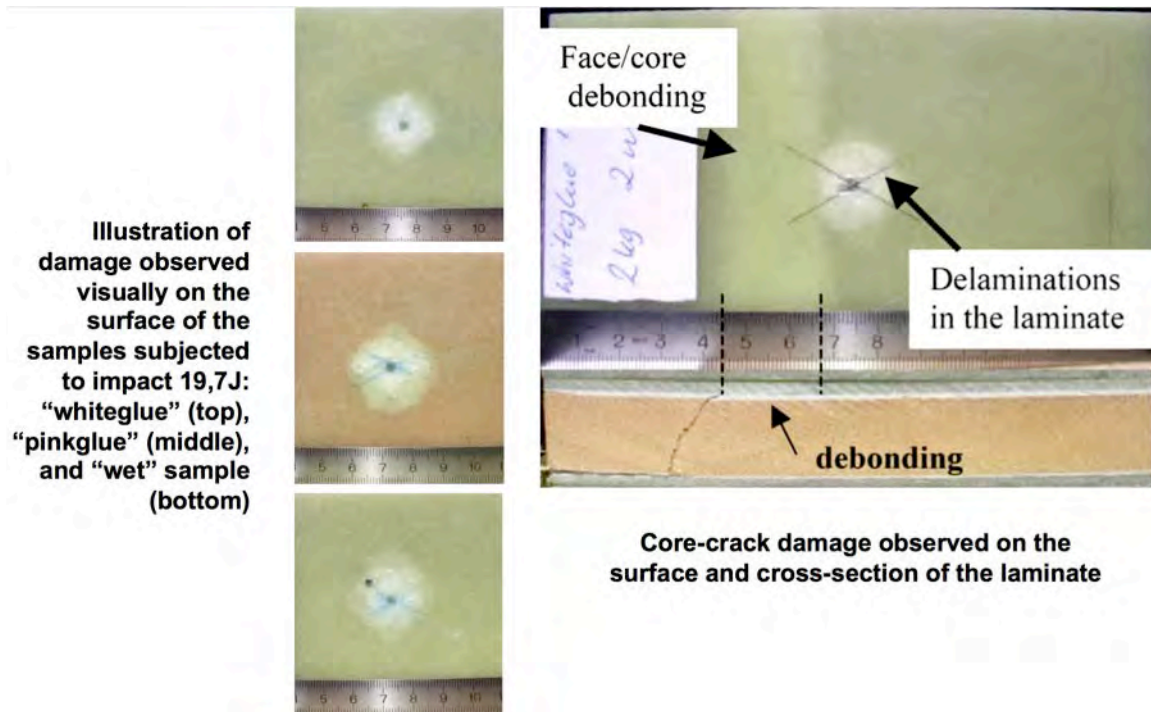


Figure 26. Sandwich laminate impact damage [Lendze 2006]

### 2.11 Matrix Cracking

Laminate cracking refers to discrete defects in the composites that are usually through thickness, as shown in Figure 27. A crack is distinct from a delaminations or disbond which refer to inter-laminar separation of material or decohesion of a bond. Matrix cracking or transverse cracking refers to the finer scale types of multiple cracking normally occurring in the central plies of a laminate. [NetComposites 2004]

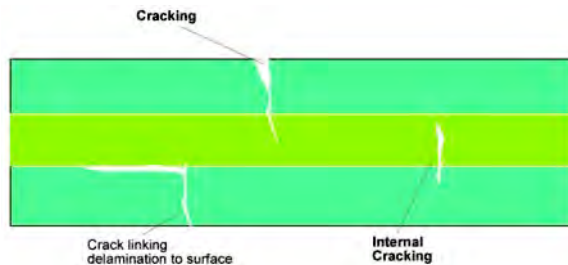
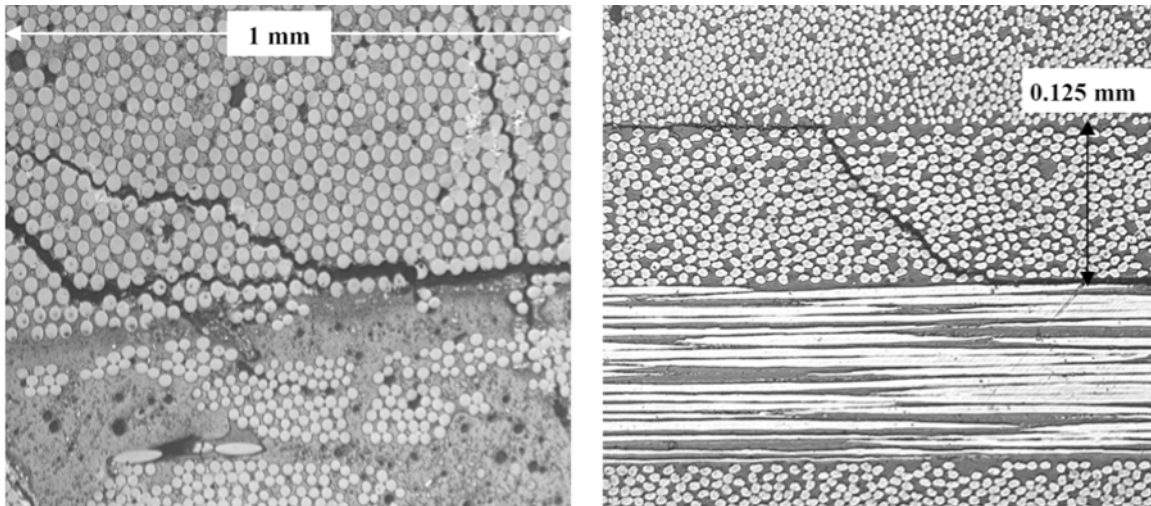


Figure 27. Schematic representation of cracks in laminates [NetComposites 2004]

Matrix cracks are caused by stresses, which can be generated by either mechanical and/or thermal loading. Thermal stresses result from differences in coefficients of thermal expansion between adjacent plies and exothermic chemical reactions. Mechanical stresses can be introduced during fabrication from resin cure shrinkage. Low failure strain resin systems are more likely to show signs of matrix cracking. Multidirectional material systems are also susceptible to matrix cracking due to the anisotropy of the thermal expansion of  $0^\circ$  and  $90^\circ$  plies, resulting from the low thermal expansion of the fiber compared to the resin. [Gower 2005]

Matrix cracking generally occurs parallel to fibers due to thermal and mechanical loading. Isolated matrix cracks can occur in processing as local fiber and matrix volumes change with part geometry. Most composites used in marine applications do not matrix crack over wide areas at working strain levels. However, aramid/epoxy materials have exhibited matrix cracking over wide areas in aircraft due to high-thermal residual stresses. Fluid ingress through the matrix cracks can further degrade sandwich face-sheet to core bonds. [Ilcewicz 2009]

Figure 28 shows micrographs of matrix cracking.



**Figure 28. Micrographs of matrix micro-cracking in (left) a woven GRP and (right) a multidirectional CFRP laminate [Gower 2005]**

### 2.12 Moisture Ingress

This type of damage usually requires another damage to be present that creates a leak path into the sandwich core. Some design details, such as porous fabric weave styles used for face-sheets (skins) or sharp discontinuities may also allow fluids to enter the core through leaks. Once the fluid gets into a sandwich laminate it can degrade the core or its bond with the face-sheets. Damage growth can be caused by freeze-thaw cycles, a pressure differential through the face-sheet and fluid degradation of the bond. [Ilcewicz 2009]

Figure 29 is a schematic of moisture ingress damage. Erosion or damage to gel coat or barrier layers can initiate damage to the laminate. The extent of damage will depend on service conditions and the particular resins used. Exposed edges and edges of adhesive bonds are particularly susceptible. [NetComposites 2004]

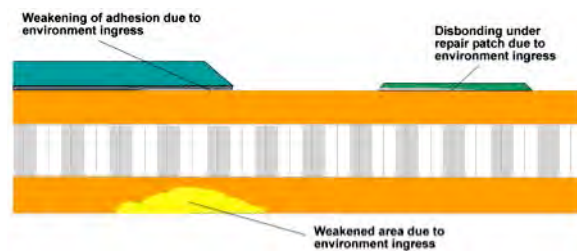


**Figure 29. Schematic representation of moisture ingress in sandwich laminates [NetComposites 2004]**

### 2.13 Pit (or pinhole)

Pits or pinholes are defined as small regular or irregular craters on the laminate surface, usually with nearly equal width and depth. Typically pinholes go through the gel coat surface. Larger pits are referred to as craters, which can only be seen on the back side of the gel coat. Pinholes arise during fabrication as a result of catalyst or contamination on molds or improper equipment operation. This type of defect in itself is not a structural concern, although it can lead to further degradation of the laminate. Figure 30 is a picture of surface pitting.

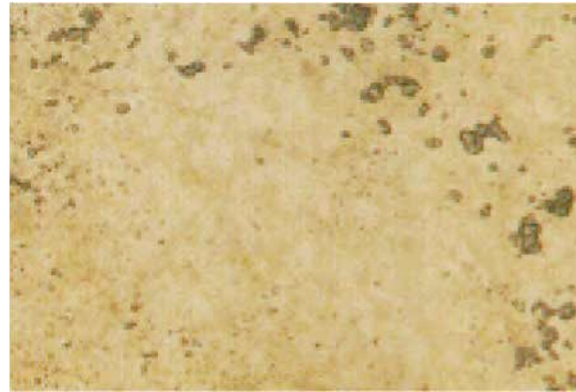


Figure 30. Image of pits or pinholes showing small regular or irregular craters on surface [Derakane 1997]

### 2.14 Ply (or Fiber) Waviness

Out-of-plane ply waviness in laminated composite material is characterized by undulations in a layer or group of layers within a multilayer laminate. Ply waviness can be caused by vacuum bagging, uneven curing, resin shrinkage or ply buckling caused by bending the composite lay-up into its final shape prior to curing. Ply waviness causes degradation of strength and fatigue life in structural applications, particularly under compressive loads. [Anastasi 2008]

Figure 31 shows images of various degrees of ply waviness. Figure 32 illustrates the angle  $\beta$  used to depict ply waviness in geometric models. Figure 33 is an extreme example of ply waviness.

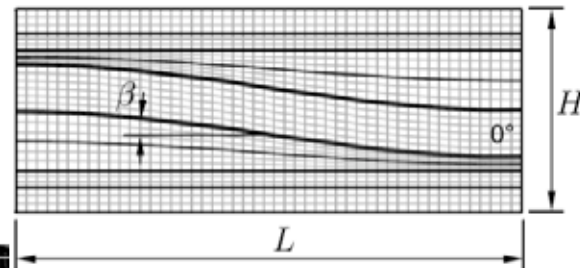


Figure 32. FE model geometry, representing one wavy  $0^\circ$  ply – the regarded geometrical features are in the order of  $10^{-1}$  mm ( $y_{ply}$  thickness) [Anastasi 2008]

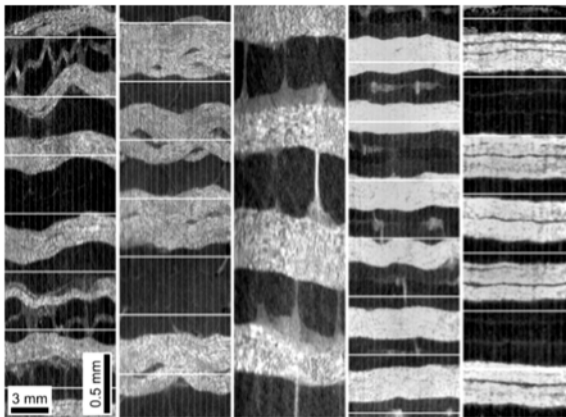
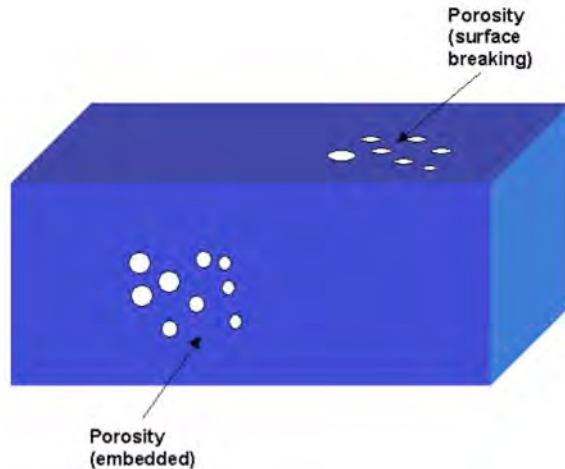


Figure 31. Different ply waviness morphologies made visible by laminate edge photographs (distorted at a ratio of 10:1); the waviness angle  $\beta$  ranges from  $5.5^\circ$  (left) to  $1.4^\circ$  (right); the wavelength  $L/H$  from 3.7 (left) to 1.5 (right) [Pansart 2009]



Figure 33. Composite sample close-up of apex showing extreme fiber-waviness [Anastasi 2008]



**Figure 34. Schematic of laminate porosity [NetComposites 2004]**

### 2.15 Porosity

Porosity can be described as a large number of small voids, each of which is too small to be of structural significance but which collectively may reduce the mechanical properties of the laminate to an unacceptable degree. Figure 34 is a schematic of porosity in composite laminates. Porosity usually occurs during the curing cycle and is caused by entrapped air, moisture or volatile products. Porosity is most common in laminates manufactured by hand lay-up. Closed molding methods are less susceptible to air entrapment if mold integrity is maintained. Single or isolated large air bubbles are also referred to as

voids (see below). These are large enough to be of structural significance and can also be individually detected and measured.

The distinction between discrete voids and porosity is somewhat subjective. In practice, porosity refers to sub-millimeter voids whereas voids of several millimeters dimension would be considered as discrete defects. Severe porosity can create stress concentrations that can affect laminate mechanical properties, such as transverse and through-thickness tensile, flexural, shear and compression strengths. [NetComposites 2004]

### 2.16 Resin Rich Area

Resin rich areas are caused by the displacement of fibers or fiber preforms during processing. This tends to occur in structures with sharp bends (i.e. small radii), steps and chamfered edges, as fiber reinforcement tends to pull around corners leaving a resin rich area near the outer radius. It can also occur locally. [Gower 2005] Resin rich defects are most commonly found with hand lay-up construction, especially in keel sump areas of yachts. These regions can have severely degraded mechanical properties.

### 2.17 Resin Starved Area

Regions of resin starvation are areas in a laminate where the reinforcement fibers are still bare and dry. This may be caused by inadequate wetting of fibers, poor consolidation during laying-up or problems with resin delivery. Resin starved regions may be difficult to detect and often occur at inner radii of curved components. [Gower 2005]

Figure 35 shows examples of resin rich and resin starved laminates. Figure 36 shows highly-magnified images of resin rich and resin starved areas in composite laminates.

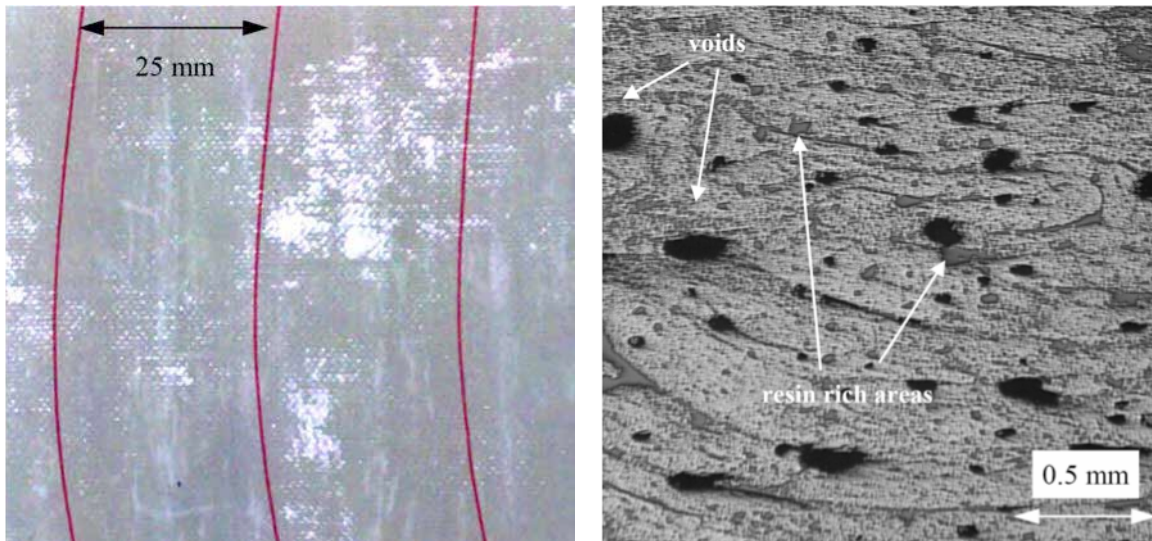


**Figure 35. Resin starved areas in a woven GRP laminate (left) and micrograph of resin rich areas in a filament wound CFRP material [Gower 2005]**

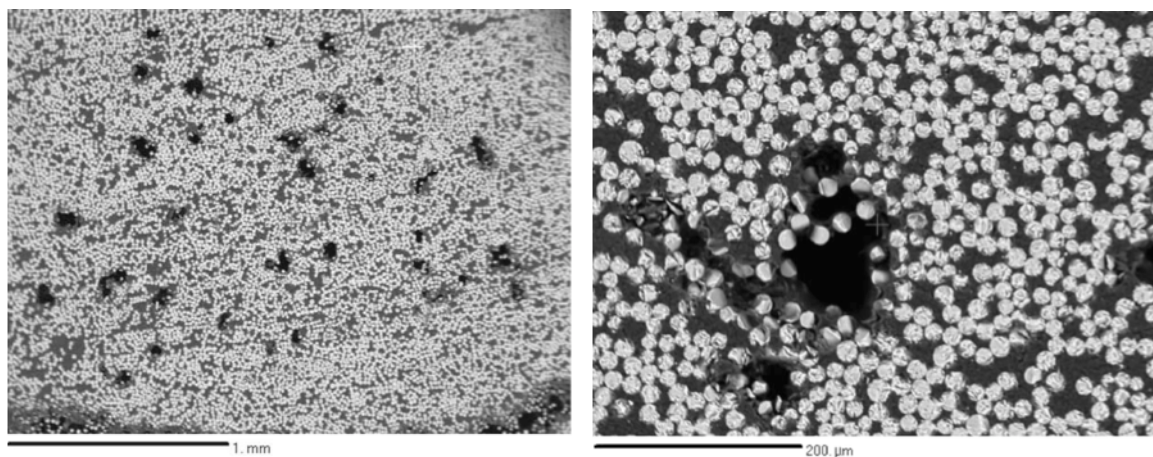


**Figure 36. Hand-polished material fabricated by the VARTM process and imaged with backscattered electron imaging. Both voids (black areas) and resin-rich areas (shown as light gray) are present. [Herzoga 2004]**

### 2.18 Skin-to-Core Disbond

A skin-to-core disbond (or debond) refers to the situation in composite sandwich structures where the skin of the composite has separated from the inner core. This may be the consequence of poor adhesion, service loading or impact damage. It is also possible that the core was never bonded to the outside skin in areas, which can occur with production manufacturing using female molds. The disbond may not be visible externally and if tight or weakly bonded may be difficult to detect using NDE methods. This is known as a kissing bond (see above). Skin-to-core disbonds can occur in hull regions that are subjected to repeated wave impact forces.

It should be noted that core disbonds are defined as a separation of the composite outer or inner skins from the core. This is different from a delamination, which refers to a similar separation between any plies or layers of the composite. Figure 37 is a schematic of skin-to-core disbond. [NetComposites 2004]



Figure 37. Schematic of skin-to-core disbond [NetComposites 2004]

Skin-to-core disbonds are one of the principal defects that can occur in manufacture, during machining and in-service and are analogous to a delamination in a solid laminate. Manufacturing disbonds can occur due to inadequate bonding or coverage of adhesive between the skin and core and also from inclusions, such as peel ply. Disbonds can also occur as a result of improper procedures used to attach hardware.

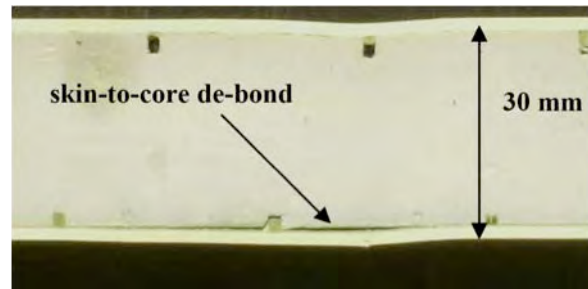


Figure 38. Photograph of skin to-core de-bond in a GRP skin, PU foam sandwich [Gower 2005]

Figure 38 shows a skin-to-core disbond in a foam-cored sandwich laminate. Figure 39 show disbonds from a fatigue test program.

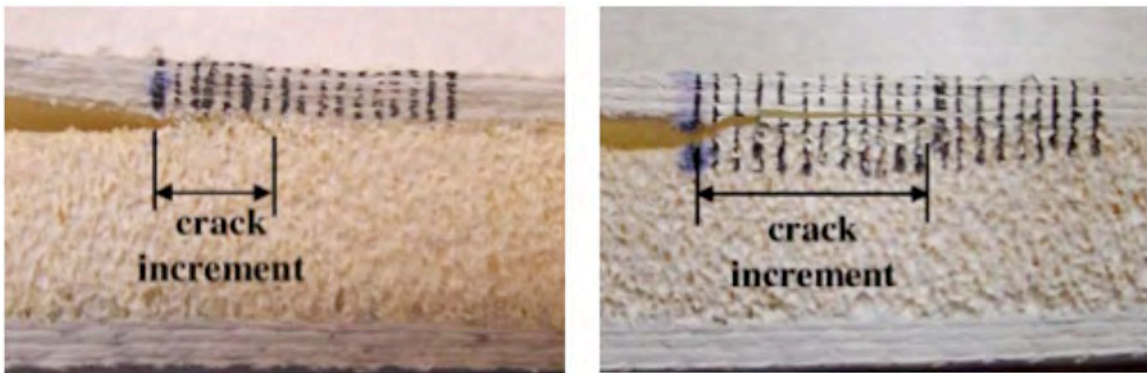


Figure 39. Compliance based crack length measurements showing crack path in PVC foam [Berggreen 2008]

### 2.19 Surface Cracking

Hairline cracks in exterior gel coat surfaces are traditionally treated as a cosmetic problem. However, barring some deficiency in manufacturing, such as thickness gauging, catalyzation or mold release technique, gel coat cracks often are the result of design inadequacies and can lead to further deterioration of the laminate. Gel coat formulations represent a fine balance between high gloss properties and material toughness.

Load sources that can exacerbate a poorly bonded sandwich panel include wave slamming, dynamic deck loading from gear or personnel, and global compressive loads that tend to seek out instable panels. Figure 40 is a schematic representation of surface cracks. [Greene 1999]

This type of damage is not critical if the damage is limited to the outer layer of resin without any damage to the fibers. If the fibers are damaged, they must be treated as a crack in the affected plies. Unlike metals, composite matrix nicks, scratches, and gouges are not likely to grow under repeated loads. [Ilcewicz 2009]

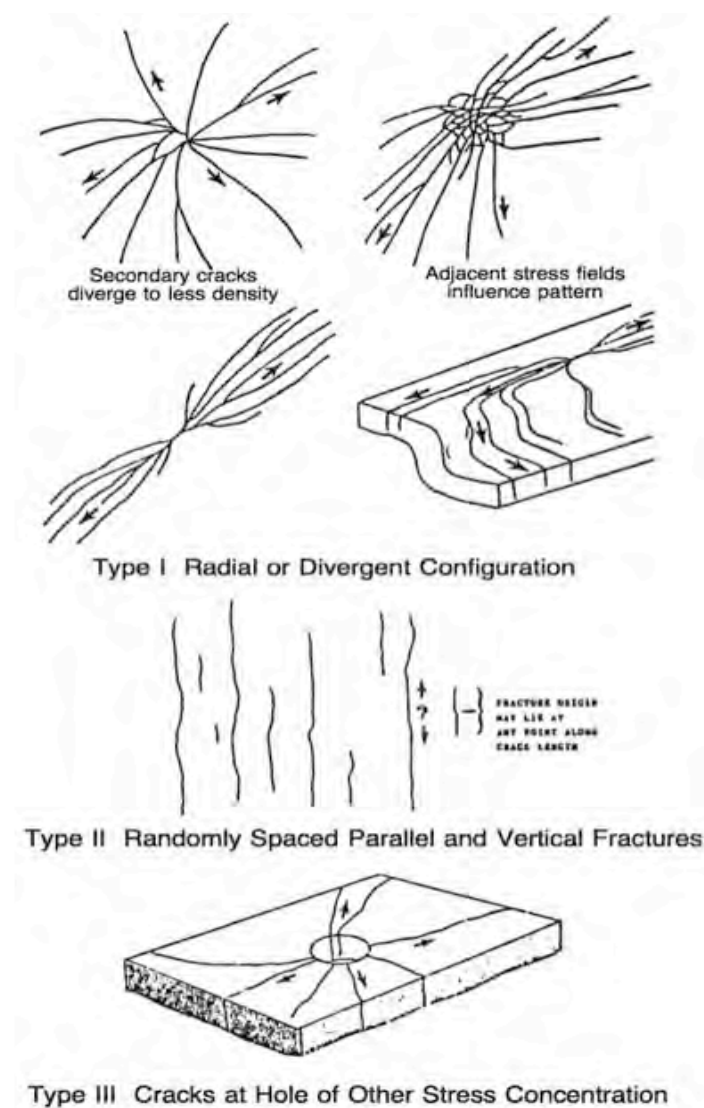


Figure 40. Schematic of surface cracks  
[Greene 1999]

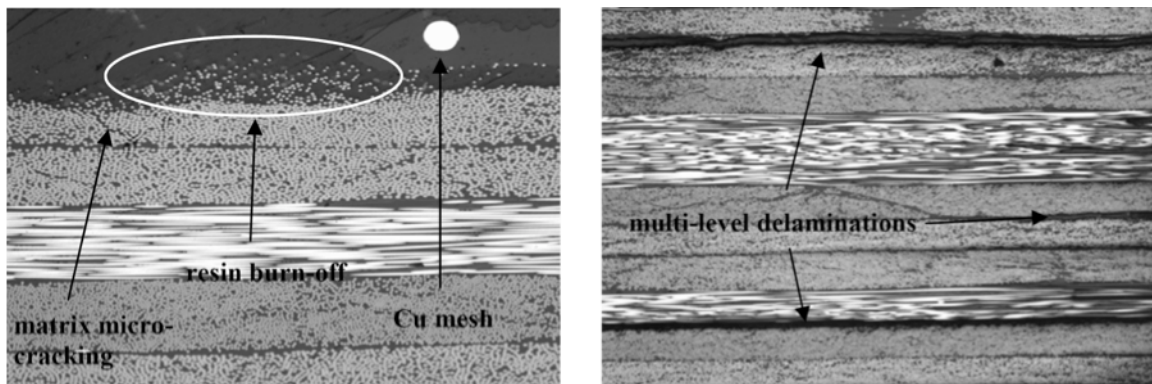
## 2.20 Thermal (and Lightning) Damage

Thermal damage is possible near sources of high temperature, such as engines and other machinery. There are usually visual indications of heat damage caused by exhaust or charring of the part surface, but it may be difficult to determine how deep into the laminate the heat damage extends. [Ilcewicz 2009]

During fabrication, material degradation due to exothermic chemical reaction of the matrix exists when dissipation of liberated heat through thermal conduction is slow. The internal temperature may be elevated to levels that induce irreversible thermal damage. This problem is particularly associated with thick sections. Extreme forms of thermal damage can be caused by phenomenon such as fire and lightning strikes. In such severe cases the resin can be burned-off from around the fibers. [Gower 2005]

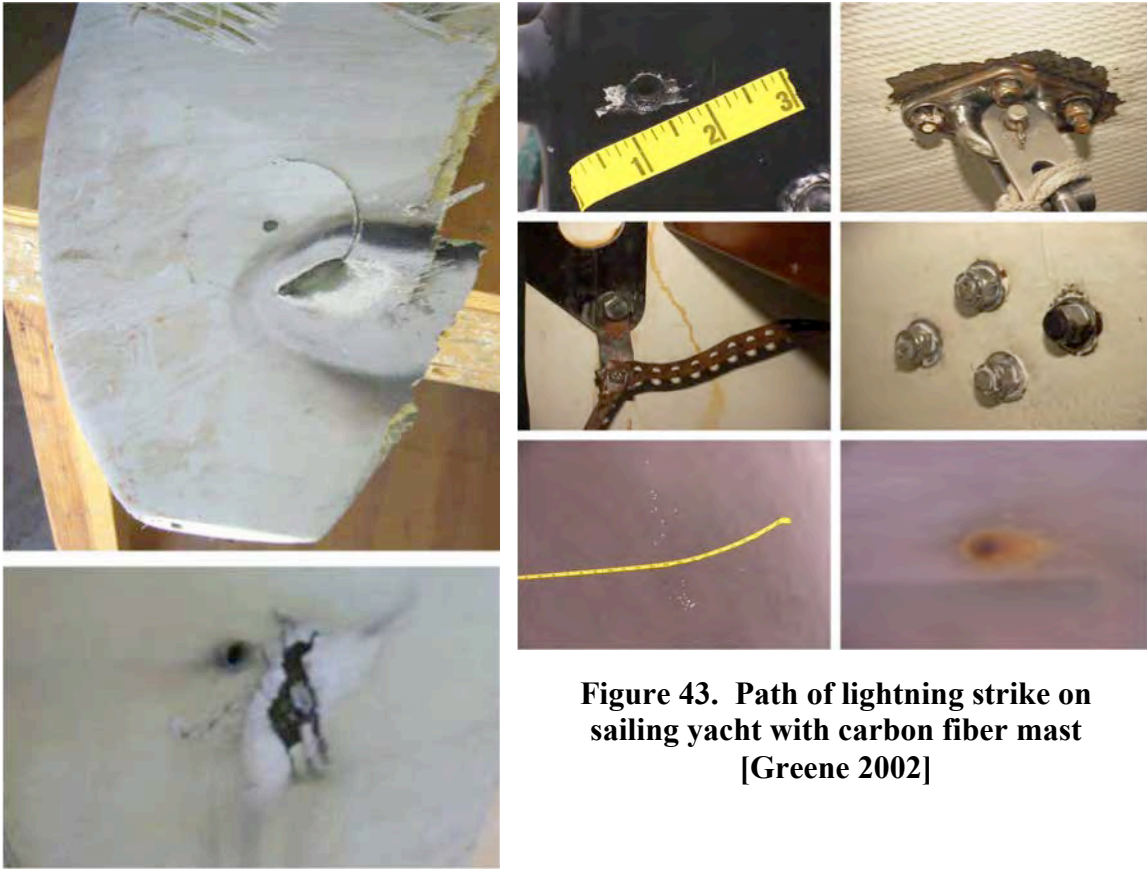
Lightning damage is usually constrained to surface layers of the skin panel. Degradation to the lightning protection system could pose potential for greater damage threats. Rare, high-energy lightning strikes may also cause considerable damage. [Ilcewicz 2009]

Figure 41 shows micrographs of thermal damage to a composite laminate.



**Figure 41. Micrographs of (left) resin burn-off and matrix micro-cracking in CFRP panel containing lightning strike protection and (right) large scale delaminations in unprotected panel [Gower 2005]**

Figure 42 shows lightning damage to a wind turbine blade. Figure 43 illustrates the discharge path of a lightning strike to a sailboat with a carbon fiber mast.



**Figure 43. Path of lightning strike on sailing yacht with carbon fiber mast [Greene 2002]**

**Figure 42. Lightning damage to wind turbine blades [Kithil 2008]**

### 2.21 Voids

Voids and porosity can occur in manufacture due to volatile resin components or air not properly controlled during cure. Single or isolated large air bubbles are referred to as voids. These are large enough to be of structural significance and can also be individually detected and measured.

Voids and/or porosity may result from trapped air between fibers, the presence of solvents/ moisture or other volatiles, or incorporation of air in the resin during mixing. These defects can occur in all composite materials and are of considerable concern as they can act as local stress concentrations. Voids can cause a reduction in structural performance (i.e. lower transverse and through-thickness tensile, flexural, shear and compression strengths, corrosion resistance and electrical properties), particularly when exposed to service environment (e.g. hot/wet) conditions for long periods. Large voids may be of sufficient size to act as delaminations, resulting in premature failure of the laminate. It is generally accepted that the void or porosity content of a component should not exceed 1-2% for high performance laminates. Figure 44 shows micrographs of voids in laminates. [Gower 2005]

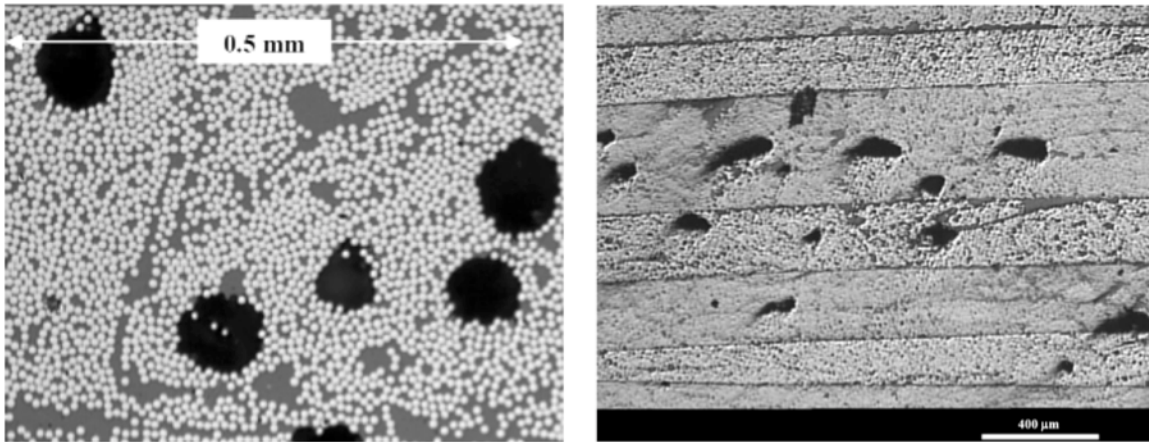


**Figure 44. Micrographs of voids in (left) unidirectional pre-preg and (right) filament wound CFRP materials [Gower 2005]**

### 3. NDE Techniques

This chapter presents a wide variety of NDE techniques that are used to inspect composite laminates in various industries. Most of the techniques are “passive” but some methods excite the structure at frequencies shown in Figure 45. Typically, defects are found when anomalies in recorded responses are noted. In the case of laser shearography, the composite laminate is “actively” stressed.

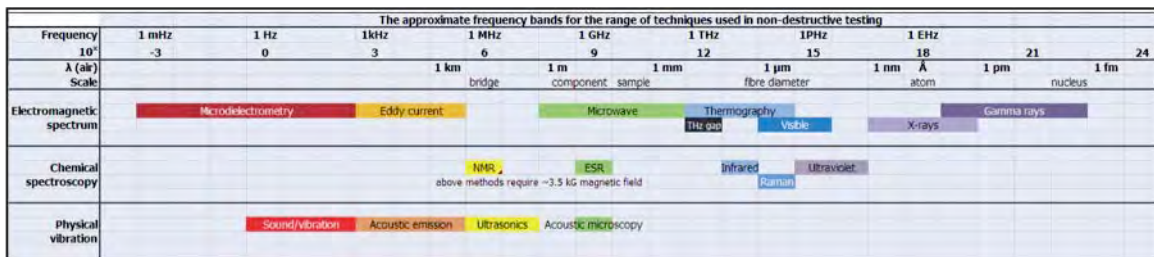


Figure 45. Approximate frequency spectrum for the range of techniques used in NDE. [www.tech.plym.ac.uk/sme/MATS324]

#### 3.1 Visual Inspection

Visual inspection is the most common form of inspection for composites and other structural systems. This is sometimes called “enhanced” or “close visual” inspection if assisted by magnifying glasses, special lighting or other tools. Still or video cameras are commonly used to provide a permanent record of the inspection.

The best quality visual inspection for transparent/translucent composite materials, such as uncoated E-glass laminates, is when access is possible from both sides with backlighting. Under these conditions, internal defects such as delaminations, fabrication defects and cracking may be seen. The effectiveness depends on fiber architecture, laminate thickness, resin type and coating. If access is limited to one side, then only apparent or obvious defects from one side will be seen.

Users often have great confidence in visual inspection, which belies the limited data available on actual reliability. Enhanced visual inspection is widely used where large areas need to be inspected. Identifiable defects include, delamination, cracks, localized (thickness) deformation, impact damage, poor wetting of fibers, inclusion, air entrapments, excessive adhesive in joints (reducing internal diameter), environmental effects (e.g. UV, erosion) and wear damage. However, for laminates that contain carbon fiber, through visual inspection is not possible. [Gower 2005] Visual inspection is usually the primary method used for defect detection, often followed up with more sophisticated NDE techniques to determine the extent of damage.

### 3.2 Tap Testing

There are many different tap-testing devices ranging from a simple coin tap, where the human ear is used to audibly sense damaged structure, to automated methods that make a recording of changes in the sound frequency and amplitude. Tap testing is used for damage inspection of both composites and bonded metallic structures. In general, the tap test works well for inspection of damages in thin skins of any type. The method is especially useful on sandwich structure with thin face-sheets and honeycomb core. It can work on solid composite laminate structure if the first few plies are delaminated, but it cannot reliably detect defects or anomalies deeper in the laminate.

The tap test is often performed with a medium-sized coin, a steel washer approximately 25 mm (1 inch) in diameter, a small tap hammer (shown in Figure 46), or an electronic device, such as the Mitsui Woodpecker WP-632DS. The Woodpecker is connected to a computer that records the sound of a good section of panel and then compares it to subsequent readings in other areas that may be damaged. The aerospace industry has evaluated three similar tap test devices: the Boeing tap hammer; the Wichitech RD3, developed by Boeing and licensed to Wichitech; and the CATT, developed by Iowa State University and licensed to Advanced Structural Imaging, Inc. The CATT has an automatic tapping carriage that eliminates any effects due to a human operator. [Ilcewicz 2009] These devices are illustrated in Figures xx and xx in the Aerospace chapter.

Experiments have been conducted to compare the efficacy of visual and tap testing methods. Studies considered variables such as inspector variation and environmental conditions during inspection. Caution needs to be used before incorporating the Probability of Detection (PoD) from these experiments, into reliability assessment because the inspections were carried out under carefully monitored conditions on flat composite panels. Also, inspectors performing PoD experiments are looking for damage that they know exists. In the field, other factors can influence PoD, such as lighting conditions, structural curvature, inspector training, access to structure, and weather conditions. Therefore, the damage detection probability is expected to be much higher for smaller damage sizes evaluated under controlled, laboratory conditions. [Huang 2005]



**Figure 46. Picture of a military specification tap hammer [Courtesy of Abaris Training Resources Incorporated]**

With tap testing, anomalies in the part are recognized by an experienced tester based on the differences in the characteristic ringing sound obtained. A trained inspector will be able to identify regions of debonding, delamination, and poor cure not necessarily identifiable by visual inspection. Identifiable defects include regions of poor cure, regions of delamination, coating debonding or thickness variations. The method is not well suited to thick components. With manual tap testing, the method is very subjective and limitations include the uniformity of tapping and the variation in backside structure, which can cause the acoustic response to differ. The hearing ability of the operator is also a key factor affecting reliability. Tap testing is still widely used, as it is a relatively low cost option. [Gower 2005]

Figure 47 represents data from a controlled laboratory environment where inspectors had a priori knowledge of defects. [Huang 2005]. This resulted in a PoD that was higher for visual inspection when compared to manual tap hammer techniques.

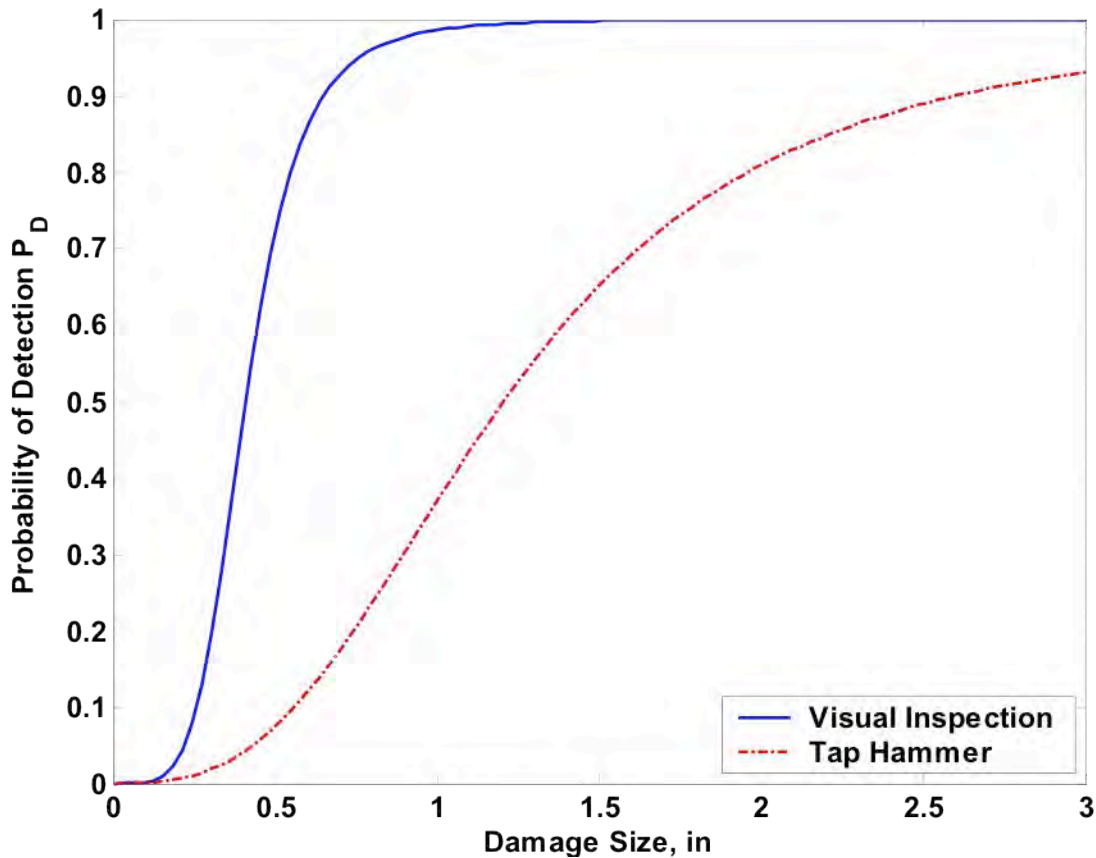


Figure 47. PoD for Visual and Tap Hammer Inspection Methods [Huang 2005]

### **3.3 Ultrasonic Inspection**

Ultrasonic testing (UT) technology has been around for more than 50 years and is the predominant non-destructive testing method for composites in the aviation and aerospace industries. It evolved from sound navigation ranging (SONAR) after World War II. [Gardiner 2010] UT uses high frequency sound energy to locate structural anomalies in composite laminates. A typical UT inspection system consists of a pulser/receiver, a transducer and a display device. The pulser/receiver is an electronic device that can produce a high voltage electrical pulse. Driven by the pulser, the transducer generates high frequency ultrasonic energy. Typical frequencies are in the range of 0.5 MHz to 15 MHz. Sound energy then travels through the structure. A couplant effectively transmits sound through the interface with the composite because sound is not transmitted well through air at frequencies usually employed for non-destructive testing; even a thin air gap between the transducer and the test piece will make typical UT inspection impossible. Discontinuities, such as cracks or delaminations, reflect the energy back from the location of the flaw surface. The reflected wave signal is then transformed into an electrical signal by the transducer and is displayed on a screen. A UT system measures what is called the time-of-flight and the amplitude of the received pulse. This information can be used to determine laminate mechanical properties such as density and elastic moduli. [Ji 1996]

An inspector using ultrasonic methods must interpret any differences found and, therefore, needs a thorough knowledge of the structure being inspected. There are generally two types of ultrasonic inspection:

- Through-transmission ultrasonics (TTU), which uses two transducers (one to send the ultrasonic wave and one to receive it after traveling through the part), is typically limited to the factory because access to both sides of the part is required.
- Pulse-echo (P/E) ultrasonics uses a single transducer and requires access to only one side of the part. This method is more predominant for inspections in the field.

Both TTU and P/E inspection can detect small defects through the thickness of a laminate and debonds between elements or face-sheets and core material. A detailed understanding of the part design features, such as local fiber architecture and internally bonded elements, is essential for determining the extent of damage. [Ilcewicz 2009] The use of calibration samples with known good laminate and defects is essential for interpreting signal traces.

#### Phased Array Systems

Conventional ultrasonic transducers for NDE have either a single active element that both generates and receives high frequency sound waves, or two paired elements, one for transmitting and one for receiving. Phased array probes can have transducer assemblies with from 16 to 256 small individual elements that can each be pulsed separately. The transducer arrays can be arranged in strips (linear array), rings (annular array) or custom configurations. Transducer frequencies are most commonly in the range from 2 MHz to 10 MHz. A phased array system requires computer control that is capable of driving the

multi-element probe. The controller receives and digitizes the returning echoes and plots the information digitally. Phased array systems can sweep a sound beam through a range of refracted angles or along a linear path. They can also focus at a number of different depths, thus increasing both flexibility and capability of UT inspection.

Phased array systems utilize the wave physics principle of phasing, whereby the time between a series of outgoing ultrasonic pulses is varied so the individual wave fronts generated by each element in the array combine with each other to add or cancel energy in predictable ways that effectively steer and shape the sound beam. Figure 48 shows some examples of ultrasonic phased array probe assemblies. [Nelligan 2007]



Figure 48. Typical ultrasonic phased array probe assemblies [Nelligan 2007]

#### A-Scan displays

An A-scan is a simple waveform presentation showing the time and amplitude of an ultrasonic signal and is used for conventional ultrasonic flaw detectors and waveform display thickness gages. An A-scan waveform represents the reflections from a single sound wave location in the test piece. The flaw detector A-scan shown in Figure 49 depicts echoes from two holes drilled into the side of a steel reference block. The columnar sound beam from a common single-element contact transducer intercepts two out of the three of the holes and generates two distinct reflections at different times that are proportional to the depth of the holes. [Nelligan 2007]

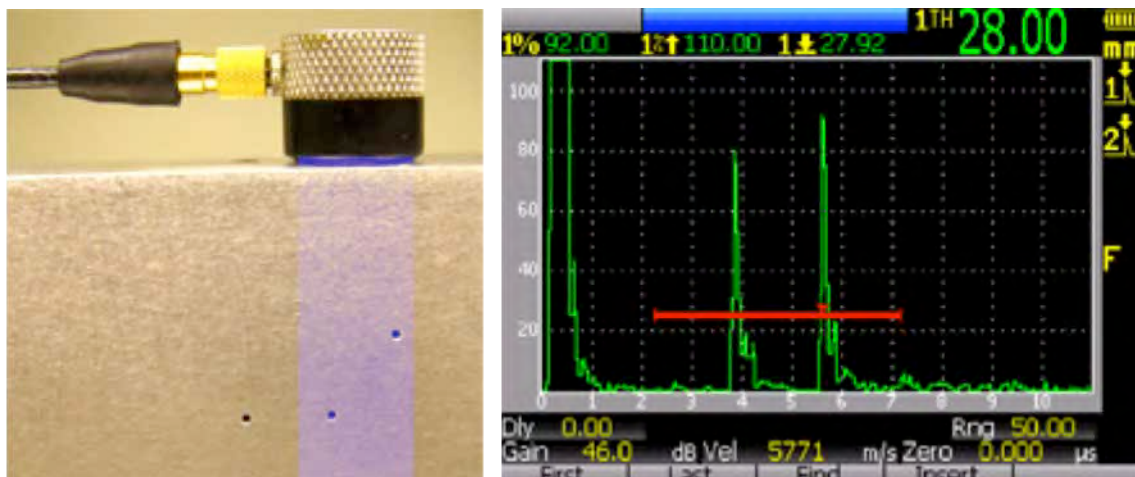
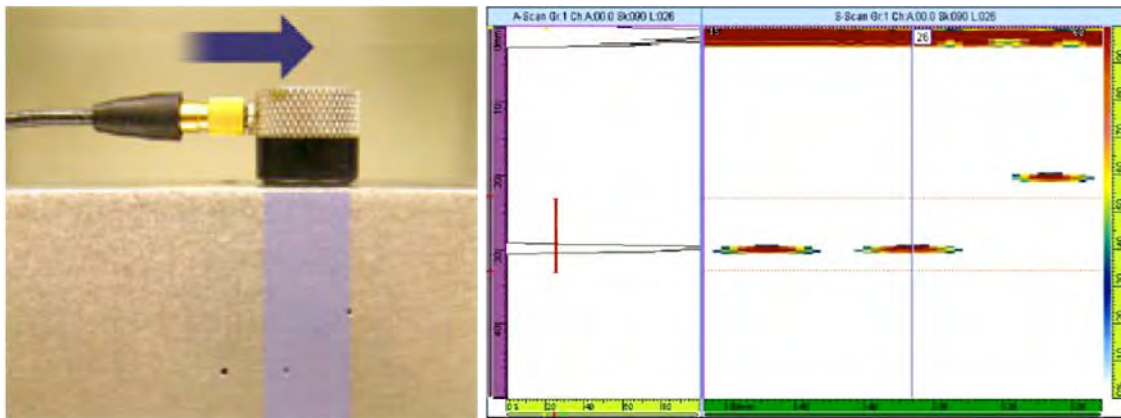


Figure 49. Single-element contact ultrasonic transducer (left) and A-scan image (right) [Nelligan 2007]

B-Scan displays

A B-scan is an image showing a cross-sectional profile through one vertical slice of the test piece, showing the depth of anomalies with respect to their linear position. B-scan imaging requires that the sound beam be scanned along the selected axis of the test piece, either mechanically or electronically, while storing relevant data. In Figure xx, the B-scan shows two deep anomalies and one shallower one, corresponding to the positions of the holes in the test block. With a conventional flaw detector, the transducer must be moved laterally across the test piece. Figure 50 shows the transducer movement necessary for a B-scan and the resulting data image. [Nelligan 2007]



**Figure 50. Ultrasonic transducer scan movement (left) and linear scan B-scan image (right) [Nelligan 2007]**

C-Scan displays

A C-scan is a two dimensional presentation of data displayed as a top or planar view of a test piece, similar in its graphic perspective to an x-ray image, where color represents the gated signal amplitude at each point in the test piece mapped to its x-y position. This type of display is probably the most intuitive to interpret.

A C-scan requires that single-element transducers must be moved in an x-y raster scan pattern over the test piece. With phased array systems, the probe is typically moved physically along one axis while the beam electronically scans along the other. Encoders that indicate precise transducer location are typically used whenever precise geometrical correspondence of the scan image to the structure is required. However, un-encoded manual scans can be useful if the inspected structure is marked as defects are noticed. [Nelligan 2007]

S-Scan displays

An S-scan or sectorial scan image shows a two-dimensional cross-sectional view based on a series of A-scans that have been plotted with respect to time delay and refracted angle. The horizontal axis corresponds to test piece width, and the vertical axis to depth. This is the most common display used for medical sonograms and industrial phased array images but is not as common for NDE applications. The sound beam sweeps through a series of angles to generate an approximately cone-shaped cross-sectional image. Figure 51 shows a portable UT device with combined A-scan and S-scan displays. [Nelligan 2007]



**Figure 51. EPOCH 1000i ultrasonic and phased array flaw detector with simultaneous A-scan and S-scan display [Olympus 2008]**

Ultrasonic Testing Transducers

Transducer frequencies influence the trade-off between penetrating power and defect detection resolution. Higher frequencies tend to provide better resolutions but they also reduce the ability to detect deep flaws. Thick composites require very low frequencies, on the order of 0.5 to 1 MHz, while higher frequencies (10 to 15 MHz) are needed to detect small defects in thin composites. Table 2 provides an overview on the applicability of UT transducers. [Gardiner 2010]

**Table 2. Effect of transducer frequency on UT inspection of composites [Gardiner 2010]**

<b>Frequency</b>	<b>Typical Spot Resolution</b>	<b>Typical Materials</b>	<b>Comments</b>
0.5 MHz	0.31 – 0.39 ins. (8mm – 10mm)	Thick laminates (closer to 1 in./25 mm thick), complex multi-layer composites	Will penetrate almost anything, but resolution is inadequate for many purposes.
5 MHz	0.19 ins. (5 mm)	Thinner solid laminates (0.2 – 0.8 ins/5 mm – 20 mm thick)	Good compromise where max resolution is not required. Can penetrate most materials that are possible to test conventionally.
15 MHz	0.03 – 0.07 ins. (1mm – 2mm)	Solid laminates, single-layer honeycombs	Gives results comparable in resolution to practical production tests.

Laser Induced Ultrasound

Laser ultrasonics is novel technique of transmitting and receiving ultrasonic waves without the need for a couplant. The received signals are evaluated very similar to the pulse-echo technique and parts can easily be scanned from a distance of about 3-4 meters. Laser energy pulses on the order of ten milliseconds cause a rapid heating and expansion of the surface, which forms elastic pulses. The reflected signals are examined using interferometry techniques. The method has been used to inspect structures with complex geometry, allowing examination of surfaces with a slope of up to about  $\pm 45^\circ$ . The limiting factor in scanning speed is the rate that pulses are applied. Sensitivity is fundamentally limited to about 45dB because there is a lower bound on the sensitivity of detecting a single phonon, whereas the upper limit is set by thermal damage prevention. Additionally, the cost and sensitivity of the laser ultrasonic technique make it unsuitable for marine applications. [Bar-Cohen 2000]

### **3.4 X-Radiography (X-Ray)**

Radiography uses localized differences in attenuation under X-ray illumination to provide a cross-sectional picture of the density of a structure. Images are typically recorded on film. Increasingly, digital or real-time recording systems are used. The method is well suited to volumetric defects and to complex components, which might be difficult to inspect by other methods. X-rays do not reveal surface defects. The method is not popular because of health and safety implications associated with the radiation source. However, portable low intensity systems that reduce the associated hazards are becoming available and are being used in the offshore industry.

In composites, X-ray inspection is typically limited to thinner walled laminates. Radiography is sensitive to major changes in density so it is good at checking adhesive joint assemblies. Identifiable defects include voids, delamination, cracks (dependant upon geometry), excesses of adhesive in joints, and improper joint assembly. [Lee 2003]

The use of x-ray on composite parts that are constructed of carbon fiber-reinforced epoxy is difficult because the absorption characteristics of the fibers and resin are similar, which is overall quite low. The properties of E-glass are better suited to the use of x-ray as an inspection method for composites. X-ray is often used to detect moisture ingress in honeycomb core of sandwich parts and is sometimes used to detect transverse cracks in laminates. [Ilcewicz 2009]

### **3.5 Eddy Current**

In eddy current inspection, an electromagnetic coil or arrays of coils are passed over the surface being examined. This induces local eddy currents below the coil, which are sensed by detection coils. The presence of a defect will affect the flow of eddy-currents. By adjusting the frequency, it is possible to move from a surface specific technique to a lower frequency method with good depth penetration that allows inspection of sandwich structures and more complex components and materials systems, such as flexible risers in the offshore industry and concrete structures. The method cannot be used with E-glass laminates, as they are non-conductive. Some success with carbon fiber laminates has been reported. [Lee 2003]

It should be noted that eddy current NDE has very limited use in detecting composite damage and for inspecting repairs for integrity. It is most commonly used to detect cracks emanating from fastener holes in metal structures without removing the fasteners. [Ilcewicz 2009]

### 3.6 Thermography

Infrared thermography measures the variations in heat emitted by an object and displays them into visible images, usually by monitoring infrared emissions using a thermal imaging camera. It is a rapidly developing technology for NDE in many applications. The imaging equipment used for thermography has improved a lot recently, which enables more rapid data acquisition and higher spatial resolution.

Thermography is used to isolate structural anomalies based on very small differences in thermal properties. The component being inspected is typically heated from one side and viewed from either the same side or the opposite side depending on access to the structure and the laminate schedule (marine sandwich laminates have very low through-thickness heat conduction). The heat application must be relatively uniform throughout the area being inspected. Uniform heating is achieved by using hot air guns, heat lamps or flash lamps in a controlled fashion.

The external application of heat creates a thermal gradient within the laminate. The movement of heat energy from the heated surface into the cooler component is a function of the material's thermal diffusivity. Thermal diffusivity is defined as the ratio of a material's thermal conductivity to its thermal capacitance. Heat will diffuse uniformly throughout a laminate until it encounters a discontinuity.

Most flaws are discontinuities having thermal properties that differ from the base material in the composite structure. A delamination, disbond or void will typically have a lower rate of thermal conductivity, resulting in heat being locally trapped in the area containing the discontinuity. The heat buildup transfers to the surface of the laminate, showing the location and approximate size of the discontinuity. High capacitance flaws, such as the ingress of water into the composite structure, result in a cooler surface over the flaw area soon after heat is applied to the surface. [Snell 2007]

Two forms of thermographic inspection methods are currently available: the passive method measures laminate response to an applied transient heat source and the active method monitors response to heating produced by applying a cyclic heat source. [Ilcewicz 2009] The active method is also referred to as pulsed or transient thermography. The rate at which temperature changes take place is often more important than the amplitude of the temperature change which is usually only a few degrees centigrade. [Gower 2005]

With pulsed thermography, the laminate is heated for few seconds and the thermal decay response at the surface is measured by an infrared camera. Defect detectability strongly depends on the temperature contrast between the defect and good areas of the structure. Temperature contrast is a function of defect features, such as area, depth and orientation. The time-dependent surface temperature response to an instantaneous heat pulse reveals a characteristic linear profile with slope  $-0.5$  when plotted on a natural logarithm scale, as shown in Figure 52.

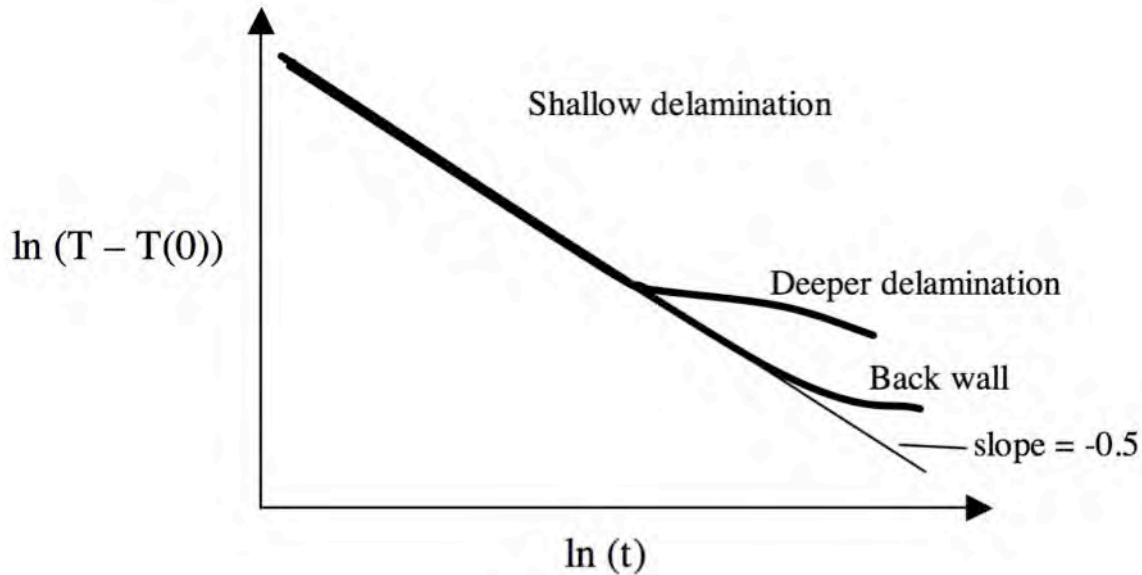


**Figure 52. Logarithmic time evolution of surface temperature is shown. Temperature decay is linear with slope  $-0.5$  until heat flow is obstructed by a subsurface defect or a boundary such as a wall. [Shepard 2005]**

Pulsed thermography works best where the diameter of a defect is greater than its depth beneath the surface. As the defect aspect ratio approaches unity or less, the maximum temperature difference between a defect and the surrounding intact areas decreases, often to level comparable to the noise level of the IR camera. This type of defect requires additional signal processing for detection. [Shepard 2004]

A form of signal processing called Thermographic Signal Reconstruction (TSR) was developed to improve the sensitivity and range of thermography NDE. TSR takes the time and temperature history of each pixel and converts it into a set of equations for advanced mathematical calculations in order to identify defects that are otherwise undetectable, vague or blurry. Because TSR is compiling images taken from first and second derivatives of time/temperature data, physical features that do not appear or are masked by reflections in the raw image are typically shown prominently in the TSR-converted display. [Shepard 2004]

Thermography requires developing a baseline of readings on an identical, undamaged laminate. This can be obtained by shooting the structure in an area away from the known or suspected damage that is indicative of the laminate being examined. TSR technology does not rely solely on display contrast and therefore damage detection is possible without a reference baseline. [Gardiner 2010]

A thermography technique that combines the advantages of both lock-in and pulse thermography is pulse phase thermography. Here, the specimen is pulse heated and frequencies of the applied thermal waves are unscrambled by computing the Fourier transform of the temperature evolution over the field of view. The phase, or magnitude, image can be presented as in modulated lock-in thermography. [Montanini 2010]

### **3.7 Moisture Meters**

These devices are often used to survey yacht hulls during surveys. This can be problematic with boats recently hauled out of the water for the purposes of a survey. Indeed, some surveyors will limit their use to topside structure only.

Most moisture meters rely on radio frequency dielectric power loss to detect moisture, which is attributed to an increase in the conductivity of the composite due to moisture absorption. However, these devices won't work with carbon fiber laminates, as the carbon fibers are electrically conductive. Therefore, contact type moisture meters can only be used on structural components that do not contain carbon fibers. Caution must also be exercised with panels that contain buried metallic doublers. These doublers will give a false indication of moisture and may cause a panel to be removed needlessly.

Digital (microwave) moisture meters used in the aerospace industry can correct readings for the density of the material. This is the most accurate system known, as the measurement enables the density to be calculated and accounted for in the readings. [Ilcewicz 2009]

### **3.8 Bond Testers**

These NDE instruments are based on mechanical impedance measurements. Bond testers are typically used to detect composite delaminations and adhesive debonds in thin laminates. Bond testers are very portable and well suited for inspection of face-sheet core separation in sandwich structures when small anomalies are not considered to be important and the laminate is fairly uniform. [Ilcewicz 2009] Gross defects, such as widespread environmental degradation and skin-to-core disbonds in sandwich structure, produce readily measurable changes in resonant frequencies. Therefore, baseline readings on known intact structure are essential.

### **3.9 Laser Shearography**

Laser shearography is an emerging NDE technology for detection of delaminations, debonding, poor adhesion and other flaws in composite materials systems. Recent development is a result of portable lasers and innovation in data processing, including phase analysis. The method can also indicate areas of reduced or increased adhesion, not simply the presence of a delamination. The main limitation of the technique is accessibility to the surface being inspected and equipment cost.

Laser shearography uses a scanning laser system to determine the surface strain fields from the difference in displacements between unloaded and loaded structure. Because laser shearography systems can detect surface changes on the order of one nanometer, the applied load does not have to be very large. It can be applied to the sample by mechanical loading, vacuum loading, heating or internal pressurization. Table 3 provides an overview of which stress methods are best for observing specific defects.

**Table 3. Shearography stress method applicability [Gardiner 2010]**

<b>Stress Method</b>	<b>Defects Detected</b>
Thermal	Impact damage, delamination, disbands in core splices
Vacuum	Disbonds in honeycomb and foam, core damage, disbands in core splices
Vibration	Disbonds in metal honeycomb structures, delamination in solid laminates
Pressure	Impact damage, delamination in filament-wound pressure vessels

The principle of shearography employs a single expanded beam of laser light, which is reflected back from the inspected structure. The camera includes an image-shearing device. The effect of shearing is to bring two separate areas on the object surface to meet at the image plane of the camera. The two overlapped areas of the sheared images interfere and produce what is called a speckle pattern. When the surface of the object is deformed, the speckle pattern is modified. Comparing the stressed and unstressed speckle patterns produces a fringe pattern, which depicts the relative displacement of the surface. Since the magnitude of shearing is small, the fringe pattern approximately represents the derivative of displacement, which is the strain of the surface. [Gower 2005]

Shearography has seen dramatic performance improvements in the last decade and greater acceptance as a means for high-speed, cost effective inspection and manufacturing process control. These performance gains have been made possible by the development of the personal computer, high resolution CCD and digital video cameras, high performance solid-state lasers and the development of phase stepping algorithms. System output images can now show structural features, surface and subsurface anomalies, and quantitative data, such as defect size, area, depth, material deformation vs. load change and material properties.

Shearography cameras generally use a Michelson type interferometer with two essential modifications. First, one mirror may be precisely tilted to induce an offset, or sheared image, of the inspected structure with respect to a second image. The sheared amount is a vector with an angle and a displacement value. The shear vector determines the sensitivity of the interferometer to surface displacement derivatives. Figure 53 illustrates the shearography principal and a portable shearography device. [Newman 2009]

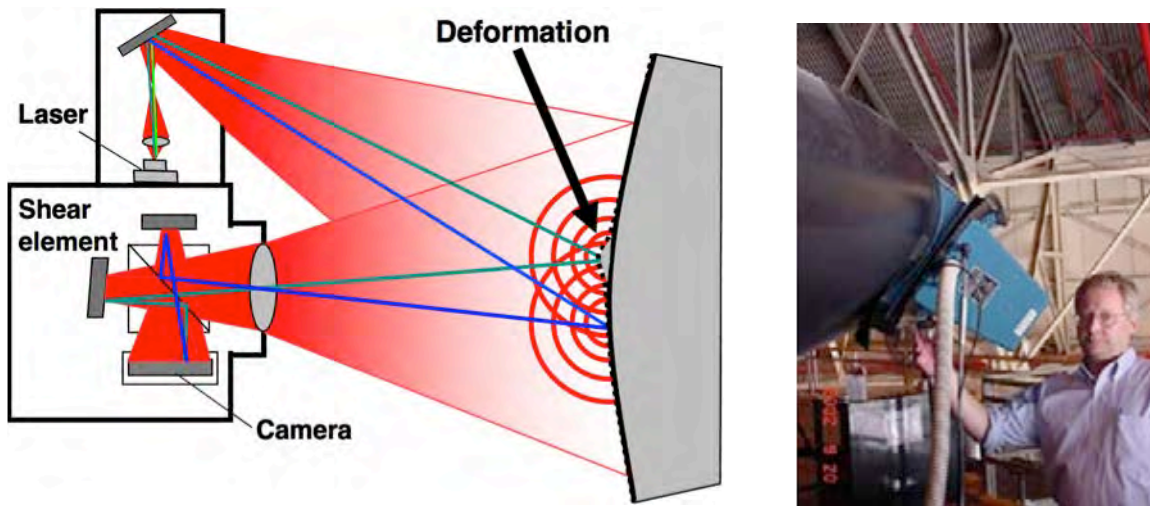


**Figure 53. Shearography principal [Collrep 2006] and portable shearography device [Newman 2009]**

### 3.10 Electron Probe Imaging

An electron microprobe is an instrument that bombards a small sample with a beam of high-energy electrons. Specimens usually are polished (especially for quantitative analysis) and must be coated with a thin film of carbon or metal to prevent the buildup of an electrical charge. Long and tedious preparation is often required for image samples with conventional light microscopy methods, and although secondary electron imaging (SEI) provides high resolution images of surface topography, the distinct components of a multi-component sample are not always discernable. Needless to say, this technique is not appropriate for in-the-field inspections of large marine structures.

Another laboratory-scale NDE process is called backscattered electron imaging (BEI). BEI shows the elemental composition variation and surface topography of a sample. Backscattered electrons are produced by the elastic interactions between the sample and the incident electron beam. These high-energy electrons can escape from much deeper than secondary electrons, so surface topography is not as accurately resolved. The number of backscattered electrons that re-emerge from within the sample is controlled by the number of collisions, which take place in the sample, which is in turn controlled by the atomic number of the components in the sample. The greater the atomic number of the sample contents, the greater the backscattered electron yield. Therefore, the image obtained from the collected backscattered electrons is essentially an atomic number contrast image. [Herzoga 2004]

### **3.11 Modal Methods**

Modal analysis involves the identification of the modal parameters of a structure in order to characterize its dynamic behavior. These modal parameters include the structure's resonant frequencies, damping ratios and mode shapes. The mode shapes represent the physical displacement of the structure at a particular resonant frequency or mode. Together, these quantities make a unique "modal model" of the structure, which describes its dynamic behavior and as such represents the inertial and stiffness properties of the structure.

The modal parameters can be obtained through dynamic analysis of a mathematical model or through vibration testing of the physical structure. To determine a structure's natural frequencies using physical testing, the structure is dynamically loaded with a shaker that is "swept" through a frequency range. Peak amplitudes in structural response correspond to natural frequencies. Traditional applications of the modal analysis approach have been to:

- Use the results of a modal test to verify and adjust a finite element model.
- Produce a mathematical model of the structure to predict the effects of structural modifications.
- Estimate the forces a structure experiences in operation through measurement of the response of the unknown forces and a mathematical description of the transfer function. [Matthews 1995]

To use modal analysis as an NDE tool, structures can be excited by ambient energy, an external shaker or embedded actuators. Embedded strain gauges, piezos or accelerometers are then used to monitor the structural dynamic response. Changes in normal vibrational modes can be correlated to loss of stiffness in a structure. Typically, analytical models or experimentally determined response-history tables are used to predict the corresponding location of damage. Interpretation of the data collected is often subjective without a detailed model of the structure. There are also detection limitations imposed by the resolution and range of the individual sensors chosen. Fidelity increases with the number of sensors mounted on the structure, but this is often cost-constrained. To illustrate the subtlety of data interpretation, Figure 54 displays the velocity magnitude response to a frequency range below 500 Hz for tested specimens. [Kessler 2001]

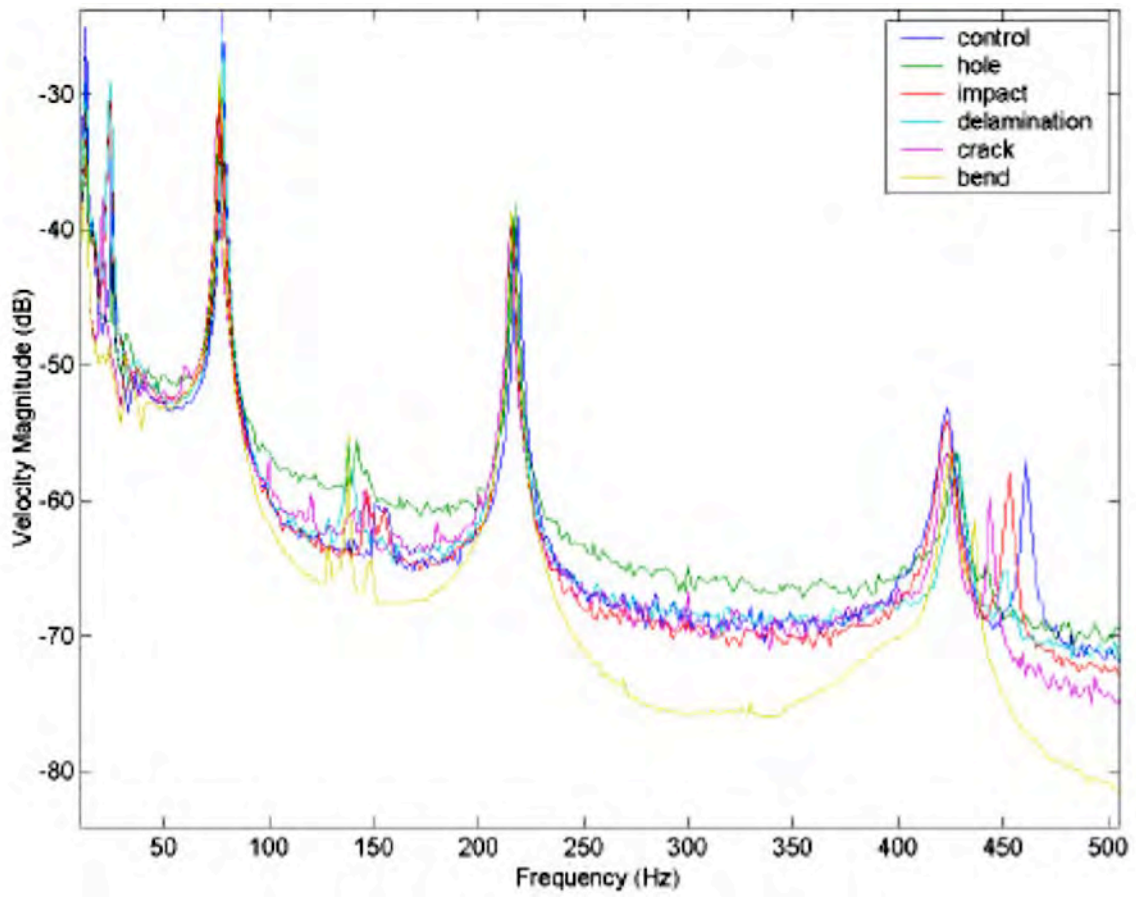


**Figure 54. Frequency response plot from vibrometer for all specimens, range of 0-500 Hz [Kessler 2001]**

### 3.12 Structural Integrity and Damage Evaluation and Damage Evaluation Routine (SIDER)

SIDER is a vibration-based inspection method that uses vibration waves that are totally invasive but not intrusive. The structure is excited at a mesh of test points (see Figure 55) and the acceleration response is measured at a few locations. Data is reduced to generate a contour map of structural stiffness irregularity. SIDER is designed for the rapid inspection of structures with large surface areas. A single inspection finds areas where there is structural variation/inconsistency associated with a localized change in stiffness. These are places with designed (deliberate) stiffness changes, manufacturing anomalies, and service-related damage. SIDER results are typically used to focus the attention of more detailed (but time consuming) inspections, e.g., UT and laser shearography. [Ratcliffe 2001] SIDER is a relatively new NDE technique that has only been conducted by the system developers and requires a carefully-trained analyst to interpret the nuanced inspection results.



**Figure 55. An instrumented hammer is used to excite a composite destroyer rudder during SIDER examination [author photo]**

### **3.13 Acoustic Emission**

Acoustic emission NDE works on the principle that regions of discontinuous composition tend to experience some form of stress concentration when loaded. In these regions energy is stored in form of a high local stress field. In composites, these stress concentrations can reach levels as high as nine times the average full-field stress. When the material cracks at internal discontinuities, a new surface is formed and the stored elastic energy is released in the form of heat and a short pulse of elastic and kinetic energy that travels from the defect and disperses into the material. This energy release is accompanied with an acoustic emission. [Hellier 2001]

Acoustic emission NDE uses sensors to monitor such emissions and determine medium to large-scale defects in composites, which would generally have structural integrity and/or strength implications. Transducers typically work within the range between 100 kHz and 30 MHz, depending on the test material. Acoustic emission can be used on whole systems and works by picking up stress waves generated by inelastic deformation. As an NDE tool, acoustic emission identifies changes in systems by comparison rather than an absolute value. Identifiable defects include delamination growth, large strains, crack growth, and fiber fracture. Acoustic emission historically had difficulty in application to large structures and false calls. [Lee 2003]

#### 4. Aerospace Damage and Repair Inspection Procedures

Methods used in the field for aerospace composite part damage detection, damage characterization, and post-repair inspection are typically less sophisticated than those employed by the OEM for their post-processing inspection. Operators and maintenance organizations use visual inspection as their main technique for initial detection of field damages, unless NDE techniques are specified by the specific maintenance planning manual or aircraft maintenance manual. Once damage is detected visually, other NDE methods are typically used to map the full extent of damage for proper disposition.

In addition to the use of visual inspection to first detect damage, more sophisticated NDE methods are essential to the subsequent damage disposition and repair processes. Many types of damage have both visual and hidden damages. Hidden damage in composites usually covers a larger area than visual indications of damage is most responsible for lost residual strength. It is essential that the proper NDE methods be applied to damage found on aerospace composite structure to map the full extent of the damage, which is needed to determine whether damage is below the Allowable Damage Limit (see Figure 56) or whether repairs are required. Since a disposition of repair size limits also depends on accurate mapping, decisions on whether the repair substantiation database is sufficient also relies on a complete inspection with the proper NDE. [Ilcewicz 2009]

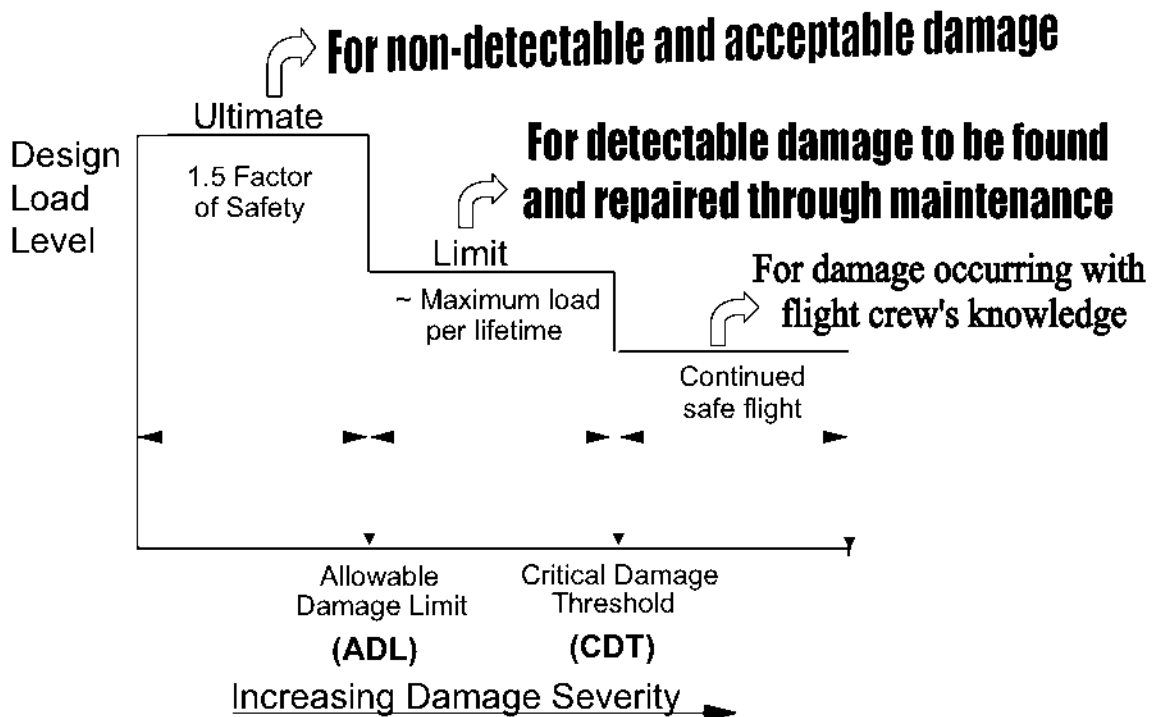
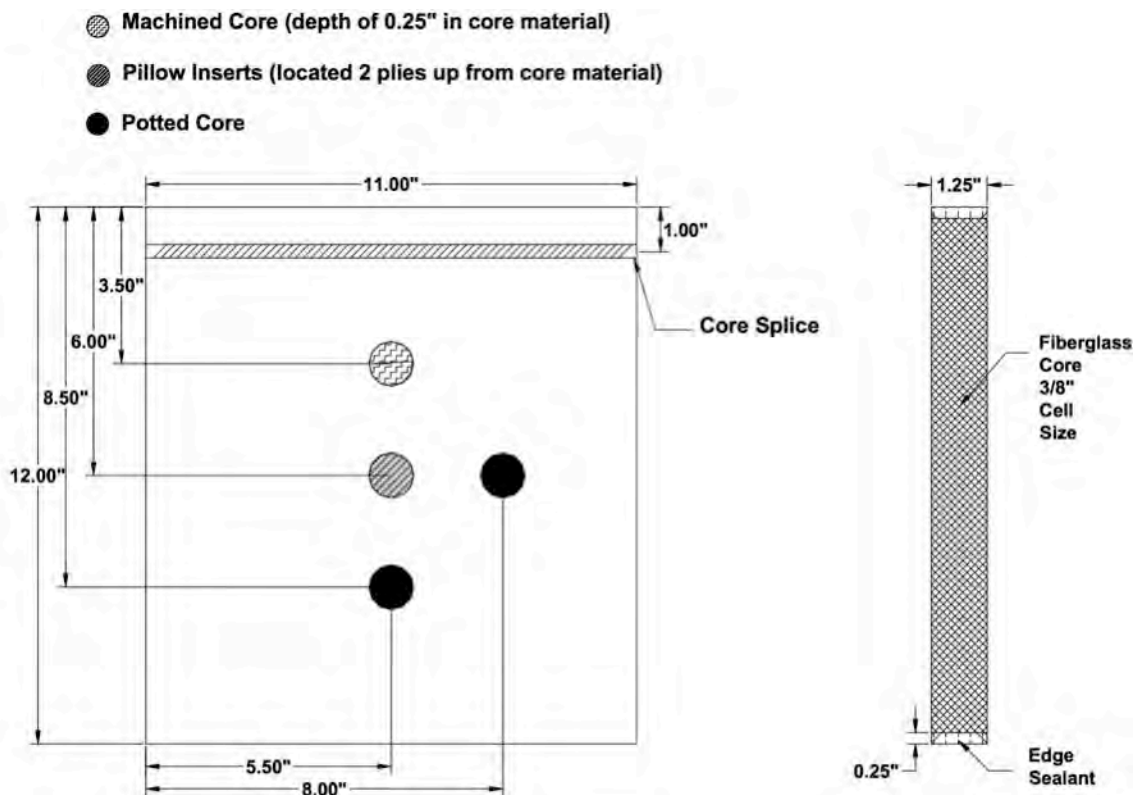


Figure 56. Aerospace structural design load and damage considerations [Ilcewicz 2009]

Accurate NDE methods are considered a necessity to ensure aircraft airworthiness and passenger safety. Traditionally, tap tests and a few ultrasonic-based inspection methods have been used to inspect composite aircraft structures. [Roach, 2008]

A test program, called Composite Flaw Detection Experiments, was undertaken at the Federal Aviation Administration (FAA) Airworthiness Assurance NDI Validation Center (AANC), operated by Sandia National Laboratories. A large number of test panels, representing the bounding conditions of construction on aircraft, were inspected using a wide array of NDE techniques.

Forty-four Nomex honeycomb core panels with either carbon/epoxy or fiberglass/epoxy skins were manufactured, with flaws ranging from 0.2 in<sup>2</sup> to 3 in<sup>2</sup> (1.29 cm<sup>2</sup> to 19.35 cm<sup>2</sup>). Figure 57 shows the configuration of honeycomb panels with imbedded flaws. The panels were shipped to airlines, third-party maintenance depots, aircraft manufacturers and NDE developer labs around the world. Industry-wide data was generated to quantify how well current inspection techniques are able to reliably find flaws in composite honeycomb structure. [Roach, 2010] The program developed Probability of Detection (PoD) curves for various laminates and NDE techniques. Figures 59 through 63 show some results from the “round-robin” study. Figure 64 shows some of the NDE devices used during the study.



**Figure 57. Schematic of a reference standard used for NDE of honeycomb-cored panels [Tomblin 2004]**

The honeycomb-cored reference panel shown in Figure 57 has been incorporated into SAE International’s Aerospace Recommended Practice 5606, “Composite Honeycomb

NDI Reference Standards,” September 2001. A companion document for solid laminates published at the same time, Aerospace Recommended Practice 5605, “Solid Composite Laminate NDI Reference Standards,” uses reference laminates shown in Figure 58.

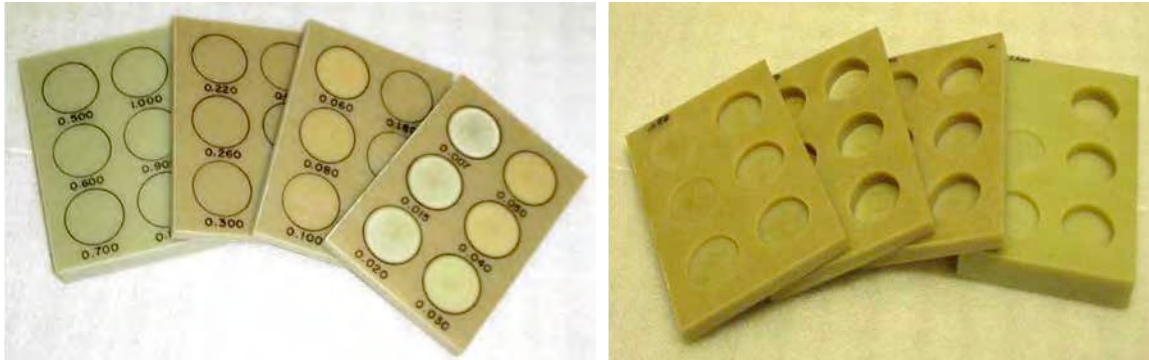


Figure 58. Reference standard used for NDE of solid laminates [Galella 2006]

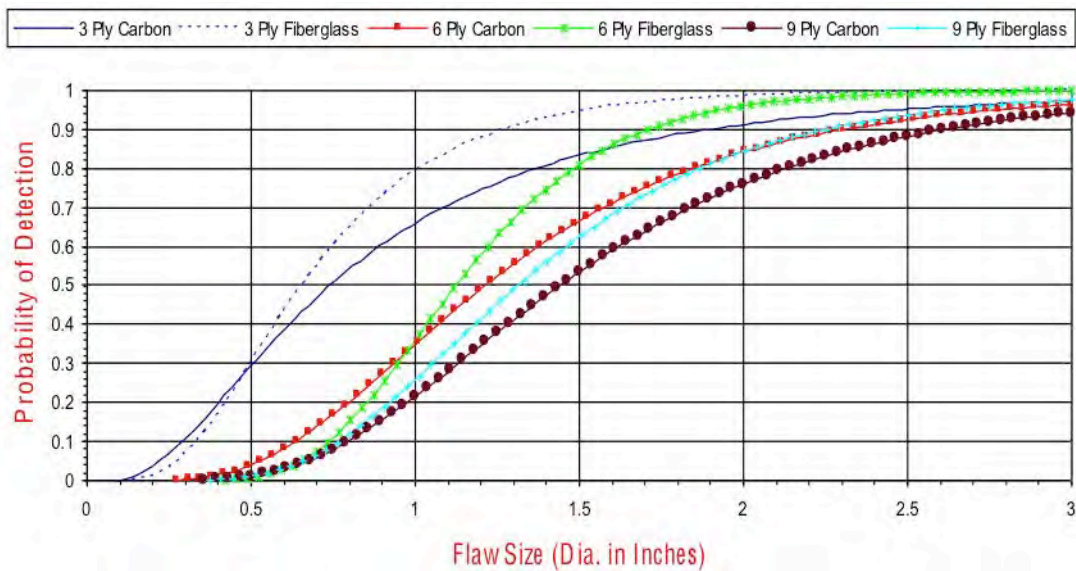


Figure 59. Probability of Detection (PoD) versus flaw size (diameter in inches) for composite sandwich panels with various skin architectures [Roach, 2008]

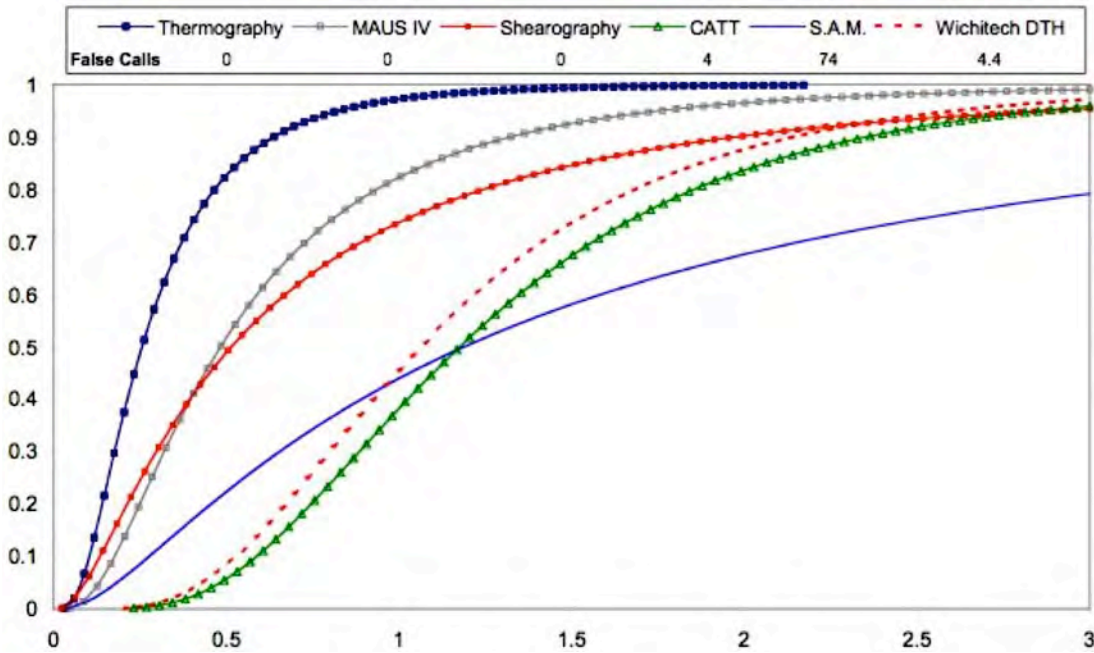


Figure 60. Probability of Detection (PoD) versus flaw size (diameter in inches) for a 9-ply carbon fiber-reinforced composite sandwich panel [Roach, 2008]

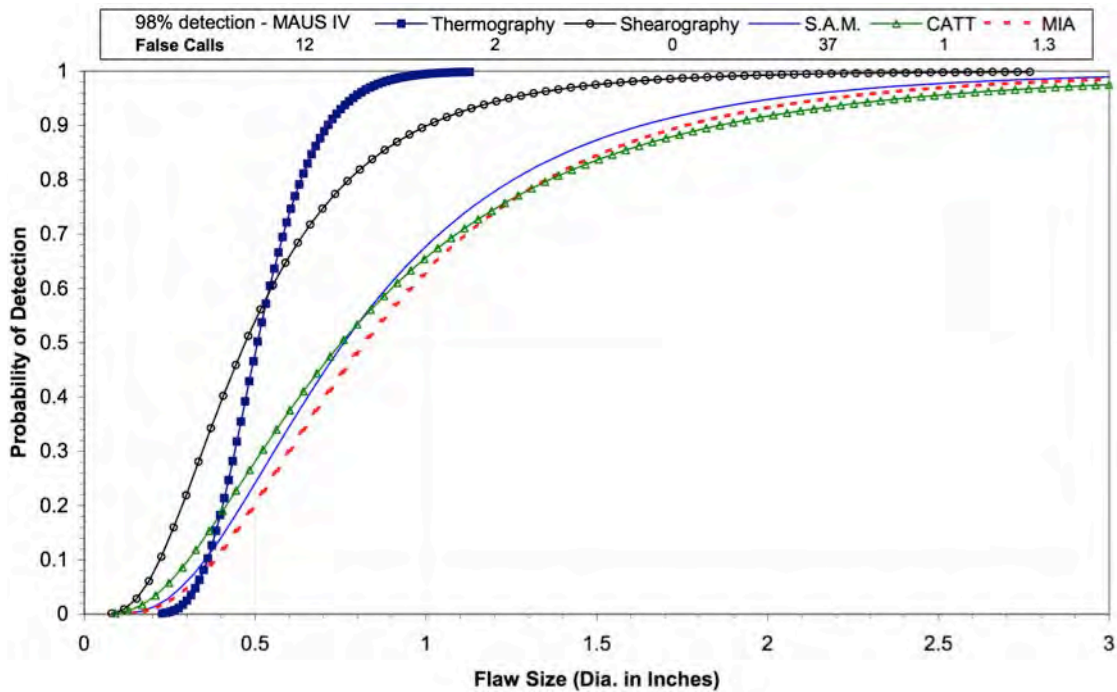


Figure 61. Comparison of advanced inspection techniques with best conventional NDE results on 6 Ply carbon [Galella 2006]

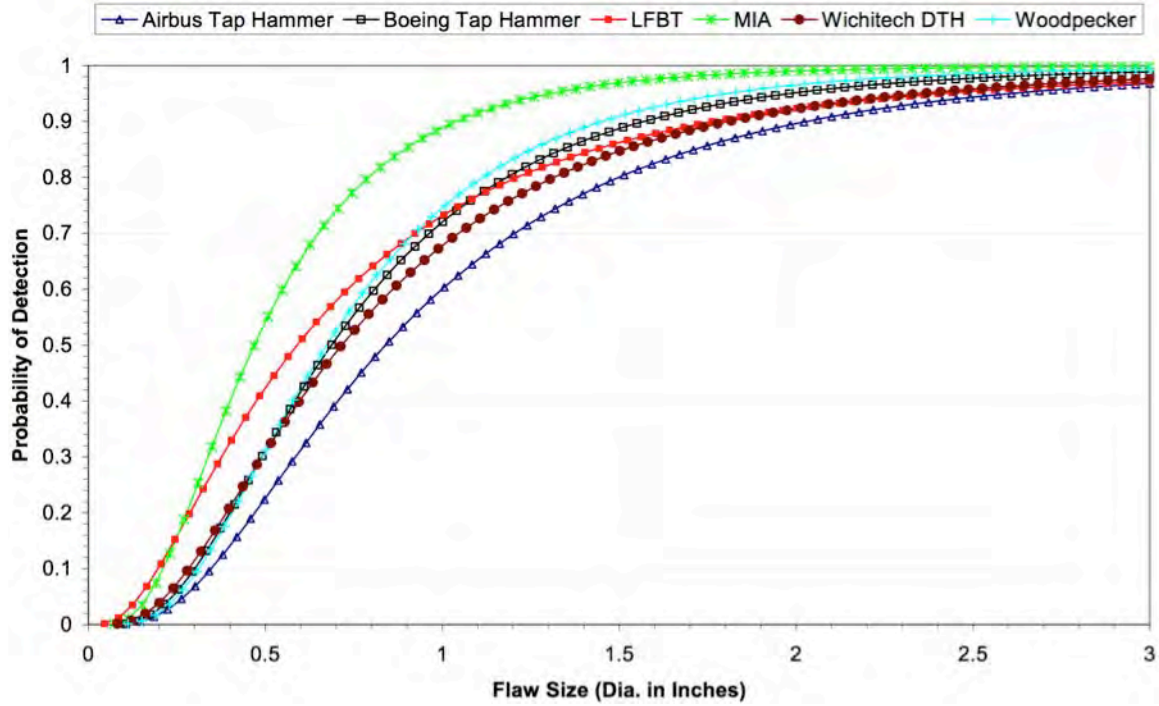


Figure 62. Cumulative PoD of all conventional NDE devices for 3 ply fiberglass honeycomb panels[Galella 2006]

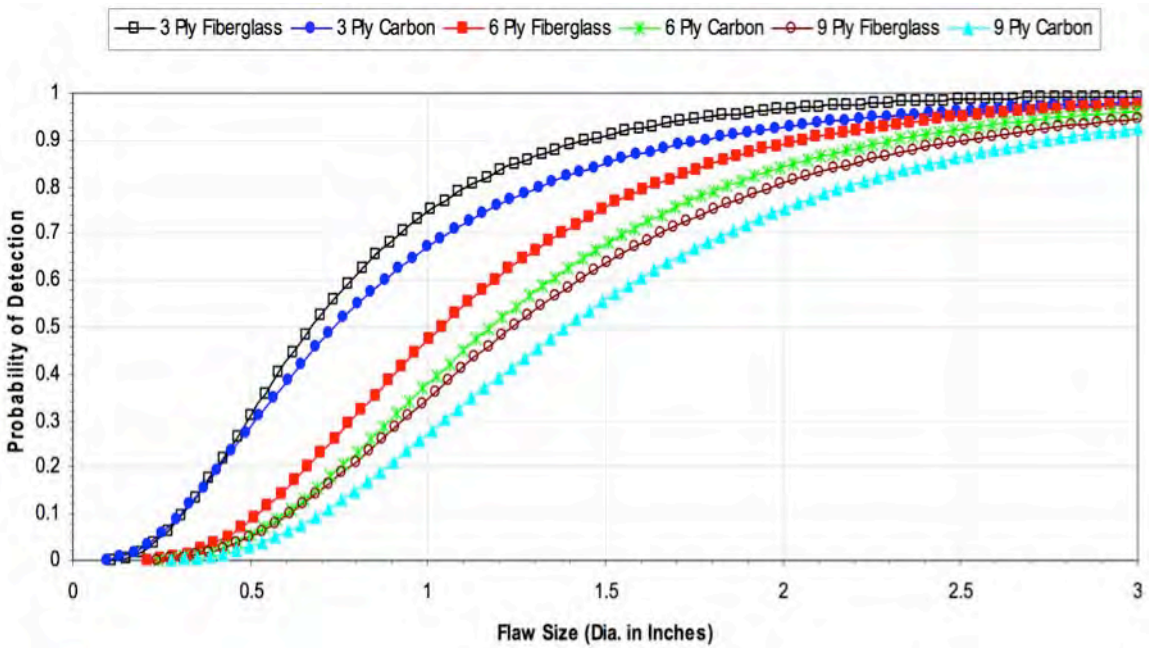
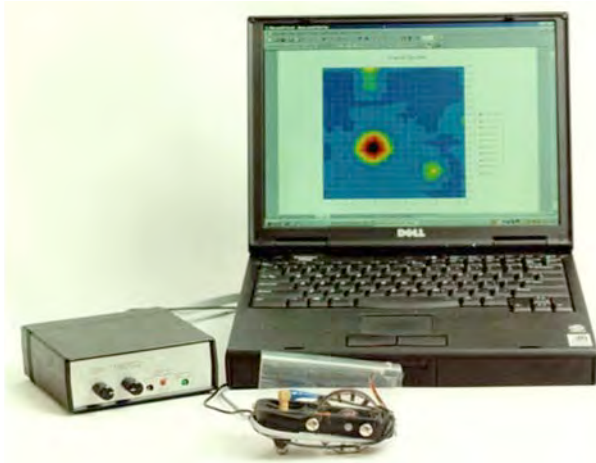


Figure 63. Cumulative PoD for Woodpecker device for all honeycomb panel types tested [Galella 2006]



**Computer Aided Tap Tester (CATT)**



**Mobile Automated Scanner (MAUS IV) UT C-scan or Low-Frequency Bond Tests (LFBT)**



**Wichitech Digital Tap Hammer (DTH)**



**Mechanical Impedance Analysis (MIA) V-95 Device**

**Figure 64. Some NDE devices evaluated during the FAA's composite flaw detection experiments [Tomblin 2004 and Galella 2006]**

Aerospace composite NDE technology can be adequate for the characterization of defects like pores, delamination or debonding within adhesive bonds but not able to ensure the detection of a weak bond ('kissing bond') and, by extension, ensure the quality of an adhesive bond. This lack remains the major issue set against a wider application of the adhesive bonding technology. Shearography and Active Thermography are reported as methods with high potential for the measurements of adhesive bond strength [Ehrhart, 2010]

Porosity in aerospace composites may degrade the stiffness of the structure. Porosity has to be detected therefore in production. At Airbus Germany the requirement is that 2.5% volume porosity is the maximum allowed. An ultrasonic testing method has been developed and qualified to detect porous areas in carbon fiber laminates. In porous areas often no intermediate echo occurs, because pores may scatter the incident sound in all directions. It has been shown that there is a good correlation between backwall echo reduction and volume porosity, as determined by micrographic analysis, see Figure 65." [Schnars 2006]

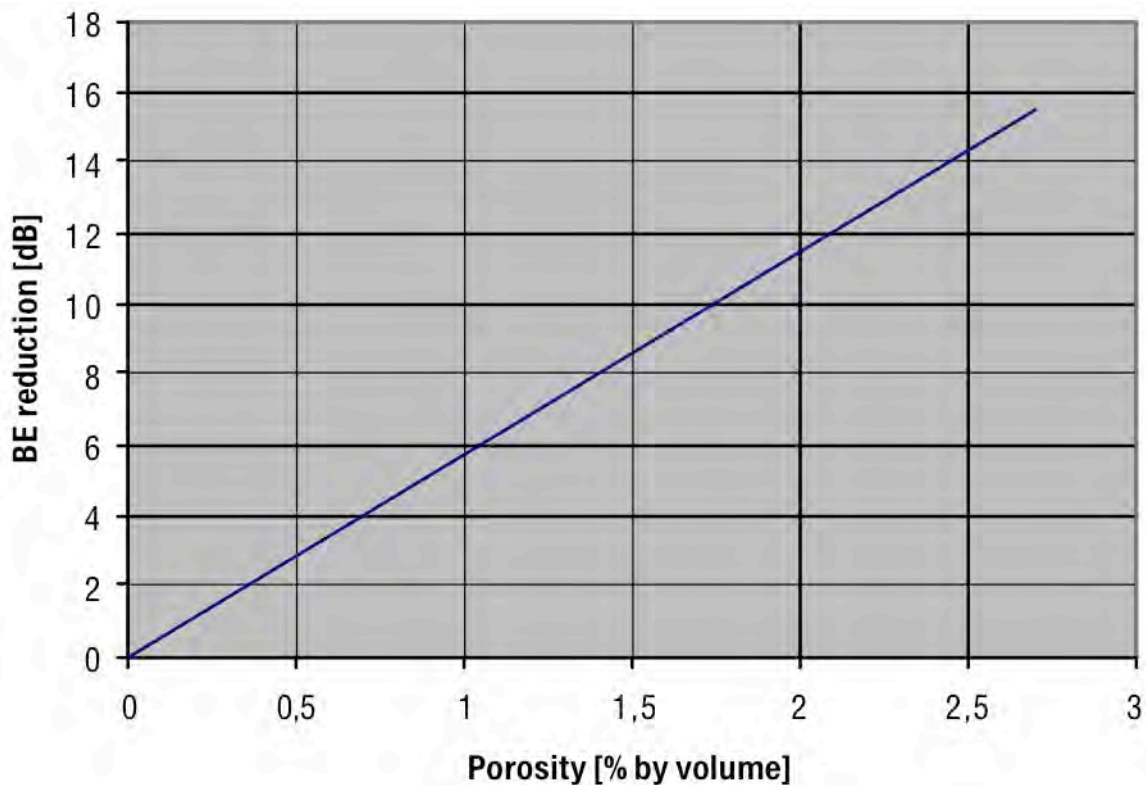


**Figure 65. Ultrasonic backwall echo reduction versus volume porosity**  
[Schnars 2006]

Ultrasonic phased array (PA) NDE systems can produce any desired wavefront electronically. PA techniques can be used to tilt and focus a sound beam for electronic scanning of a sound beam. Another advantage with respect to single element transducers is the availability of display images (B-scan, C-scan, S-scan) instead of only A-scans, which allows better interpretation of signals inside complex structures. An example of PA inspection of a bonded aircraft stringer is shown in Figure 66. [Schnars 2006]

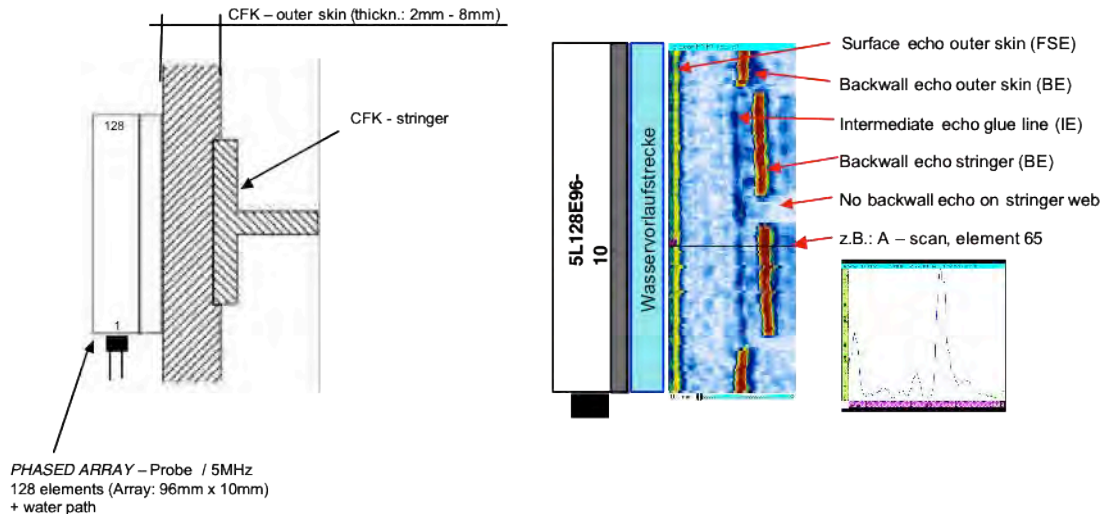


**Figure 66. Phased array inspection of stringer skin bonding [Schnars 2006]**

While in service, aerospace composite structures may suffer damage from a number of natural and man-made causes. For both solid laminates and sandwich structures, the most significant damage is caused by mechanical impact. Lower velocity impacts on composites often lead to non-visual damage on the surface but significant damage internally. Impact damage can result from dropped tools or from collision with ground handling equipment. Bird strikes in flight can cause considerable damage to the radome on to the wing leading edge. [Hsu 2008]

The inspection requirements recommended by aircraft manufacturers and required by aviation regulatory agencies have rarely gone beyond visual inspection and manual tap testing. Considering the large size of aircraft structures, it is not practical, nor is it necessary to conduct large area inspection scans without a clear cause justified by prior incidences. In exceptional cases, advanced NDE beyond that of visual inspection and tap testing have been recommended for primary composite structures. A recent example was the repetitive ultrasonic inspection and other checks recommended for the composite rudders on Airbus A300/310 reported in the news media. [Pasztor 2006] However, as the use of composite increases, especially in the next generation of airplanes, there will be a greater need for NDE procedures for quality assurance by the manufacturers. [Hsu 2008]

“The Australian Defence Force (ADF) has recently acquired a fleet of Multi Role Helicopters. While ballistic impact damage in battle is the most obvious and extreme threat, peacetime operation also includes a range of hazards. For example, helicopter

rotor wash can cause ground debris to impact various parts of the aircraft. Other impacts might occur in the course of normal maintenance where bumps, knocks and dropped tools are inevitable. Impact by hail is another potential source of damage. Although a number of NDE techniques are known to be effective for thin laminates, infrared thermography holds particular appeal for aerospace composite structure because it is faster than over most other techniques. [Rajic 2010]

To validate Flash Thermography (FT) as a valid NDE method for helicopter structure, a test sample was manufactured by bonding a 3 mm thick carbon-epoxy laminate to aluminum honeycomb core with a 3/16" (5 mm) cell size. Varying amounts of water were injected into clusters of cells arranged as shown in Figure 67. The defect was detectable for all of the considered cases, including the 5% fill volume in a single cell, suggesting a detection threshold near that level. [Rajic 2010]

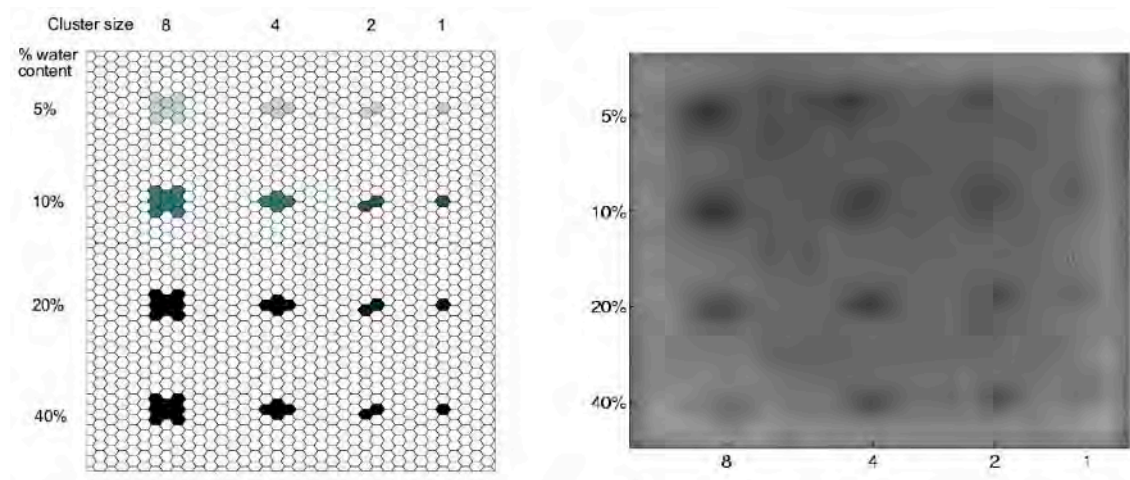


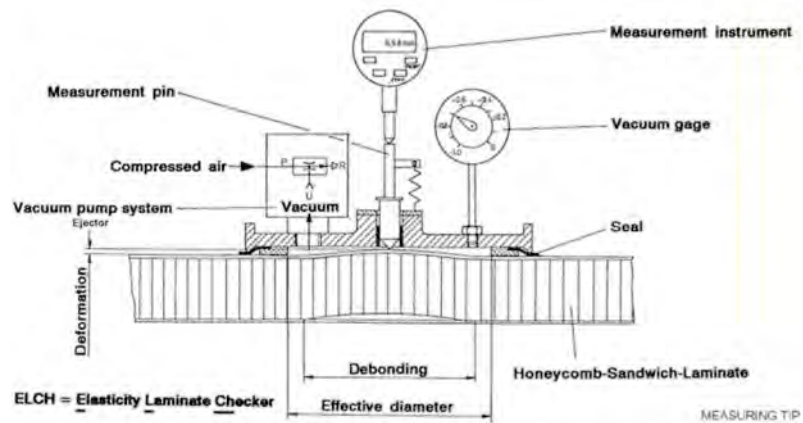
**Figure 67. Schematic (left) showing layout of entrapped water in a honeycomb panel, and a processed thermographic image (right) [Rajic 2010]**

Recent in-service occurrences triggered Airbus to increase the number of in-service NDE methods to inspect honeycomb sandwich structures. The introduction of scheduled health checks for some sandwich structures (control surfaces) necessitated large area inspections. This motivated Airbus to develop a set of procedures to perform those inspections. [Bisle 2010]

Airbus evaluated various NDE methods, some of which are illustrated in Figure 68. An extensive PoD exercise was done, that gives a clear view about the capabilities NDE procedures. Figure 69 provides an overview of the Airbus assessment of various NDE methods.



Mitsui Woodpecker



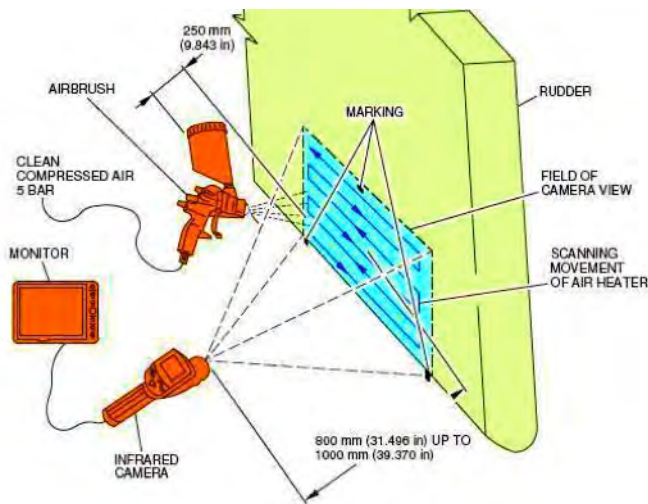
Elastic Laminate Checker (ELCH)



BondMaster 1000



Ultrasonic Tester



Thermography Evaluation Arrangement



Shearography Evaluation Arrangement

Figure 68. Various NDE technologies evaluated by Airbus [Bisle 2010]

	Test procedure	Outer skin Bonding	Inner Skin Bonding	Fluid	Estimated Insp. Time	Flaw size	Training	Remarks – Availability - Advantages – Constrains
FIT (field inspection technology)	Tap Test / Woodpecker	Green	Red	Red	4h 3h	25 mm 50 mm	No	• High human factor!
	ELCH	Green	Green	Red	2x4 h (2 Operators)	100mm	No / Introduction	• Simple, reliable, qualified • Development for improvement: OPTO-ELCH
	BONDMASTER	no procedure	no procedure	Red	2x8h (2 Operators)	25mm	UT II + Special course	• Portable, reliable • Competing with UT
	Ultrasonic	Green	Green	Green	48h	25mm	UT II +	• Procedure available • Equipment common • Not for large areas
	X-Ray	Red	Red	Green	4-8h	1 cell	RT II	• Everywhere available • Safety?
	Thermography	Red	Red	Green	4-h	1-3 cells	IRT Level I limited	• Relatively Cheap • Small and highly portable • Easy to use
Close to FIT	OptoELCH	In Development	In Development	Red	2x4 h (2 Operators)	25mm	Introduction	• Simple, reliable, compact, cheap
	Shearography	With Adaption Possible	too expensive	In Development	16h	25mm	SH II No course avail.	• Expensive/bulky • No quantitative deformation indication • Missing inspector certification scheme

■ Applicability Verified   
 ■ In Development   
 ■ Potential   
 ■ Not Applicable  
 With Adaption Possible

Figure 69. Comparison of the effectiveness of NDE techniques for honeycomb sandwich structures by Airbus [Bisle 2010]

Most processing anomalies that are allowed to enter the aerospace composites field are much smaller than damage considered from service. This is a result of more advanced NDE procedures used in the factory.

There are many types of composite defects and damage that can arise to aircraft composite structure in the field. Field damages can result from (1) dropped tools, (2) service vehicle, jetway, or work-stand collisions, (3) aircraft-handling accidents, (4) dropped parts, (5) improperly installed fasteners, (6) bird strikes, (7) foreign object impacts (e.g., runway debris), (8) overheating, (9) fluid contamination, (10) flight overloads, and (11) sonic fatigue. [Ilcewicz 2009]

## **5. Wind Turbine Blades**

Wind turbine blades are almost exclusively built using traditional composite construction methods. Typical manufacturing defects that are found in wind turbine blades include:

- Porosity
- Debonding
- Delaminations
- Improper Matrix Distribution
- Fiber misalignment
- Improper Fiber/Resin Ratio
- Bonding defects
- Foreign Inclusions
- Incompletely cured matrix
- Matrix Cracking [Cairns 2010]

In service, several damage mechanisms for composite wind turbine blades include degradation of the rotor hub attachment points, blade fatigue damage, and environmental damage such as lightning strikes to the blade exterior. The rotor blades are typically bolted to the central hub and this creates a critical stress concentration area. The bonds between different parts of the blade structure are also likely locations of damage propagation.

Blade strength and fatigue life is related to the degradation of the composite material and the manufacture of the blade. These degradations may include delaminations and debonding. The blades are also susceptible to environmental damage such as leading edge erosion and lightning strikes. Various blade degradations and damage are shown in Figures 70 through 72.

Several challenges exist for developing an inspection program for the blades. In addition to access issues, there is limited ability to detect underlying degradations such as delamination and debonding. Access to the blades is a challenge for two reasons. First, the height of the blades necessitates the use of rope access personnel or some other means of safely placing an inspector close to the blades along their length. Second, there is limited access to the blade interior (skin interior and spar). These concerns are amplified offshore where no easy and stable access is available such as truck-mounted aerial lifts utilized onshore. A purpose-built lift boat for the wind farm is required to provide an aerial lift platform to inspect and repair the blades.

Degradation detection is limited because, unlike the above and below water structure, the blades are composite materials. While the aerospace industry has pioneered many non-destructive inspection techniques for large composite structures, the aforementioned access issues may limit their adoption directly to the offshore wind turbine blade inspection. A typical visual inspection of the blade from below with binoculars will identify surface defects (leading or trailing edge damage, lightning strikes, coating failures, etc.), but will not capture any interior anomalies. Tap tests and ultrasonic testing may identify internal anomalies such as voids, delaminations, and debonding, however

they are not well suited for capturing in-the-field inspection results. More advanced techniques such as thermography or shearography may provide improved blade coverage however their portability and application in-service can be problematic. Any of these techniques must be applied to a long structure with a large surface area and many potential locations of degradation.

One method to overcome some of the challenges for composite inspection currently being developed by the aerospace industry is structural health monitoring (SHM). SHM utilizes active sensors ranging from traditional strain gages or fiber Bragg gratings. Real-time damage detection sensors (acoustic emissions) are able to provide continual feedback on the blade condition and highlighting potential damaging events. Once identified, the monitoring results are used to target more detailed inspection activities to the area of interest and provide information pertinent to an analytical assessment. Note that while an SHM program would be used in conjunction with a typical inspection program, it is not currently practical to implement in service. [Sheppard 2010]

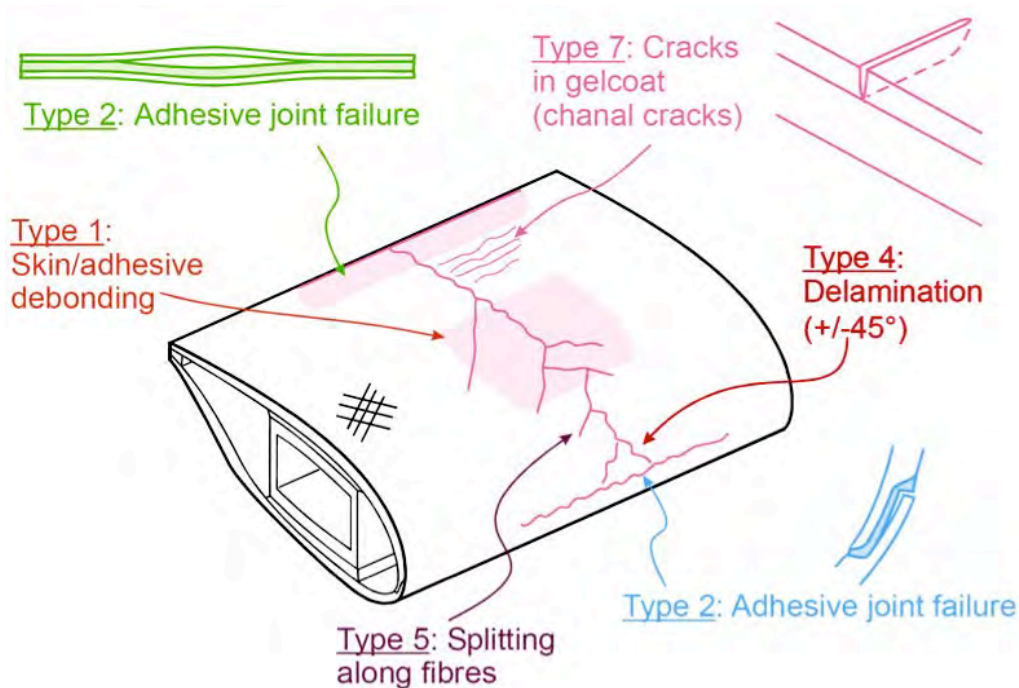


**Figure 70. Blade damage Types 1 (skin/adhesive debonding) and 2 (adhesive joint failure between skins) at the leading as well as the trailing edge. Types 4 (delamination driven by a buckling load), 5 (laminare failure in compression) and 7 (gel-coat cracking and gel-coat/skin debonding) [Sørensen 2004]**

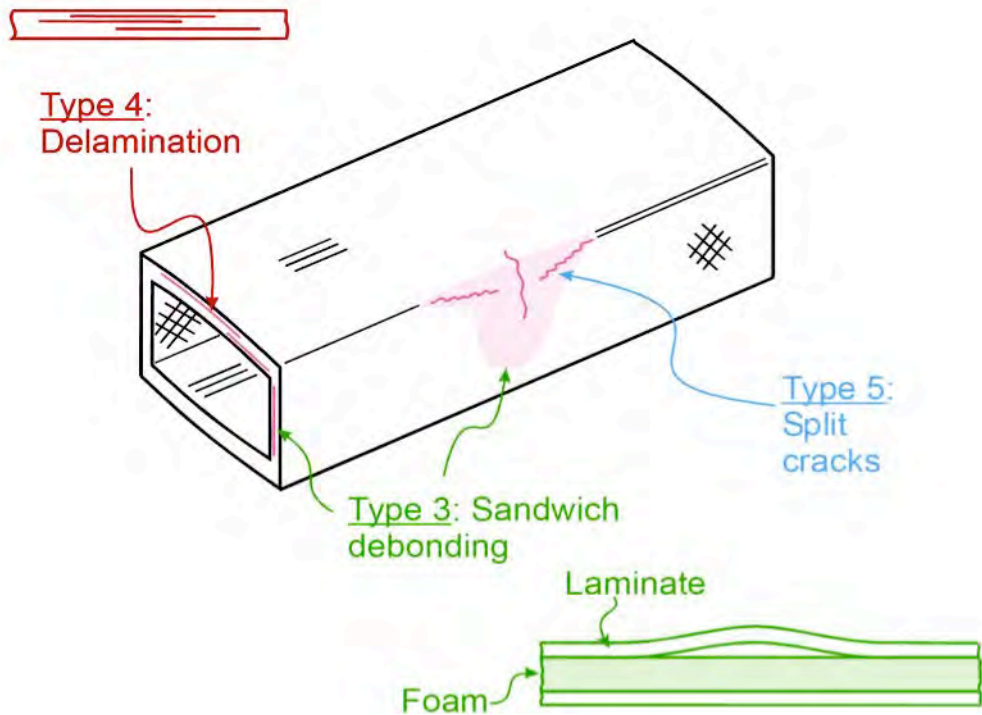


Figure 71. Blade damage types 4 (delamination driven by buckling load) in upper flange and 5 (fiber failure in tension; laminate failure in compression) in the web [Sørensen 2004]

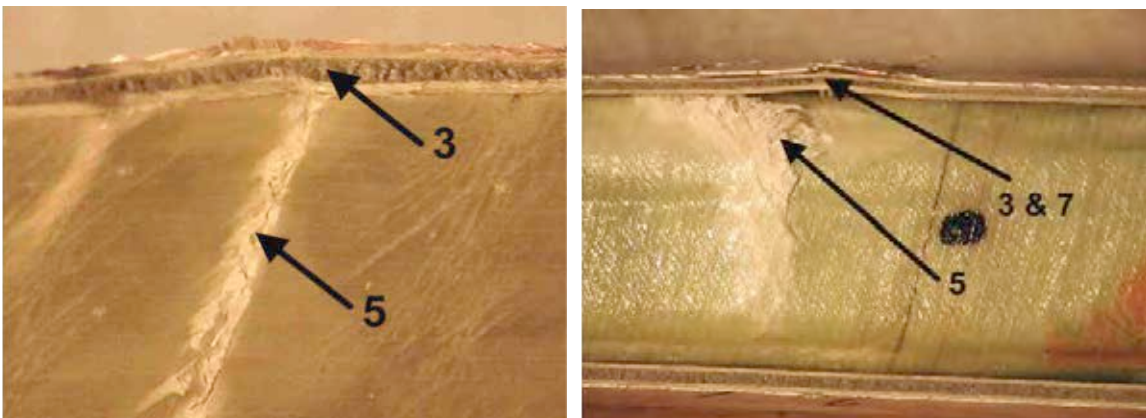


Figure 72. 3 – Blade damage formation and growth at the interface between face and core in sandwich panels in skins and main spar web (sandwich panel face/core debonding); 5 - Splitting and fracture of separate fibers in laminates of the skin and main spar (fiber failure in tension; laminate failure in compression) and 7 - Formation and growth of cracks in the gel-coat; debonding of the gel-coat from the skin (gel-coat cracking and gel-coat/skin debonding) [Sørensen 2004]

Of particular interest is how blades respond to an offshore environment and what degradations affect them. Figure 73 shows the kind of mechanisms that affect blades leading to erosion and other blade damage that should be identified as part of an inspection program. [Sheppard 2010]



**Figure 73. Wind blade damage showing: Leading Edge Erosion, Severe Blade Damage (left) , Delamination (center) and Lightning Damage to Blade [Knight & Carver]**

### 5.1 Blade Inspection Program

Blade damage is difficult to identify with general visual inspection techniques even when augmented with binoculars or similar equipment. Remote monitoring of blade performance (e.g., through power performance data analysis) should be planned and implemented by a qualified engineer to provide regular feedback on blade performance and proactively identify potential blade issues. Sheppard proposes a rigorous inspection program for composite wind turbine blades, as summarized below.

#### Critical Inspection Areas

The following areas should receive primary attention when developing an inspection program due to their importance to maintaining blade integrity:

- Blade attachment bolts
- Blade condition
- Areas of previous repair or damage

#### Inspection Cycles

##### *Annual Inspections*

General visual inspection of blade should be assisted by binoculars or other equipment to provide sufficient detail to identify the following anomalies:

- Material degradation (e.g., fiber or matrix failure, delamination, stress fracture, stiffness degradation, etc.)
- Blade damage (e.g., impact, lightning, etc.)
- Erosion particularly at leading edge
- Corrosion at attachment points

Where possible to access the blades from the nacelle, this vantage shall be used to observe the entire blade remotely and as much of the blade root exterior and interior as possible looking for the anomalies identified above.

*Intermediate Inspections*

This inspection cycle should be performed at a 3 to 5 year interval and documented with a written report including video and photographs. Non-destructive testing of the connection bolts connecting the blades to the turbine system is required.

*Additional Inspections*

When anomalous conditions are identified it may be necessary to expand the inspection scope or implement techniques that are able to provide more information for review of the extent of the anomaly. Of primary importance is the adequate documentation of the anomaly before the inspection team is demobilized.

Photos, video, sketches and measurements of the anomalous condition that can be made with the available equipment should be taken so that proper response can be determined. A qualified engineer should be consulted to determine the scope and technique of the additional inspection, keeping in mind the access and safety issues involved in getting personnel and equipment close to the blades.

Close visual inspections from no more than arm's length of the area as necessary with measurements of the anomaly and other investigation as directed by a qualified engineer using approved NDE methods.

Power performance data analysis may be used in addition to visual inspections to identify potential blade anomalies. Appropriate NDE techniques should be employed to further evaluate the condition of the blade and the blade material if either of the following is true:

- The anomalous visual or power performance results are not due to anticipated blade wear, material buildup or other mechanism considered in the design of the blades, or;
- The operator cannot demonstrate that the anomalous condition will not result in a loss of structural integrity prior to the next scheduled inspection cycle.

Of particular importance to blade integrity is evaluation of the shear web bonds and the leading and trailing edge bonds. [Sheppard 2010]

**5.2 Blade Flaw Characterization**

Montana State University has developed a wind blade flaw characterization metric that evaluates the statistical relevance of flaw occurrence. Their method incorporates the concept of inspection limitations – where flaws are there but we can't see them. The severity designation is derived iteratively. The database is ranked by criteria severity in relation to each other, essentially scoring flaw designations for each criteria.

Figure 74 shows the classification system developed to define the critical geometric parameters of blade manufacturing flaws. [Cairns 2010]

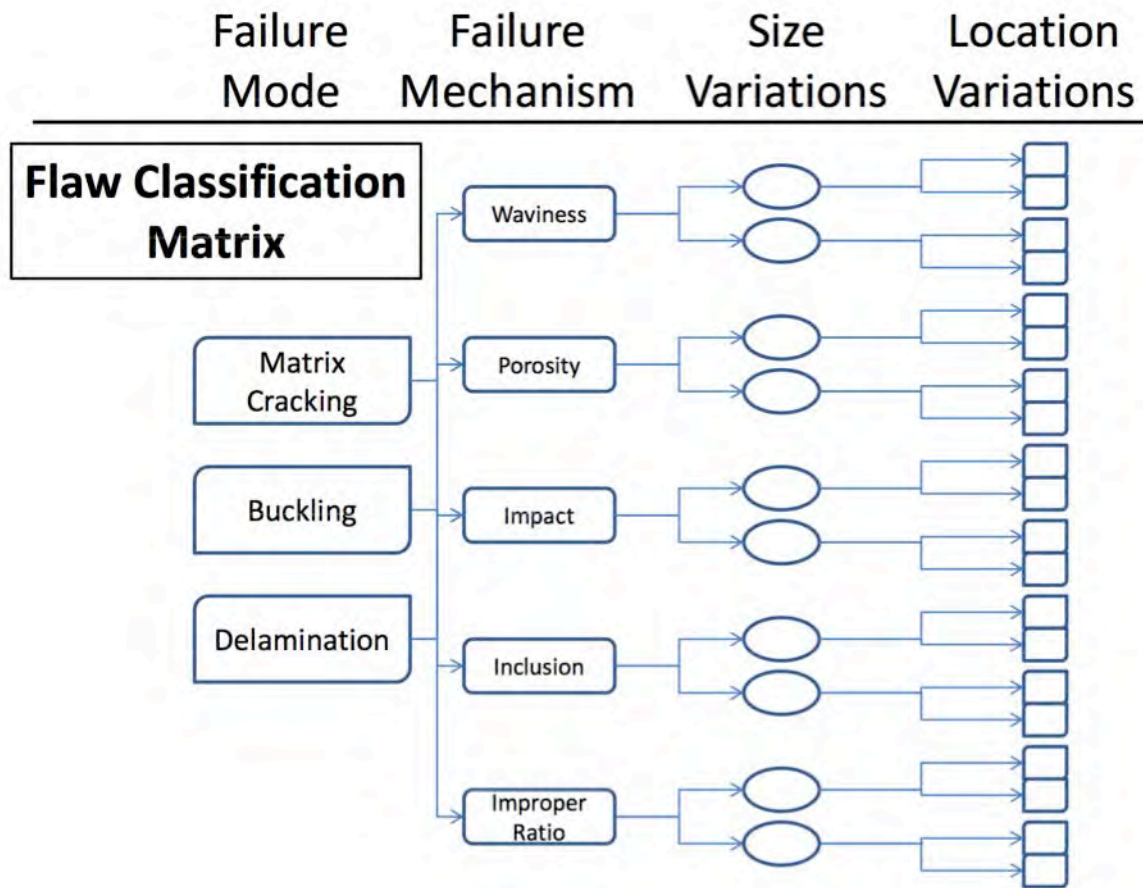


Figure 74. Classification and quantification of blade defects [Cairns 2010]

In a November 2010 discussion with Marco Zvanik of Composotech Structures, it was noted that the wind blade industry uses a variety of NDE techniques. They of course rely heavily on visual inspection but are increasingly using ultrasonics and shearography. The use of X-ray is limited because it is not “user friendly” at all. Zvanik noted that it takes trained technical personnel to be able to interpret electronic NDE data. NDE at manufacturer’s facilities tends to be more automated because the NDE equipment is fixed in an indoor environment. [Zvanik 2010]

## **6. Test Panel Program**

In order to evaluate the efficacy of proposed NDE techniques, various marine composite test panels with embedded defects were collected or fabricated for this project. With the assistance of Professor Paul Miller of the U.S. Naval Academy, test panels that were evaluated for the Navy's 44-foot sail training vessel were made available to this program. The panels included solid laminates, that were representative of the vessel's bilge area, and sandwich panels evaluated as candidate hull and deck laminates. A number of these panels had impact damage from testing that took place during the Navy's laminate down-select process. [Arvidson 2001]

The only type of damage that we could realistically induce with existing panels was impact damage. Therefore, panels with embedded flaws were fabricated to supplement the range of marine composite panels offered by Dr. Miller. The design and fabrication of these panels are detailed later in this chapter. For the solid laminates we were also able to machine cavities into the back face to simulate voids.

The test panel size was standardized to 24 by 24 inches in order to embed a number of defects in a single panel and still maintain easy transportability. A 1 by 1 inch reference grid was placed on the inspection side of each panel. Our goal was to make none of the embedded defects visible in order to objectively evaluate various NDE techniques on the same panel.

In order to "bound" the problem of how much impact energy should be used to create only internal laminate damage, a number of previous composite laminate impact damage were investigated. The wide range of impact energies, laminate constructions and resulting damage are presented herein as background.

### **6.1 Previous Composite Laminate Impact Test Programs**

Designers of composite structures have focused a lot of research into understanding damage mechanisms resulting from foreign object or wave impact. Lightweight, sandwich structures are of particular interest as the threat from impact damage often determines the minimum required skin thickness. Various non-standard test protocols have been proposed in an attempt to better simulate real world damage scenarios.

#### Aerospace Laminates

Typical sandwich laminates used in the aerospace industry use thin gage composite facesheets (0.020" to 0.045") that are co-cured to honeycomb and foam cores. The Federal Aviation Administration investigated the impact damage resistance of sandwich laminates as well as testing and inspection methods. [Tomblin 2001] They determined that a larger diameter impactor produces a very benign appearing damage state, wherein, no surface fracture/cracks nor visually perceptible levels of indentation exist, but the subsequent NDE did indicate a very large damaged region. The investigators examined a number of previous impact studies and noted impact energies up to 100 ft-lbs were used, as shown in Figure 75.

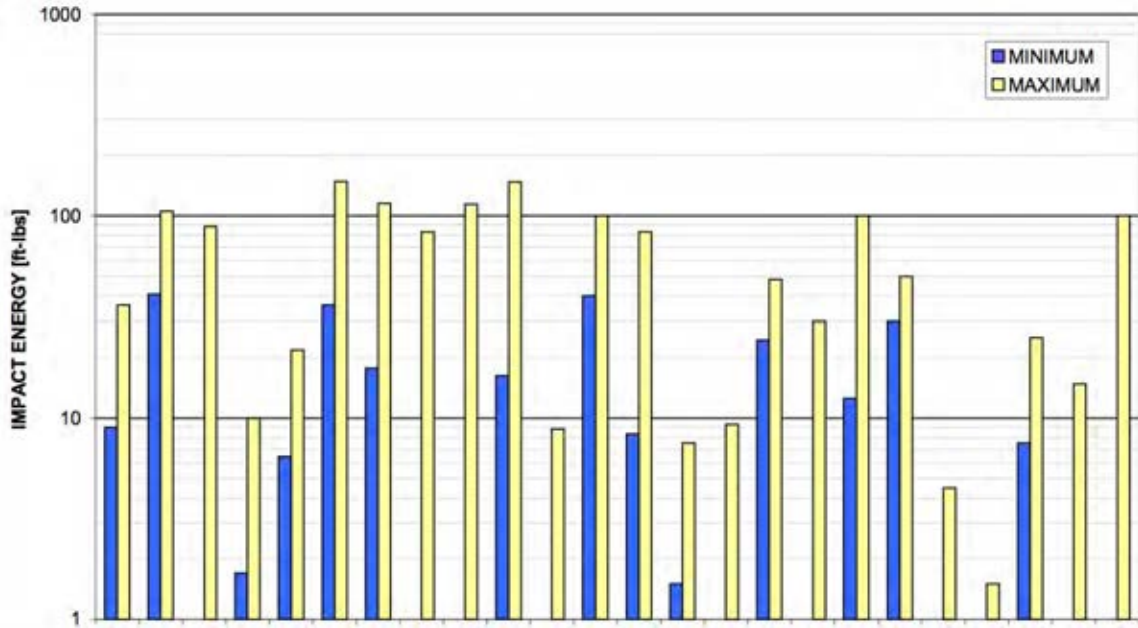


**Figure 75. Impact energies used for previous aerospace sandwich laminate impact test studies [Tomblin 2001]**

Since the investigators did not want produce visible impact damage, impact energies from 85 to 150 *inch-lbs* were used. Impactor diameters of 1, 2 and 3 inches were used that resulted in NDE-detected damage ranging from 0.10 to 3.31 inches in diameter. The curvatures in the contact region tended to equal that of the impactor, which clearly explains the onset of skin fracture at lower impact energies for the small diameter impactor. Figure 76 shows the NDE pattern damage a schematic representation of the core crushing phenomenon.

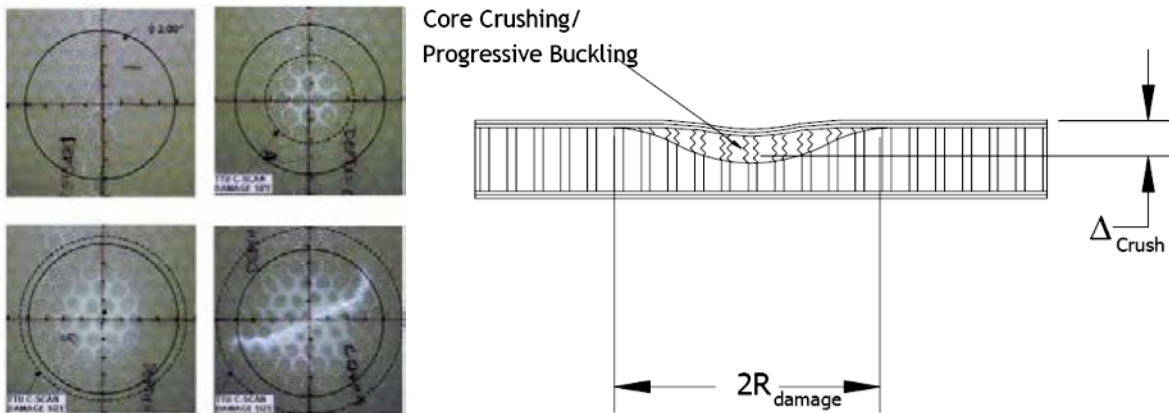


**Figure 76. Impact damage apparent only with NDE (left) and core crushing process (right) [Tomblin 2001]**

Boatbuilding Laminates

In 1996 Martin Hildebrand of Finland’s Technical Research Center noted that when he researched sandwich panel testing he came up with eight references and each used their own test method. Test variables include impact energy, impactor mass, impact velocity, and impactor geometry. Hildebrand looked at the laminates shown in Table 4 and found some correlation between laminate thickness and absorbed energy. Table 5 describes the impactor and impact energies studied.

**Table 4. Laminates studied by Hildebrand, 1996**

		thickness, mm	density, kg/m <sup>3</sup>	% fiber, weight	absorbed energy, J
1	Glass mat - polyester	2.6	3.61	22%	10.1
2	Glass/aramid - polyester	3.5	5.58	28%	33.5
3	Glass-polyester	3.8	6.37	41%	46.5
4	Spray-up laminate	6.9	9.08	20%	40.0
5	Glass - polyester	7.1	11.30	32%	62.2
6	Glass/aramid - polyester	7.7	11.00	23%	56.1
7	Glass-polyester	11.5	16.90	24%	108.2

**Table 5. Impact energies studied by Hildebrand, 1996**

Hemispherical impactor tip	diameter:	20 mm	
	support diameter:	40 mm	
	maximum energy used:	600 joules	(5310 in-lbs)

Marine Composite Laminates

In 1999 the Marine Materials Laboratory in Plouzané, France looked at a variety of marine composite laminates over an extreme range of impact energies, as shown in Table 6. The “impactors” ranged from a simple drop weight to a full-size shipping container weighing a whopping four tons. Specimens were tested to failure for this exercise but it instructive to note.

Three types of impact scenarios were studied. First, a falling weight, involving energies up to 3 kJ, and steel impactors weighing up to 50 kg were dropped onto composite sandwich panels. The second type of test was the simulation of wave impact (slamming) using a 20 kg flexible bladder impactor. The third test released containers weighing up to 4 tons from heights up to 3 meters onto large steel and composite floor structures. Table 7 provides a summary of impact energies.

The large scale tests served primarily as a demonstration of the feasibility of using composite materials for floor structures on offshore installations. The impact behavior of the pultruded composite structure was shown to satisfy the qualification criterion

specified. Also, the modular design of the pultruded composite floor allowed easy replacement of the damaged elements. [Choqueuse 1999]

**Table 6. Laminates studied by Marine Materials Laboratory, [Choqueuse 1999]**

Material	Thickness	Geometries tested, mm	Type of test
GRP/PVC foam sandwich	Skins: 2 mm Core: 20 mm	300 x 300 up to 800 x 800	Drop weight Slamming
GRP/Phenolic foam sandwich	Skins: 2 mm Core: 50 mm	2000 x 1000 4000 x 5000	Drop weight Container
CFRP stiffened laminate	5 mm	1200 x 600	Slamming
Sandwich (foam,	Skins: 1 mm Core: 20-35 mm		
Pultruded box sections	7 to 15 mm section 250 x 300	Single 5 m element 14 elements	Drop weight Container
Acier E24 78 kg/m <sup>2</sup>	9 mm	2000 x 1000	Drop weight Container
	6 mm	4000 x 5000	

**Table 7. Impact Energies studied by Marine Materials Laboratory, [Choqueuse 1999]**

Drop weight

Falling weight tower employed here is 6 metres high with mass up to 50kg  
 maximum: 3 kJ  
 tested: 75 J

Slamming

Impactor: an elastomeric ball (diameter 30 cm) filled with sand to a total weight of 20kg  
 Drop height: 50 cm to 8 m  
 mininum: 868 in-lbs  
 maximum: 13,900 in-lbs

Container

A 4 ton container is dropped from a height of up to 3 meters  
 mininum: 21,700 in-lbs  
 maximum: 520,650 in-lbs

## 6.2 Project Test Panels

The test panel program utilized both a variety of marine composite panels available from past research efforts and a set purposely built for this project. A description of the panels is presented to illustrate the variety of laminates used for NDE and in order to estimate a correlation between impact energies and resulting damage.

### Solid Laminates

The solid laminates made available to this project were fabricated by Pearson Yachts as quality assurance specimens molded concurrently with the Navy 44 sail training boats. Derakane 8084 vinylester resin was used to infuse a stack of triaxial E-glass reinforcement. The dimensions of the panels varied, as shown in Table 8. Most of the panels were approximately one inch thick. Table 8 shows that panels 1-3 were designated for impact damage investigations and panels 4-7 were machined as per the layout specified in Figures 77 - 80. Unlike traditional aerospace solid composite calibration blocks (see Figure 58 in Aerospace chapter), our pattern was randomized with different depth cavities machined on each panel. An opaque piece of poster board was adhered to the back of the panels to prevent NDE inspectors from seeing where the panels were machined.

**Table 8. Solid laminates built by Pearson Yachts**

Layer	Panel Construction			Panel Designation	Panel Size	
	Designation	Description	Vendor		1" thick	Damage Type
surface	gel coat			Pearson 1	35" wide	impact damage
outer ply	1.5 oz mat				12" high	
ply 1	E-TLX 2400 @ 90°	0°/+45°/-45° Triaxial	Vectorply	Pearson 2	37" wide	impact damage
ply 2	E-TLX 2400 @ 0°	0°/+45°/-45° Triaxial	Vectorply		20" high	
ply 3	E-TLX 2400 @ 90°	0°/+45°/-45° Triaxial	Vectorply	Pearson 3	38" wide	impact damage
ply 4	E-TLX 2400 @ 0°	0°/+45°/-45° Triaxial	Vectorply		18" high	
ply5	E-TLX 2400 @ 90°	0°/+45°/-45° Triaxial	Vectorply	Pearson 4	37" wide	void simulation
ply 6	E-TLX 2400 @ 0°	0°/+45°/-45° Triaxial	Vectorply		20" high	
ply 7	E-TLX 2400 @ 90°	0°/+45°/-45° Triaxial	Vectorply	Pearson 5	37" wide	1/2", 1", 2" & 3" to 60%
pl 8	E-TLX 2400 @ 0°	0°/+45°/-45° Triaxial	Vectorply		23" high	
ply 9	E-TLX 2400 @ 90°	0°/+45°/-45° Triaxial	Vectorply	Pearson 6	36" wide	1/2", 1", 2" & 3" to 40%
ply 10	E-TLX 2400 @ 0°	0°/+45°/-45° Triaxial	Vectorply		25" high	
ply 11	E-TLX 2400 @ 90°	0°/+45°/-45° Triaxial	Vectorply	Pearson 7	37" wide	1/2", 1", 2" & 3" to 20%
resin	Derakane 8084	vinylester	Dow Chemical		25" high	

Only the four machined solid laminates were retained for the NDE round robin trial. The remaining panels were subjected to impact loads but it was not possible to impart internal or back face damage without a corresponding large surface damage area.

Because the panels were fabricated with clear gel coat, it was very easy to visibly identify where the machining was done, as light is easily transmitted through these regions. Pieces of foam board were cut and placed in the cavities and another piece of foam board was adhered to the back of the panel. It was still possible to notice where the panel defects were so the front face of the panels was painted with several layers of white polyurethane paint and a reference grid was applied.

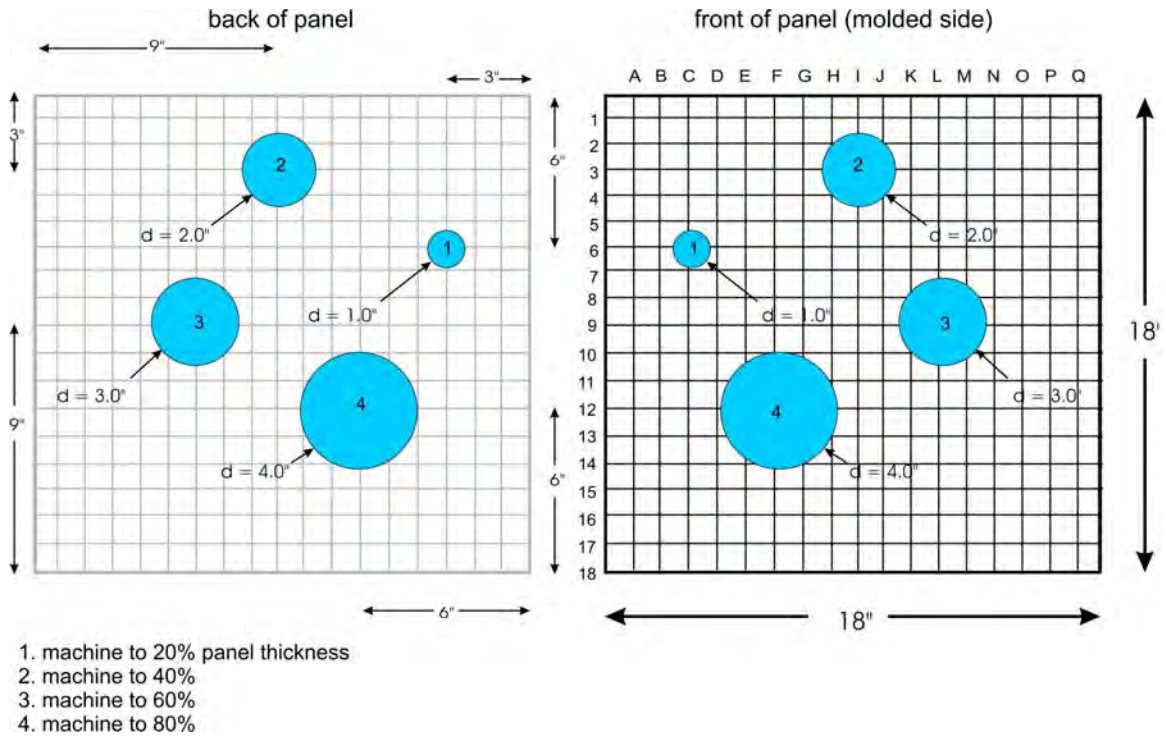


Figure 77. Void simulation cavity machining diagram for Pearson 4 test panel

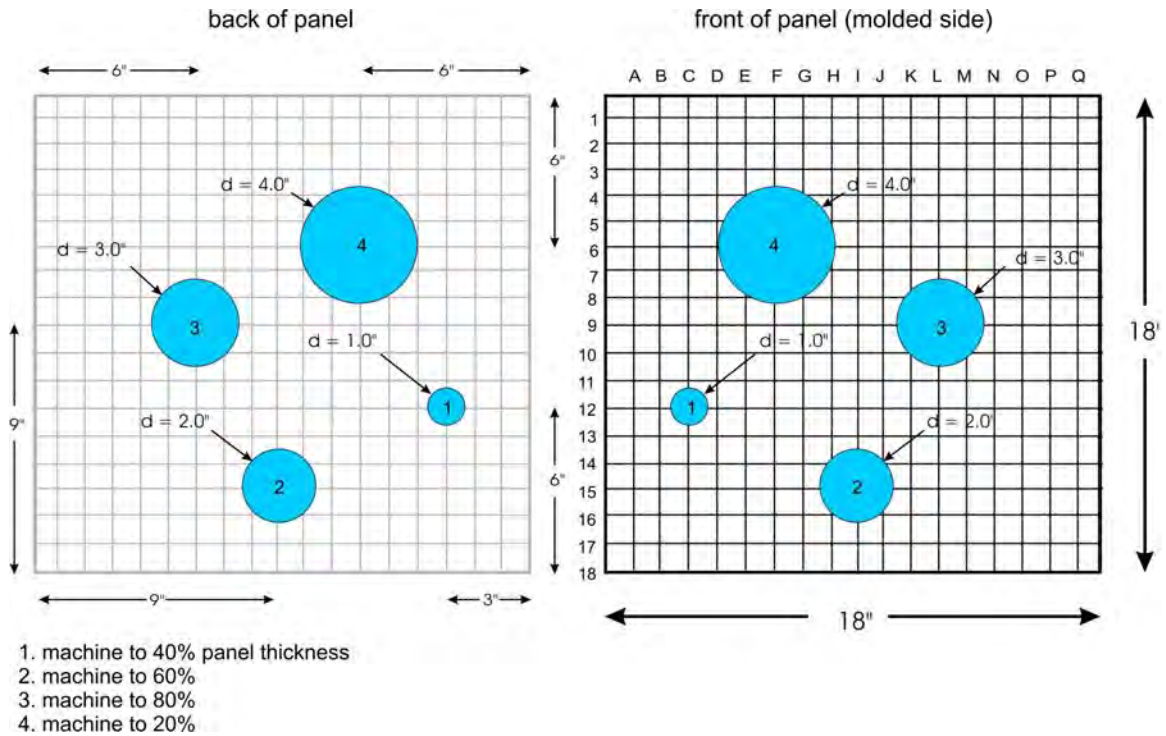


Figure 78. Void simulation cavity machining diagram for Pearson 5 test panel

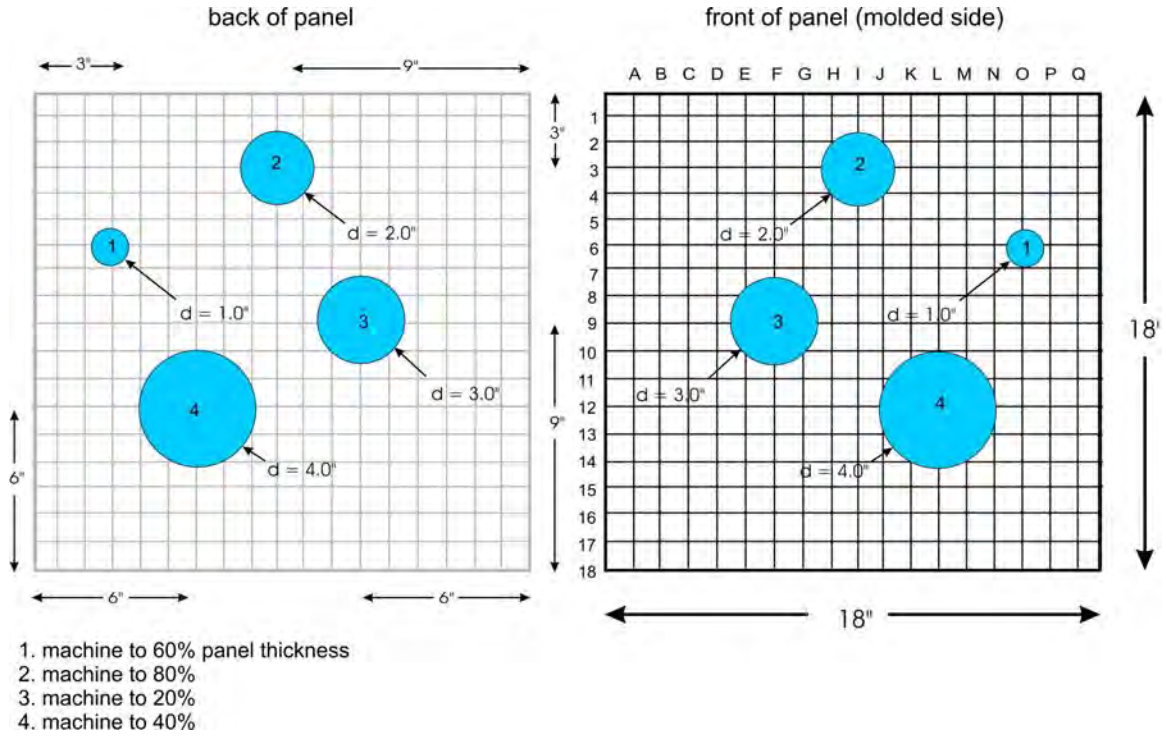


Figure 79. Void simulation cavity machining diagram for Pearson 6 test panel

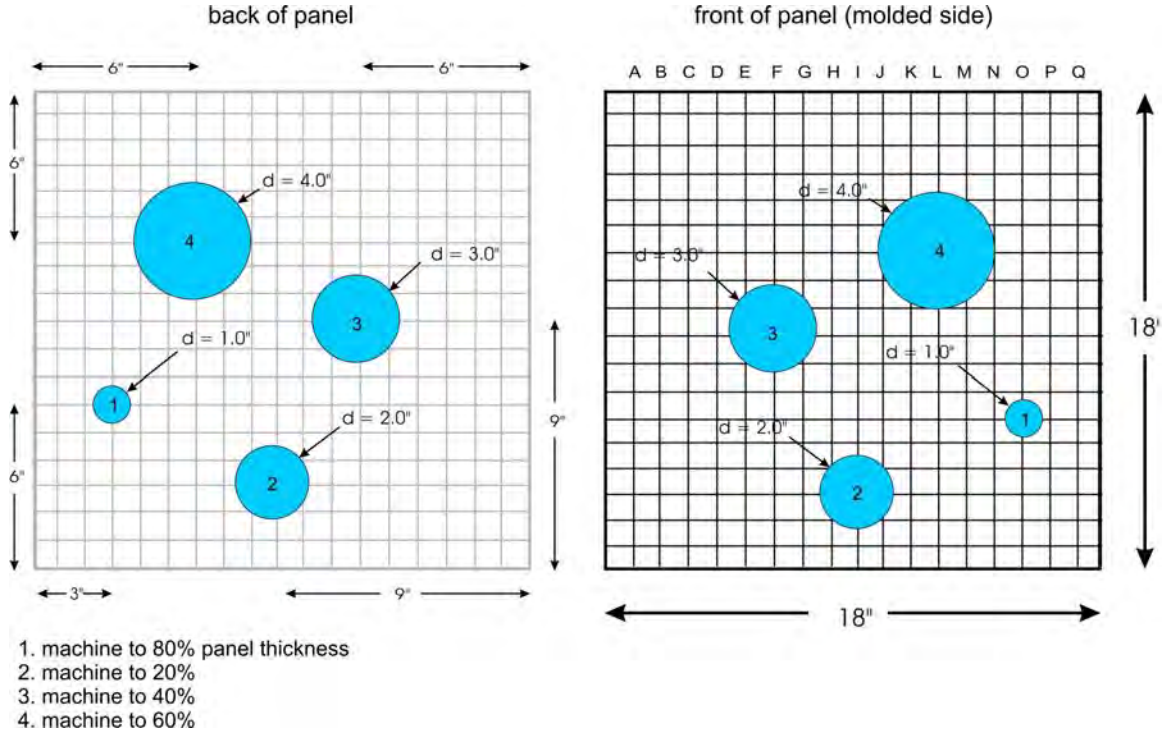


Figure 80. Void simulation cavity machining diagram for Pearson 7 test panel

Sandwich Panels from Previous Studies

A variety of marine composite panels have been tested by Dr. Paul Miller at the U.S. Naval Academy over the years and these panels were made available to this project for NDE investigations. Some of the panels were damaged from previous testing but most were subjected to impact damage using a test arrangement designed for this project. Figures xx through xx provide descriptions of the USNA test panels.

Figures 81 through 85 show laminate schedules, thicknesses and pictures of the USNA panels.

Panel Dimensions, inches		
Width	Height	Thickness
24	12	0.95

Layer	Description
Finish	blue paint
1	3/4 oz CSM
2	24 oz double bias
3	18 oz woven roving
4	18 oz woven roving
5	1" ATC Corecell A600
6	18 oz woven roving
7	24 oz double bias
8	18 oz woven roving

	Actual
	Thickness, ins
Core	0.65
Outer Skin	0.20
Inner Skin	0.10
Total:	0.95



Panel Dimensions, inches		
Width	Height	Thickness
24	24	0.50

Layer	Description
Finish	Gelcoat
1	0.005" chopped fibers
2	0.023" 3/4 oz gun roving
3	1.5 oz mat
4	3/4 oz mat
5	0.375" balsa core
6	1.5 oz mat
7	10 oz cloth

	Actual
	Thickness, ins
Core	0.35
Outer Skin	0.10
Inner Skin	0.05
Total:	0.50



**Figure 81. Description of USNA 1 panel that weighs 2.72 lbs/ft<sup>2</sup> (left) and USNA 2 panel at 1.55 lbs/ft<sup>2</sup> (right)**

Panel Dimensions, inches		
Width	Height	Thickness
24	24	1.38

Layer	Description
1	5.6 oz boat cloth
2	+45 deg 1/8" cedar
3	-45 deg 1/8" cedar
4	3.7 oz boat cloth
5	18.4 oz carbon cloth
6	1" Superlite 45 balsa core
7	3.7 oz boat cloth
8	18.4 oz carbon cloth
9	12 oz double bias carbon fabric
10	11 oz carbon cloth
11	11 oz carbon cloth
12	3.7 oz boat cloth

	Actual Thickness, ins
Core	0.98
Outer Skin	0.30
Inner Skin	0.10
Total:	1.38



Panel Dimensions, inches		
Width	Height	Thickness
22.5	16	1.11

Layer	Description
Finish	Gelcoat
1	3/4 oz CSM
2	24 oz double bias
3	18 oz woven roving
4	18 oz woven roving
5	1" ATC Corecell A600
6	18 oz woven roving
7	24 oz double bias
8	18 oz woven roving

	Actual Thickness, ins
Core	0.95
Outer Skin	0.10
Inner Skin	0.06
Total:	1.11



Figure 82. Description of USNA 3 panel that weighs 2.21 lbs/ft<sup>2</sup> (left) and USNA 4 panel at 2.48 lbs/ft<sup>2</sup> (right)

Panel Dimensions, inches		
Width	Height	Thickness
22.5	16	0.95

Layer	Description
Finish	Gelcoat
1	18 oz woven roving
2	24 oz double bias
3	18 oz woven roving
4	1" ATC Corecell A600
5	18 oz woven roving
6	24 oz double bias
7	18 oz woven roving

	Actual Thickness, ins
Core	0.73
Outer Skin	0.14
Inner Skin	0.08
Total:	0.95



Panel Dimensions, inches		
Width	Height	Thickness
22.5	15.75	0.62

Layer	Description
Finish	Gelcoat
1	18 oz woven roving
2	24 oz double bias
3	18 oz woven roving
4	24 oz double bias
5	18 oz woven roving
6	24 oz double bias
7	18 oz woven roving
8	24 oz double bias
9	18 oz woven roving
10	24 oz double bias
11	18 oz woven roving
12	24 oz double bias
13	18 oz woven roving
14	24 oz double bias
15	18 oz woven roving
16	24 oz double bias
17	18 oz woven roving
18	24 oz double bias



Figure 83. Description of USNA 5 panel that weighs 2.22 lbs/ft<sup>2</sup> (left) and USNA 6 panel at 6.07 lbs/ft<sup>2</sup> (right)

Panel Dimensions, inches		
Width	Height	Thickness
38	17	1.19

Layer	Description
Finish	Gelcoat
1	24 oz double bias
2	18 oz woven roving
3	18 oz woven roving
4	1" ATC Corecell A600
5	18 oz woven roving
6	24 oz double bias
7	18 oz woven roving
8	18 oz woven roving

	Actual Thickness, ins
Core	0.96
Outer Skin	0.15
Inner Skin	0.08
Total:	1.19

Panel Dimensions, inches		
Width	Height	Thickness
38	18	1.16

Layer	Description
Finish	Gelcoat
1	24 oz double bias
2	18 oz woven roving
3	18 oz woven roving
4	1" ATC Corecell A600
5	18 oz woven roving
6	24 oz double bias
7	18 oz woven roving
8	18 oz woven roving

	Actual Thickness, ins
Core	0.96
Outer Skin	0.12
Inner Skin	0.08
Total:	1.16



Figure 84. Description of USNA 7 panel that weighs 2.88 lbs/ft<sup>2</sup> (left) and USNA 8 panel at 2.58 lbs/ft<sup>2</sup> (right)

Panel Dimensions, inches		
Width	Height	Thickness
36	17	0.90

Layer	Description
Finish	Gelcoat
1	3/4 oz CSM
2	18 oz woven roving
3	17 oz double bias
4	18 oz woven roving
5	0.75" ATC Corecell A600
6	18 oz woven roving
7	17 oz double bias
8	18 oz woven roving
9	3/4 oz CSM

	Actual Thickness, ins
Core	0.70
Outer Skin	0.12
Inner Skin	0.08
Total:	0.90

Panel Dimensions, inches		
Width	Height	Thickness
23.38	25.38	1.05

Layer	Description
1	4 oz boat cloth
2	11 oz carbon cloth
3	18.4 carbon cloth
4	1" Superlite 45 balsa core
5	18.4 carbon cloth
6	11 oz carbon cloth

	Actual Thickness, ins
Core	0.85
Outer Skin	0.12
Inner Skin	0.08
Total:	1.05

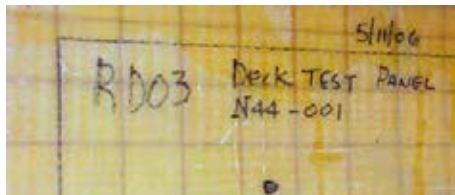


Figure 85. Description of USNA 9 panel that weighs 2.29 lbs/ft<sup>2</sup> (left) and USNA 10 panel at 1.74 lbs/ft<sup>2</sup> (right)

Fabricated Test Panels

Eric Greene Associates contracted with Osprey Marine Composites of Deale, Maryland to fabricate a series of test panels with embedded defects for this project. We settled on two types of panels that paralleled the construction used to develop allowable defect sizes early in the project. Namely, an E-glass foam-cored panel (about 3 lb/ft<sup>2</sup>) and a carbon fiber balsa-cored panel (about 2 lbs/ft<sup>2</sup>). The laminate schedules for these panels are shown in Table 9.

**Table 9. Fabricated test panels**

	Panel Construction				Panel Designation	Panel Size	Damage Type																																																																																																	
	Layer	Designation	Description	Vendor																																																																																																				
Panels built by Osprey Marine	surface	gel coat	white		Osprey 1	24" wide 24" high	delamination simulation 1/2", 1", 2", 3" & 4" @ 3 depths																																																																																																	
	outer ply	1.5 oz mat						ply 1	E-BXM 170	+45°/-45° Biaxial	Vectorply	Osprey 2	24" wide 24" high	water ingress 1", 2", 3" & 4"	ply 2	E-LTM 180	0°/90° Biaxial	Vectorply	ply 3	E-BXM 170	+45°/-45° Biaxial	Vectorply	Osprey 3	24" wide 24" high	core shear 3", 6" & 12"	core	1" Divinycell H80 PVC foam	5.0 lbs/ft <sup>3</sup>	Diab	ply 4	E-BXM 170	+45°/-45° Biaxial	Vectorply	Osprey 4	24" wide 24" high	impact non-visible damage	ply5	E-LTM 180	0°/90° Biaxial	Vectorply	ply 6	E-BXM 170	+45°/-45° Biaxial	Vectorply				resin	Derakane 8084	vinylester	Dow Chemical					Layer	Designation	Description	Vendor				surface	gel coat	clear			Osprey 5	24" wide 24" high	delamination simulation 1/2", 1", 2", 3" & 4" @ 3 depths	ply 1	carbon fiber 16.38 oz. twill weave @ 0°	carbon 90°/0°	Vectorply	ply 2	carbon fiber 16.38 oz. twill weave @ 90°	carbon 90°/0°	Vectorply	Osprey 6	24" wide 24" high	water ingress 1", 2", 3" & 4"	core	1" Baltek SB.50 balsa	5.9 lbs/ft <sup>3</sup>	3A Composites	ply5	carbon fiber 16.38 oz. twill weave @ 90°	carbon 90°/0°	Vectorply	Osprey 7	24" wide 24" high	core shear 3", 6" & 12"	ply 6	carbon fiber 16.38 oz. twill weave @ 0°	carbon 90°/0°	Vectorply	resin	Derakane 8084	vinylester	Dow Chemical	Osprey 8	24" wide 24" high	impact non-visible damage	
	ply 1	E-BXM 170	+45°/-45° Biaxial	Vectorply	Osprey 2	24" wide 24" high	water ingress 1", 2", 3" & 4"																																																																																																	
	ply 2	E-LTM 180	0°/90° Biaxial	Vectorply				ply 3	E-BXM 170	+45°/-45° Biaxial	Vectorply	Osprey 3	24" wide 24" high	core shear 3", 6" & 12"	core	1" Divinycell H80 PVC foam	5.0 lbs/ft <sup>3</sup>	Diab	ply 4	E-BXM 170	+45°/-45° Biaxial	Vectorply	Osprey 4	24" wide 24" high	impact non-visible damage	ply5	E-LTM 180	0°/90° Biaxial	Vectorply	ply 6	E-BXM 170	+45°/-45° Biaxial	Vectorply				resin	Derakane 8084	vinylester	Dow Chemical					Layer	Designation	Description	Vendor				surface	gel coat	clear			Osprey 5	24" wide 24" high	delamination simulation 1/2", 1", 2", 3" & 4" @ 3 depths	ply 1	carbon fiber 16.38 oz. twill weave @ 0°	carbon 90°/0°	Vectorply	ply 2	carbon fiber 16.38 oz. twill weave @ 90°	carbon 90°/0°	Vectorply	Osprey 6	24" wide 24" high	water ingress 1", 2", 3" & 4"	core	1" Baltek SB.50 balsa	5.9 lbs/ft <sup>3</sup>	3A Composites	ply5	carbon fiber 16.38 oz. twill weave @ 90°	carbon 90°/0°	Vectorply	Osprey 7	24" wide 24" high	core shear 3", 6" & 12"	ply 6	carbon fiber 16.38 oz. twill weave @ 0°	carbon 90°/0°	Vectorply	resin	Derakane 8084	vinylester	Dow Chemical	Osprey 8	24" wide 24" high	impact non-visible damage												
	ply 3	E-BXM 170	+45°/-45° Biaxial	Vectorply	Osprey 3	24" wide 24" high	core shear 3", 6" & 12"																																																																																																	
	core	1" Divinycell H80 PVC foam	5.0 lbs/ft <sup>3</sup>	Diab				ply 4	E-BXM 170	+45°/-45° Biaxial	Vectorply	Osprey 4	24" wide 24" high	impact non-visible damage	ply5	E-LTM 180	0°/90° Biaxial	Vectorply	ply 6	E-BXM 170	+45°/-45° Biaxial	Vectorply				resin	Derakane 8084	vinylester	Dow Chemical					Layer	Designation	Description	Vendor				surface	gel coat	clear			Osprey 5	24" wide 24" high	delamination simulation 1/2", 1", 2", 3" & 4" @ 3 depths	ply 1	carbon fiber 16.38 oz. twill weave @ 0°	carbon 90°/0°	Vectorply	ply 2	carbon fiber 16.38 oz. twill weave @ 90°	carbon 90°/0°	Vectorply	Osprey 6	24" wide 24" high	water ingress 1", 2", 3" & 4"	core	1" Baltek SB.50 balsa	5.9 lbs/ft <sup>3</sup>	3A Composites	ply5	carbon fiber 16.38 oz. twill weave @ 90°	carbon 90°/0°	Vectorply	Osprey 7	24" wide 24" high	core shear 3", 6" & 12"	ply 6	carbon fiber 16.38 oz. twill weave @ 0°	carbon 90°/0°	Vectorply	resin	Derakane 8084	vinylester	Dow Chemical	Osprey 8	24" wide 24" high	impact non-visible damage																							
	ply 4	E-BXM 170	+45°/-45° Biaxial	Vectorply	Osprey 4	24" wide 24" high	impact non-visible damage																																																																																																	
	ply5	E-LTM 180	0°/90° Biaxial	Vectorply				ply 6	E-BXM 170	+45°/-45° Biaxial	Vectorply				resin	Derakane 8084	vinylester	Dow Chemical					Layer	Designation	Description	Vendor				surface	gel coat	clear			Osprey 5	24" wide 24" high	delamination simulation 1/2", 1", 2", 3" & 4" @ 3 depths	ply 1	carbon fiber 16.38 oz. twill weave @ 0°	carbon 90°/0°	Vectorply	ply 2	carbon fiber 16.38 oz. twill weave @ 90°	carbon 90°/0°	Vectorply	Osprey 6	24" wide 24" high	water ingress 1", 2", 3" & 4"	core	1" Baltek SB.50 balsa	5.9 lbs/ft <sup>3</sup>	3A Composites	ply5	carbon fiber 16.38 oz. twill weave @ 90°	carbon 90°/0°	Vectorply	Osprey 7	24" wide 24" high	core shear 3", 6" & 12"	ply 6	carbon fiber 16.38 oz. twill weave @ 0°	carbon 90°/0°	Vectorply	resin	Derakane 8084	vinylester	Dow Chemical	Osprey 8	24" wide 24" high	impact non-visible damage																																		
	ply 6	E-BXM 170	+45°/-45° Biaxial	Vectorply																																																																																																				
	resin	Derakane 8084	vinylester	Dow Chemical																																																																																																				
		Layer	Designation	Description	Vendor																																																																																																			
	surface	gel coat	clear			Osprey 5	24" wide 24" high	delamination simulation 1/2", 1", 2", 3" & 4" @ 3 depths																																																																																																
	ply 1	carbon fiber 16.38 oz. twill weave @ 0°	carbon 90°/0°	Vectorply	ply 2				carbon fiber 16.38 oz. twill weave @ 90°	carbon 90°/0°	Vectorply	Osprey 6	24" wide 24" high	water ingress 1", 2", 3" & 4"	core	1" Baltek SB.50 balsa	5.9 lbs/ft <sup>3</sup>	3A Composites	ply5	carbon fiber 16.38 oz. twill weave @ 90°	carbon 90°/0°	Vectorply	Osprey 7	24" wide 24" high	core shear 3", 6" & 12"	ply 6	carbon fiber 16.38 oz. twill weave @ 0°	carbon 90°/0°	Vectorply	resin	Derakane 8084	vinylester	Dow Chemical	Osprey 8	24" wide 24" high	impact non-visible damage																																																																				
	ply 2	carbon fiber 16.38 oz. twill weave @ 90°	carbon 90°/0°	Vectorply	Osprey 6	24" wide 24" high	water ingress 1", 2", 3" & 4"																																																																																																	
	core	1" Baltek SB.50 balsa	5.9 lbs/ft <sup>3</sup>	3A Composites				ply5	carbon fiber 16.38 oz. twill weave @ 90°	carbon 90°/0°	Vectorply	Osprey 7	24" wide 24" high	core shear 3", 6" & 12"	ply 6	carbon fiber 16.38 oz. twill weave @ 0°	carbon 90°/0°	Vectorply	resin	Derakane 8084	vinylester	Dow Chemical	Osprey 8	24" wide 24" high	impact non-visible damage																																																																															
	ply5	carbon fiber 16.38 oz. twill weave @ 90°	carbon 90°/0°	Vectorply	Osprey 7	24" wide 24" high	core shear 3", 6" & 12"																																																																																																	
ply 6	carbon fiber 16.38 oz. twill weave @ 0°	carbon 90°/0°	Vectorply	resin				Derakane 8084	vinylester	Dow Chemical	Osprey 8	24" wide 24" high	impact non-visible damage																																																																																											
resin	Derakane 8084	vinylester	Dow Chemical	Osprey 8	24" wide 24" high	impact non-visible damage																																																																																																		

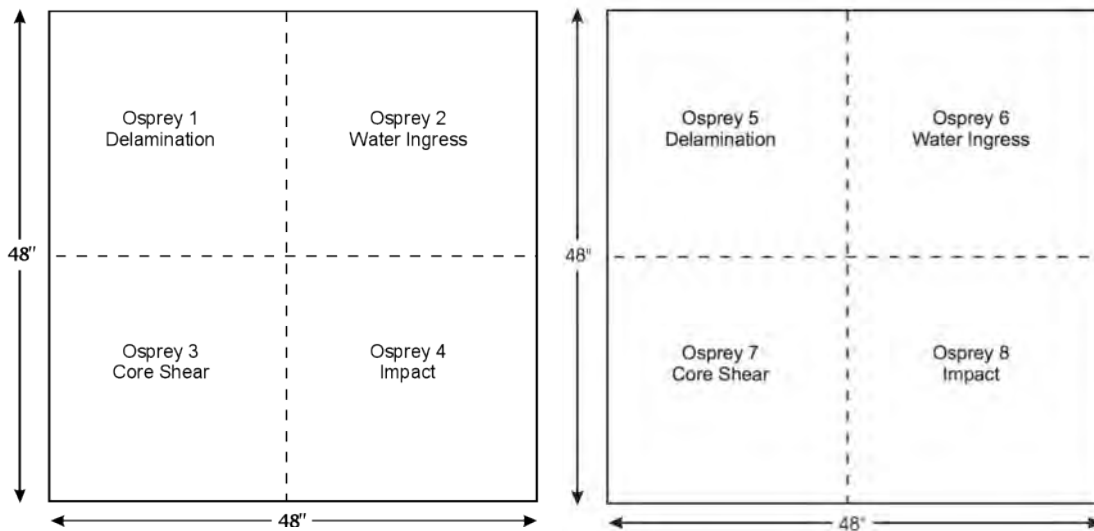
Figure 86 shows how four panels were cut from each of the four-foot by four-foot laminated panels. Figure 87 shows how peel ply material was placed strategically in the laminate to simulate delaminations. Figure 90 shows the cut peel ply material. This was done for panels Osprey 1 and Osprey 5. Mylar material was considered to simulate delamination but this material has shown to have a distinct ultrasonic signature, which may easier to detect than an actual delamination or kissing bond.

Figure 88 shows the locations and fabrication schematic for simulating water trapped under the outer skin of a hull laminate. After the outer skin was laminated to the core, a hole-saw was used to cut one to four inch diameter cavities (see Figure 91), where about ¼ inches of water was poured. The core plug was then replaced using bonding putty to ensure watertight integrity.

Many of the panels that were subjected to impact loads incurred some degree of core shear damage. However, we don't have a priori knowledge of the damage location sites and severity before NDE inspection. Therefore, core shear was simulated by cutting the core prior to panel fabrication, as shown in Figure 89. It was not feasible to cut the balsa core cleanly at 45° so peel ply was placed along the kerf cuts at 90° to the skins.

Osprey panels 4 and 8 were subjected to impact loads conducted at the US Naval Academy Structures Laboratory. Impact energy levels were chosen to produce only internal panel damage.

Figure 91 shows the one-inch reference grid that was drawn on the E-glass and carbon fiber test panels built by Osprey Marine.



**Figure 86. Layout of E-glass @ 3.29 lbs/ft<sup>2</sup> test panel (left) and carbon fiber panel @ 2.16 lbs/ft<sup>2</sup> (right). Note in photograph that the area where water ingress was simulated is clearly visible before being covered.**

A piece of black ¼-inch foam board was adhered to the back of all the test panels using black duct tape. This was done to facilitate handling and to mask any back face damage that may be visible.

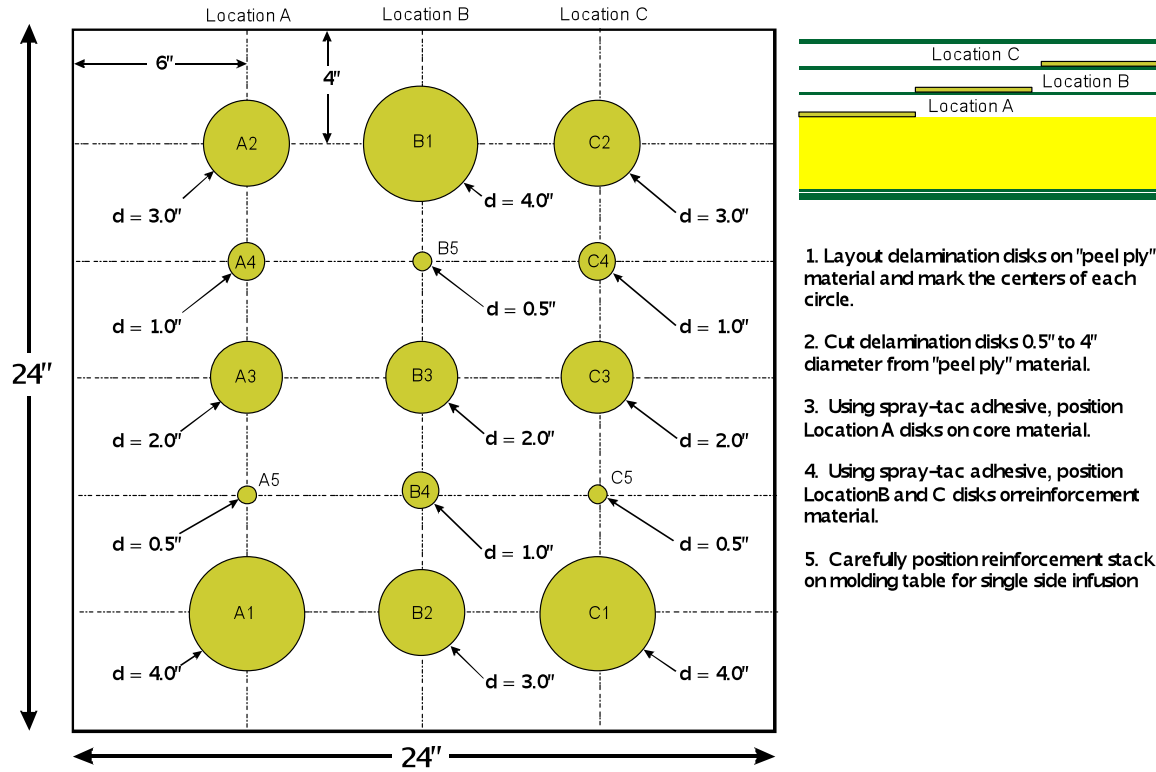


Figure 87. Test panel delamination arrangement

1. Layout delamination disks on "peel ply" material and mark the centers of each circle.
2. Cut delamination disks 0.5" to 4" diameter from "peel ply" material.
3. Using spray-tac adhesive, position Location A disks on core material.
4. Using spray-tac adhesive, position Location B and C disks on reinforcement material.
5. Carefully position reinforcement stack on molding table for single side infusion

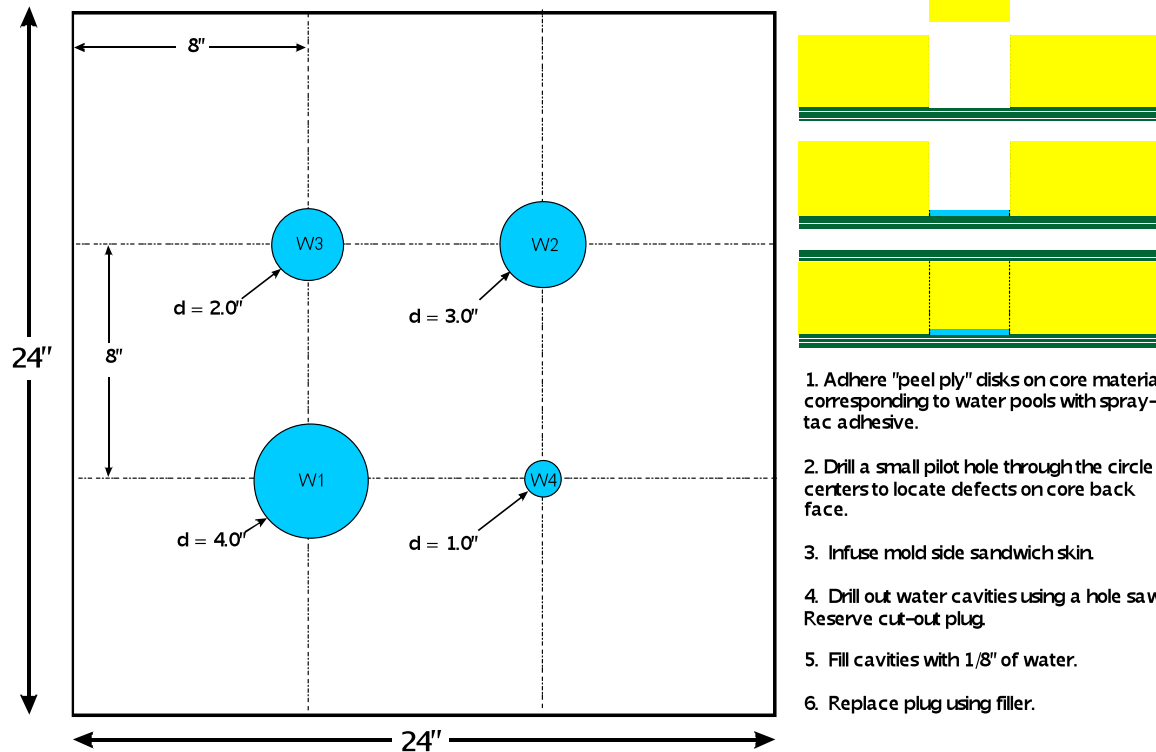


Figure 88. Test panel water ingress arrangement

1. Adhere "peel ply" disks on core material corresponding to water pools with spray-tac adhesive.
2. Drill a small pilot hole through the circle centers to locate defects on core back face.
3. Infuse mold side sandwich skin.
4. Drill out water cavities using a hole saw Reserve cut-out plug.
5. Fill cavities with 1/8" of water.
6. Replace plug using filler.

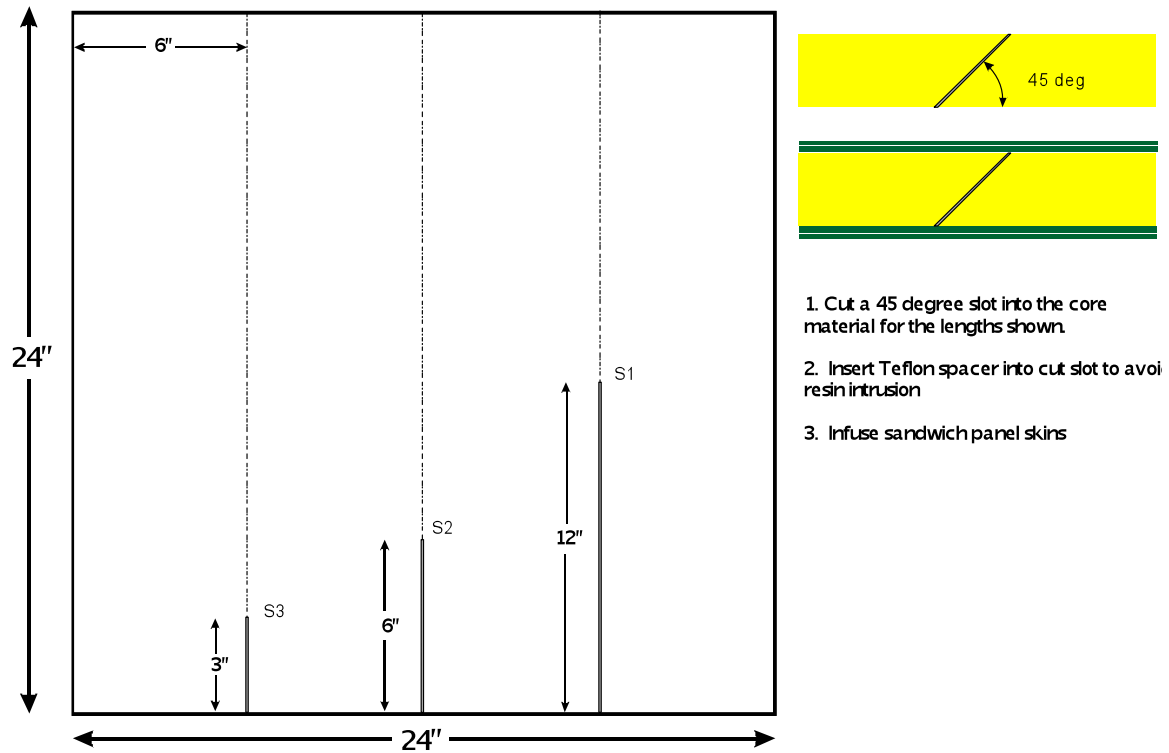


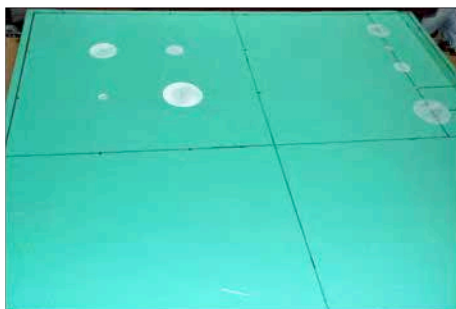
Figure 89. Test panel shear defect arrangement



Peel ply 0.5, 1, 2, 3, and 4 inches diameter used to simulate delamination



45° saw cuts (3, 6 and 12 inches long) in core used to simulate core shear failure

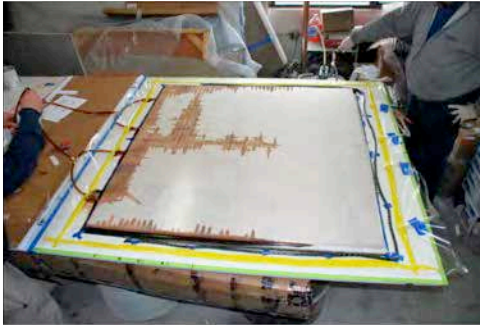


Peel ply used to create water void (left) and for delamination (right)



Removed core (left) and replacement plugs (right) used to entrap water behind skin

Figure 90. Test panel construction



Beginning of infusion process used to wet-out the outer skin



Hole saw is used to create a 1/8 inch deep void for water to be encapsulated



Inner skin is laminated by hand



Vacuum bag is used to consolidate hand-laminated inner skin

**Figure 91. Test panel construction (continued)**

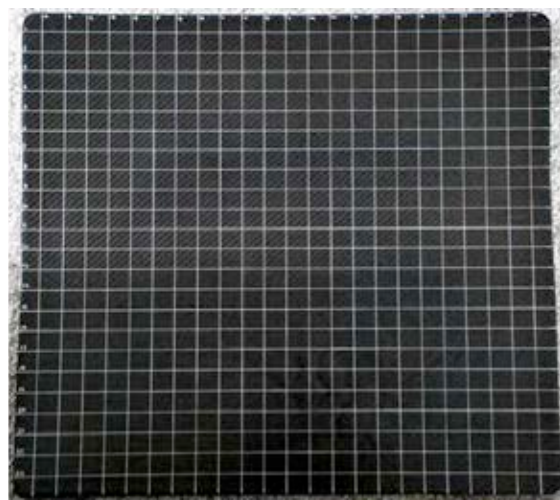
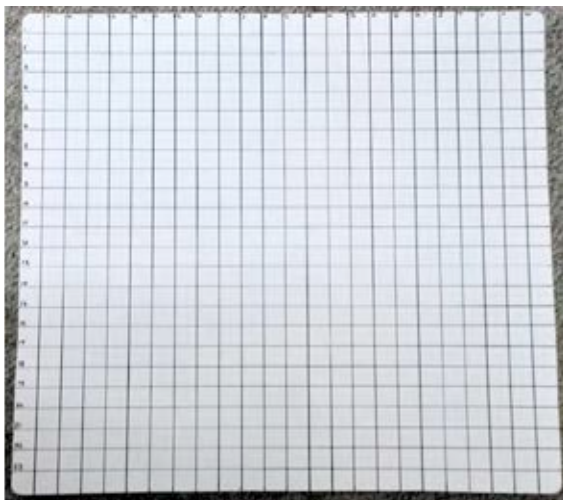


**Figure 92. E-glass panel (left) and carbon panel (right) with 1-inch grid drawn on outer skin to serve as reference for damage location identification.**

### 6.3 Induced Impact Damage

A simple drop weight impact device was developed for this program in order to induce internal damage to the test panels without causing visible surface damage. This allowed us to evaluate the efficacy of various NDE methods for detecting impact damage when visible inspection methods are inadequate. The impact testing was done at the U.S. Naval Academy Structures Laboratory with the assistance of Dr. Paul Miller. A variety of different composite panels were impacted with a range of impact energies. The damage location sites were selected randomly to facilitate “round robin” evaluation of the panels without a priori knowledge of the damage location sites.

#### Impact Tester Design

Based on studies reported earlier in this section, an impact test apparatus was designed that could deliver impact energies up to about 250 foot-pounds. Previous investigations [Hildebrand 1996] have shown that the shape of the impactor tip greatly influences the resulting surface damage. Since our goal was to avoid visible damage, an oval shaped impactor head was used. A rubber coated barbell weight was epoxied into a PVC tube to create the desired impactor, as shown in Figure 93.



**Figure 93. Rubber coated barbell is epoxied into PVC tube to form impactor**

The impactor delivery tube was made from a larger diameter PVC tube that accommodated a maximum drop height of 12 feet. The impactor was held in place by a halyard and snap shackle, as shown in Figure 94. Once the impactor was raised to the desired height, a separate lanyard was used to allow the weight to freefall. The impactor was allowed to completely exit the delivery tube, so secondary impacts were not direct hits on the target area. The delivery tube made it possible to accurately focus the impact event over a precise location on the grid pattern drawn on the surface of the test panels. Figure 95 shows the impact tester attached to the reaction frame in the Naval Academy’s Structures Laboratory. Note the added ceiling clearance in way of the tester that made it possible to accommodate a twelve foot drop height.



Figure 94. Detail of impactor release mechanism



Figure 95. Impact tester at the US Naval Academy Structures Laboratory

Impact Test Results

Since the goal impact testing was to produce damage that could not be detected by visual inspection, it was necessary to determine critical impact energies for each type of composite panel. We started with the Navy 44 deck laminate, as it represented a mid-range of panel durability. Using a trial impact energy of 245 foot-pounds produced visible indent damage near the center of the panel. A drop at 132 ft-lbs near the edge produced only damage in the core. Based on these results, 200 ft-lbs was used as the upper limit for most of the test panels. This value was adjusted based on our perceived durability of each particular panel.

A total of twelve panels were subjected to impact damage. Ten of these were the USNA panels and two were the panels built by Osprey Marine, one E-glass and the other carbon fiber. Each panel was subjected to low, medium and high impact energies at random locations. Table 10 provides a summary of impact energies used for each panel.

**Table 10. Impact energies used to damage test panels**

Panel	Impact Energy, ft-lbs			Comments
	Low	Med	High	
USNA 1	25	50	100	Panel had existing damage along bottom edge
USNA 2	25	35	50	
USNA 3	75	100	150	
USNA 4*	100		150	Panel had existing core damage; 150 ft-lb hit destroyed core
USNA 5*	25		50	
USNA 6	200		250	
USNA 7*	25	75	100	Surface dent visible after 100 ft-lb hit
USNA 8*	50	75	150	Surface dent @ 150 ft-lbs; barely visible damage (BVD) @ 75 ft-lbs
USNA 9	25	50	75	75 ft-lb hit was over previous damage; BVD @ 50 ft-lbs
USNA 10	50	75	100	Core shear at the edge of the panel @ 100 ft-lbs
Osprey 4	100	150	200	
Osprey 8	25	50	150	Visible surface cracking @ 150 ft-lbs; BVD @ 50 ft-lbs
* these panels were not retained for use in the NDE round robin test program				

## 7. Test Panel NDE

The section describes the NDE techniques used to evaluate defects in our test panels.

### 7.1 Laser Shearography

Panels were examined using laser shearography on September 8, 2011 at Laser Technology, Inc. The testing was conducted in their vacuum chamber, as shown in Figure 96. The panels were stressed either by vacuum or with heat lamps. All of the equipment was remotely operated (including positioning) from outside of the chamber.

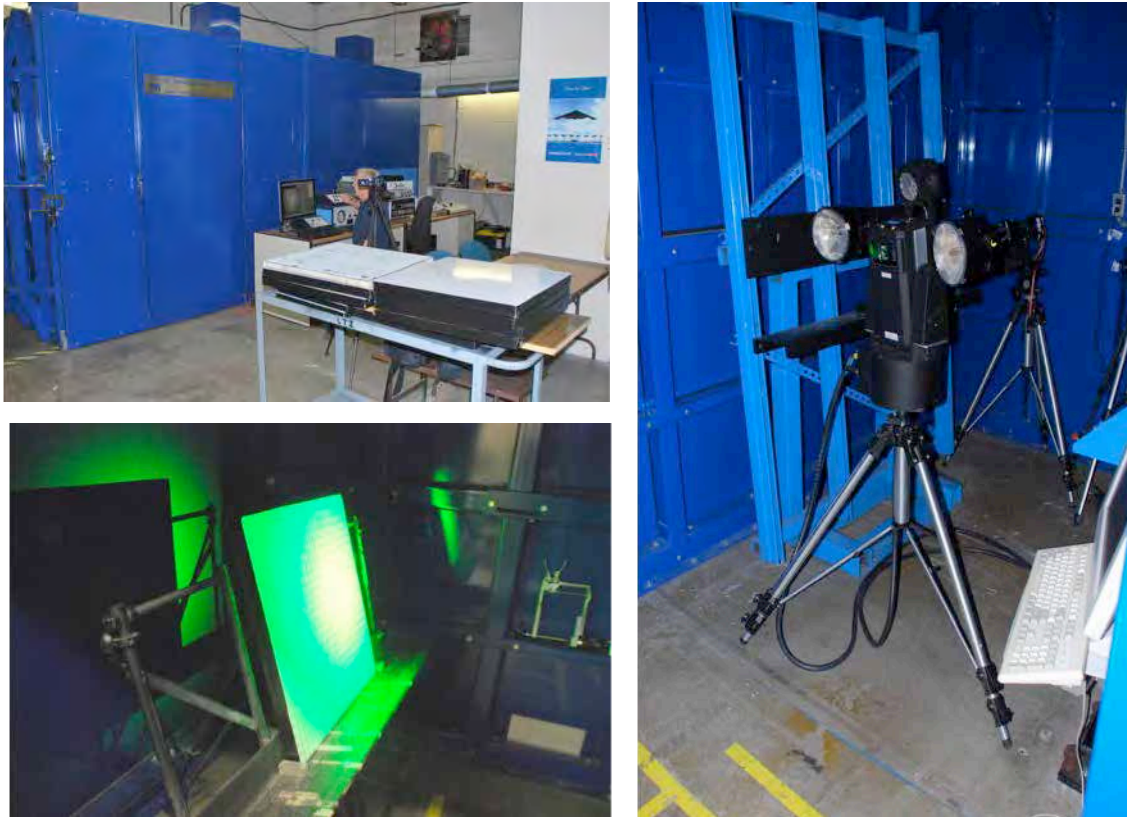


**Figure 96. Vacuum chamber used to stress parts of various geometries (upper left); test panel with laser shearography optics focused on the surface (lower left); and laser shearography camera (right) [author photos]**

The general procedure for laser shearography NDE is as follows:

1. Focus on panel surface in unstressed state
2. Take reference image
3. View changes while ramping up vacuum or thermal insult
4. Freeze resulting image, interpret and store

Figure 97 through 105 illustrate the defects in the evaluated test panels and the results of the laser shearography evaluation effort. Shearography proved to be a very effective NDE tool for marine composite construction, except with panels built using clear gel coat that required the application of a coating to restrict the laser light from transmitting through the laminate.

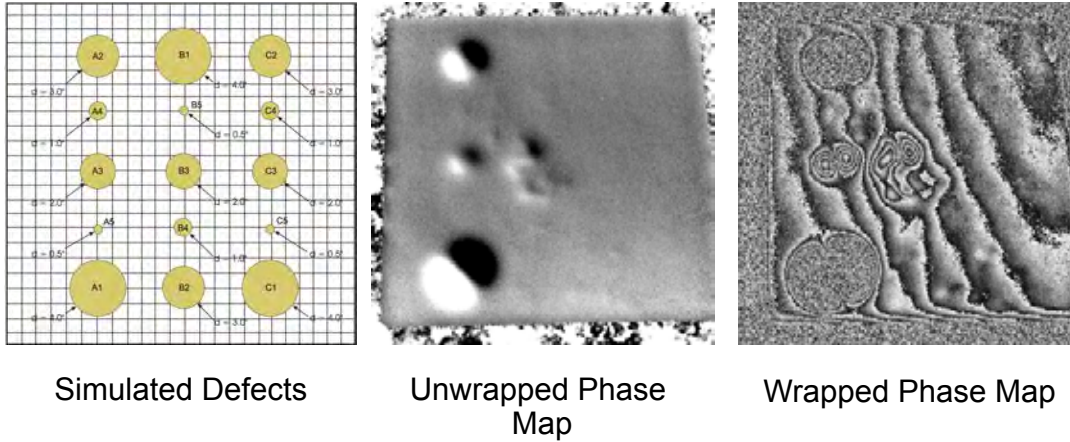


Figure 97. Panel "Osprey 1" with simulated delaminations and shearograms

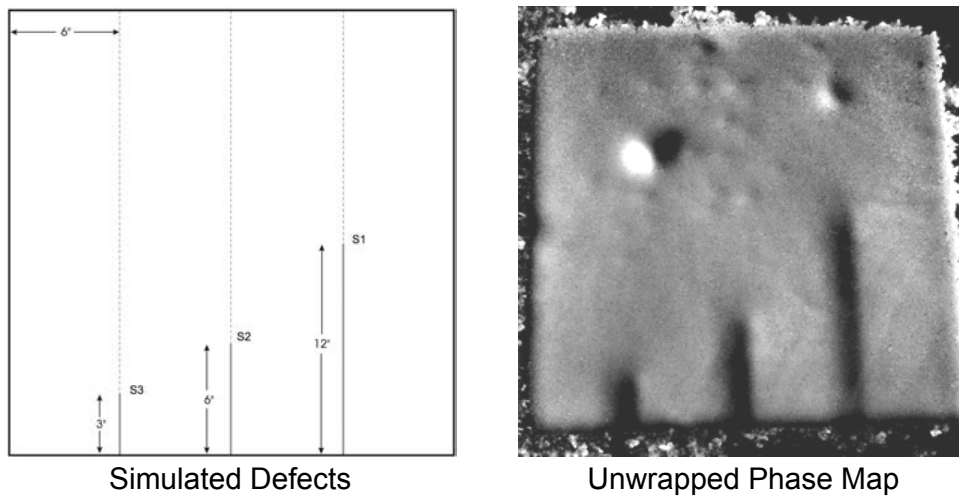


Figure 98. Panel "Osprey 3" with simulated core shear and shearograms

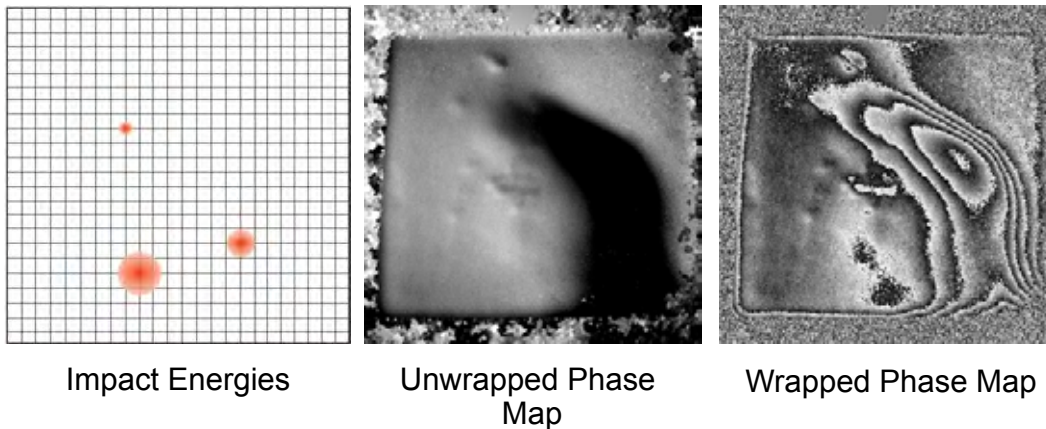


Figure 99. Panel "Osprey 4" with induced impact damage and shearograms

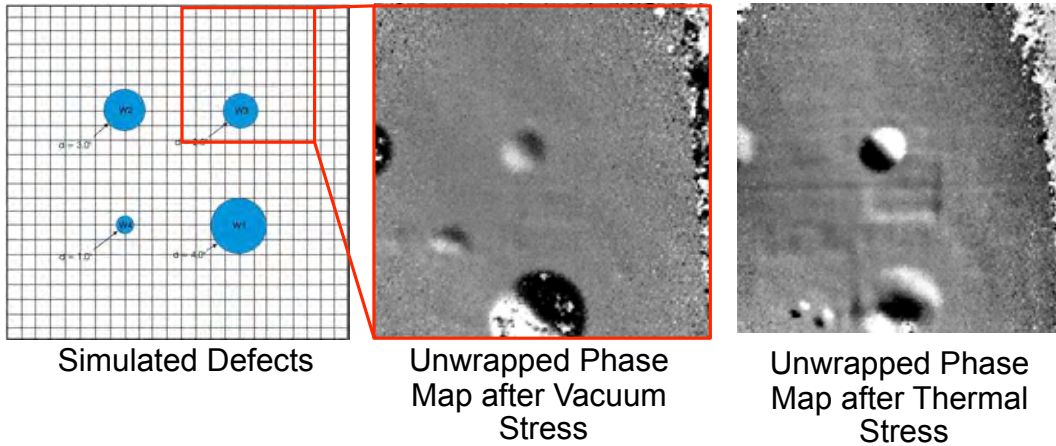


Figure 100. Panel “Osprey 6” with simulated water ingress and shearograms

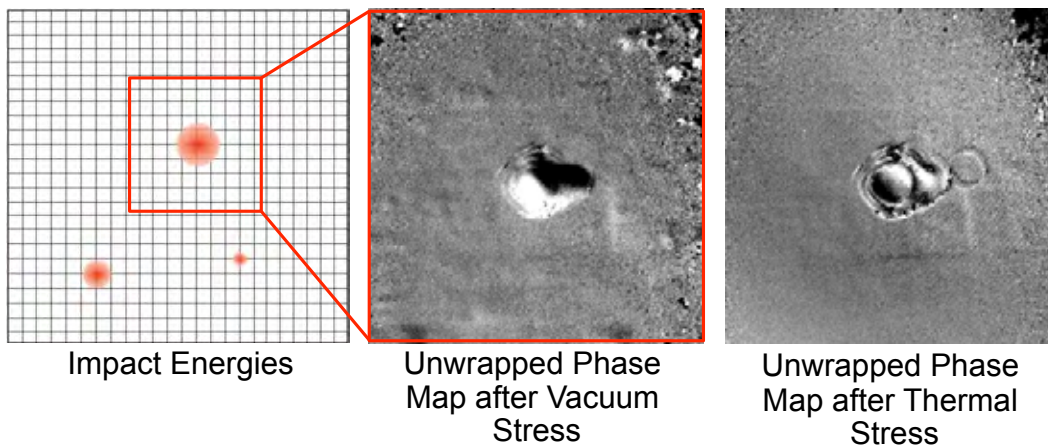


Figure 101. Panel “Osprey 8” with induced impact damage and shearograms

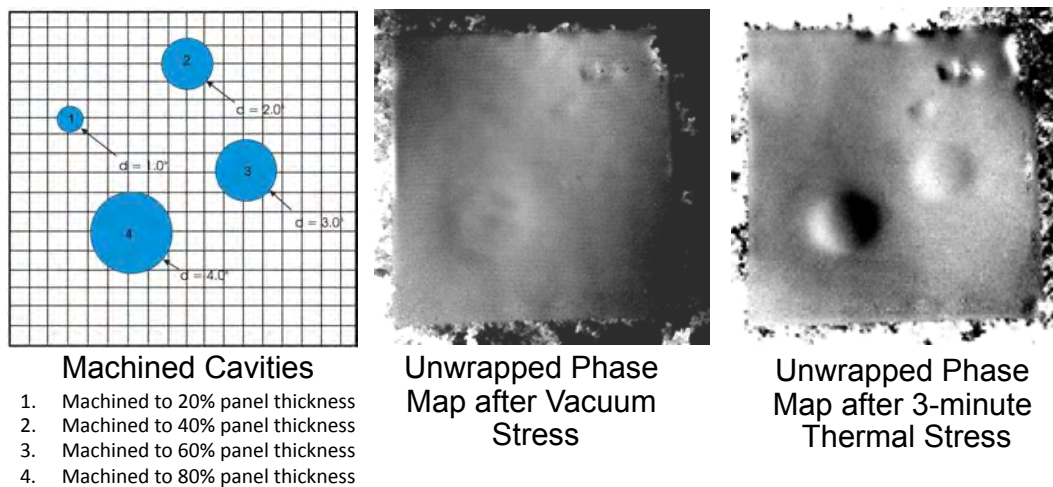


Figure 102. Panel “Pearson 4” with machined back-face cavities and shearograms

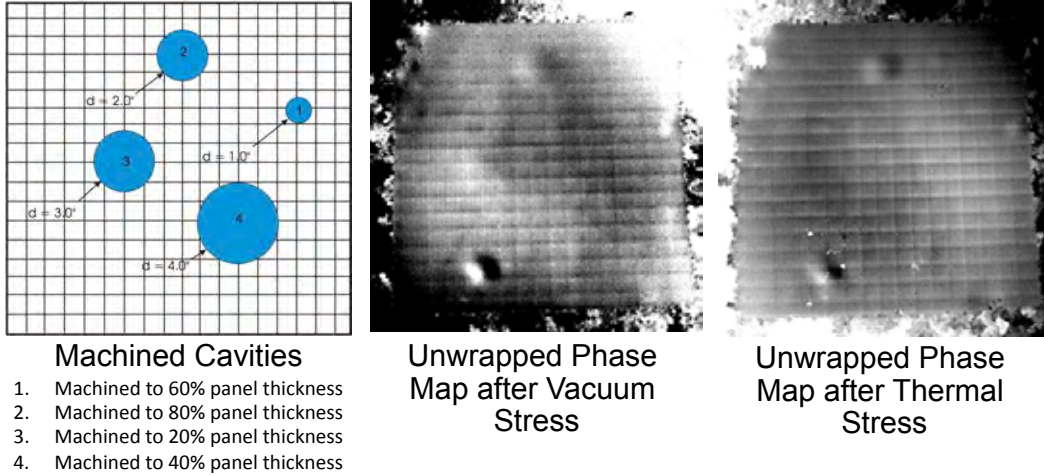


Figure 103. Panel “Pearson 6” with machined back-face cavities and shearograms

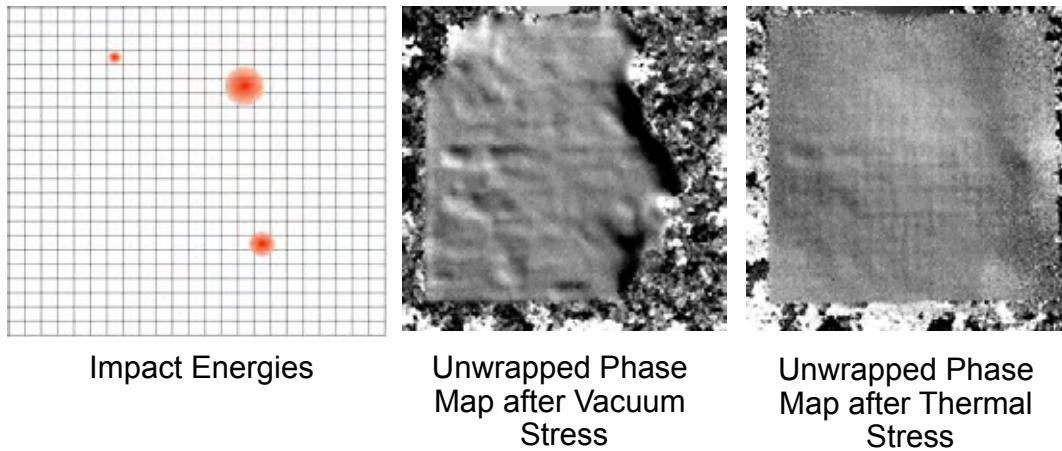


Figure 104. Panel “USNA 3” with induced impact damage and shearograms

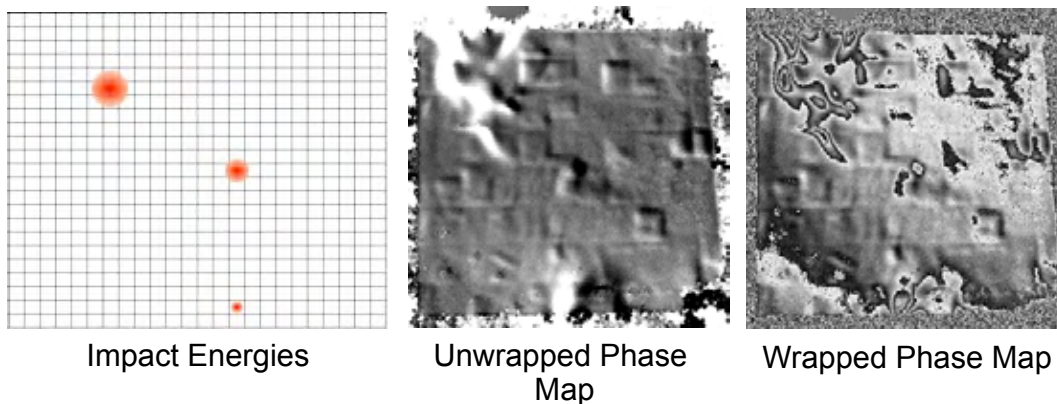


Figure 105. Panel “USNA 10” with induced impact damage and shearograms

## 7.2 Ultrasonic Inspection

Four test panels were evaluated on September 13, 2011 at Imperium, Inc. using their i600 Acoustocam PE portable ultrasonic NDE equipment based on digital acoustic video camera technology. The i600 uses a patented Application Specific Integrated Circuit (“ASIC”) called DAV. This chip is an imaging array for ultrasound similar to the approach used for conventional digital cam recorders. The Acoustocam is designed for non-specialized users featuring a touch-screen graphical user interface that operates on top of Microsoft Windows<sup>®</sup> XP. Figure 106 shows the Acoustocam equipment being used to evaluate



**Figure 106. Acoustocam i600 used to inspect a project carbon fiber panel with simulated delaminations [author photo]**

Figures 107 through 109 show saved A-scan and C-scan images for the defects shown in the figures.

In general, UT was not shown to be an effective method for surveying large areas of marine composite construction but was effective to quantify the extent and depth of defects at known damage sites.

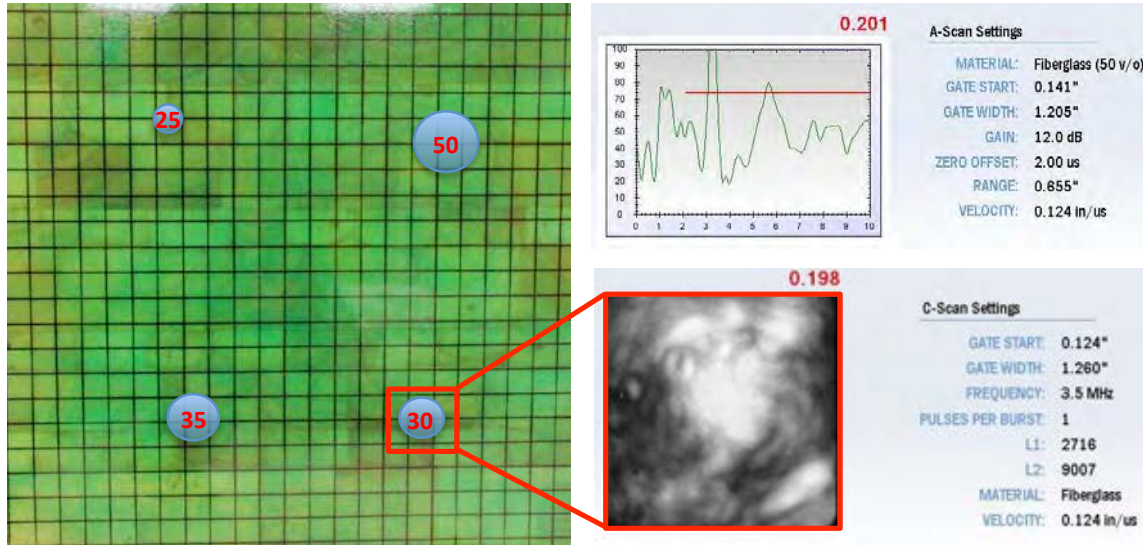


Figure 107. Impact energies on E-glass laminate (left) and corresponding ultrasonic NDE data (right) [data courtesy of Imperium, Inc.]

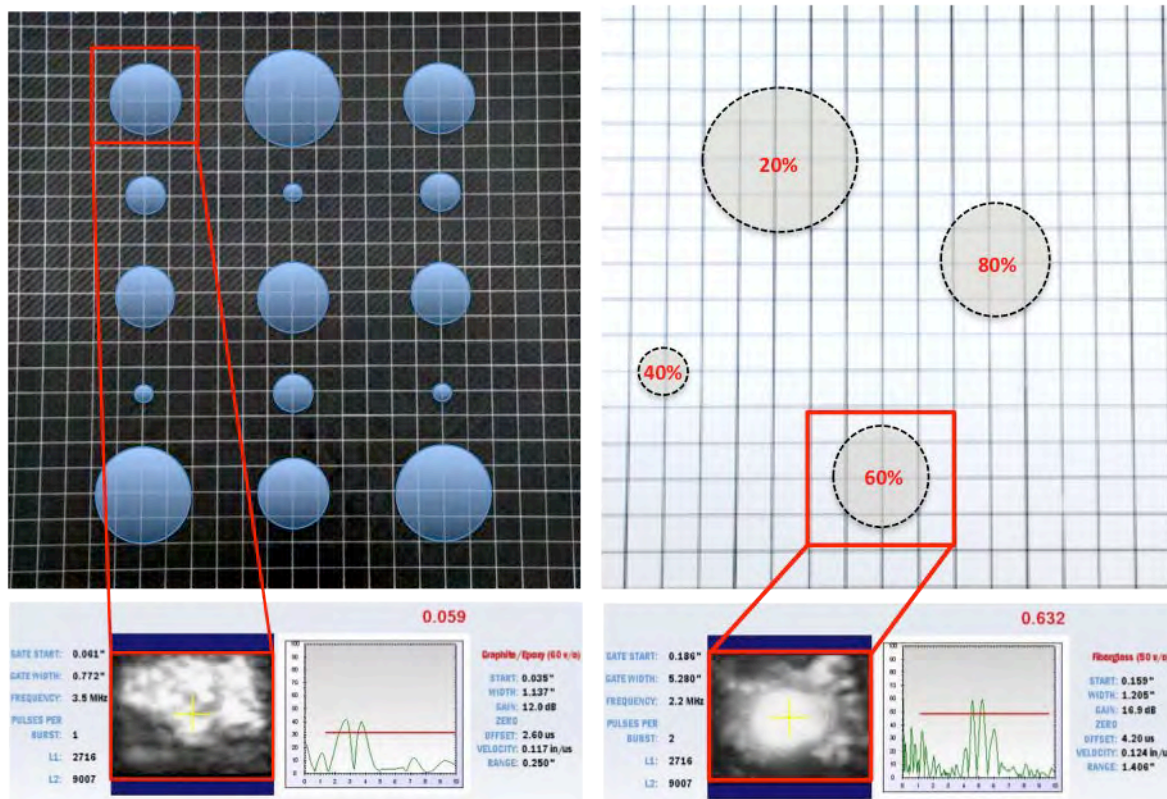


Figure 108. Simulated delamination damage (top) and corresponding ultrasonic NDE data (bottom) [data courtesy of Imperium, Inc.]

Figure 109. Machined cavities (top) and corresponding ultrasonic NDE data (bottom) [data courtesy of Imperium, Inc.]

### 7.3 Infrared Thermography

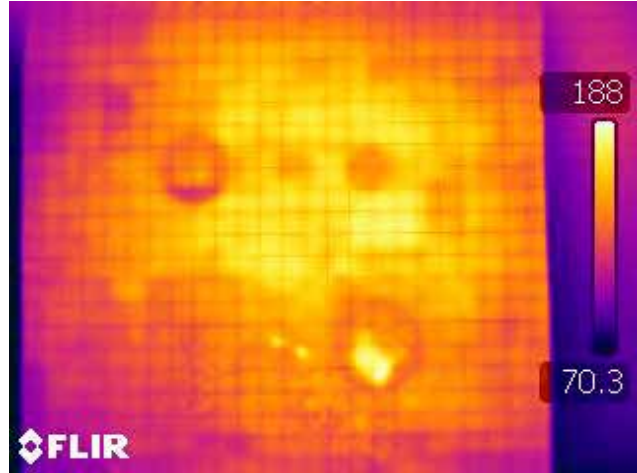
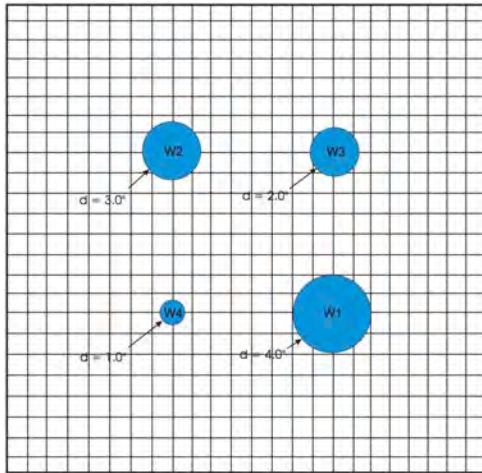
Fourteen test panels were examined using infrared thermography by Mark Ashton of Independent Marine Systems on September 26, 2011. The inspection took place in a storage shed at the New England Boatworks facility in Portsmouth, RI to ensure a uniform ambient temperature and minimize reflected light on the panels. The panels were uniformly heated and analyzed with an FLIR T300 infrared camera, as shown in Figure 110.



**Figure 110. Mark Ashton is shown capturing (left) and analyzing the IR image (right) [author photos]**

Figures 111 through 114 show photographs and diagrams of damaged panels and the resulting infrared thermograms from Independent Marine Systems. The heat was applied to the panels in a uniform manner but over varying timeframes to achieve optimal thermal response. The edges of the panels are not representative of most marine composite structures and therefore produced some anomalies in the IR data.

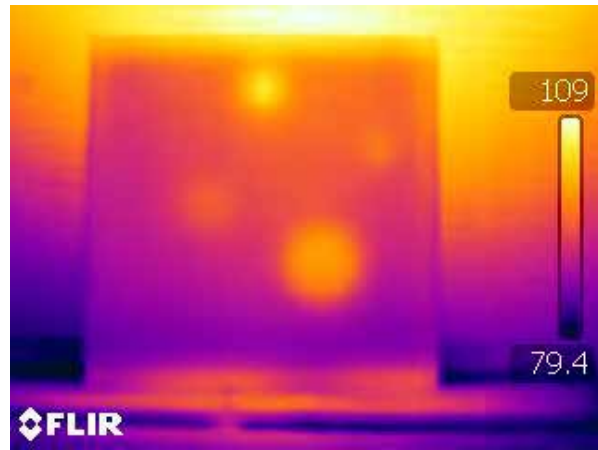
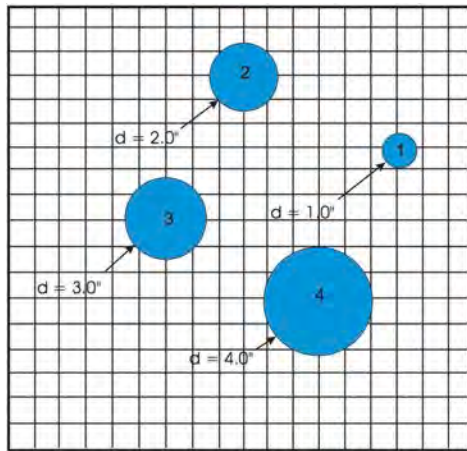
Figure 111 shows that moisture ingress was easily detected using infrared thermography. All of the water pockets embedded in the core showed up in the thermogram. Figure 112 illustrates that IR NDE was also very effective for finding delaminations in thick laminates, even over  $\frac{3}{4}$  of an inch below the surface. Figure 113 and 114 showed that IR can be an effective tool to determine the extent of impact damage when the surface has been punctured. We did not have as much success finding internal impact damage when there was no visible surface damage. IR NDE also had a difficult time finding “kissing bonds,” which were simulated in Osprey panels 1 and 5 by placing peel ply in the laminate stack.



Simulated Defects

Thermogram

Figure 111. Panel “Osprey 6” with simulated water ingress and thermogram



Machined Cavities

Thermogram

1. Machined to 60% panel thickness
2. Machined to 80% panel thickness
3. Machined to 20% panel thickness
4. Machined to 40% panel thickness

Figure 112. Panel “Pearson 6” with machined back-face cavities and thermogram

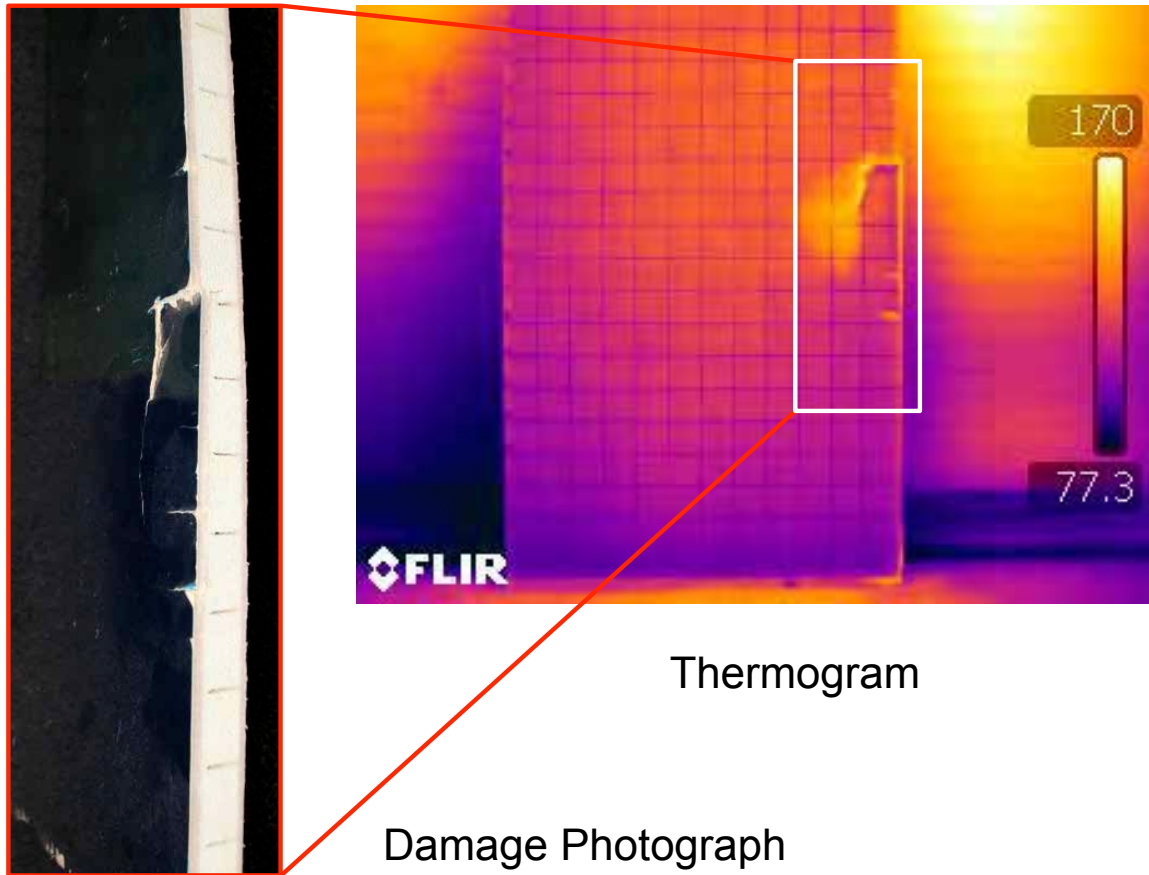


Figure 113. Panel "USNA 3" with impact damage and thermogram

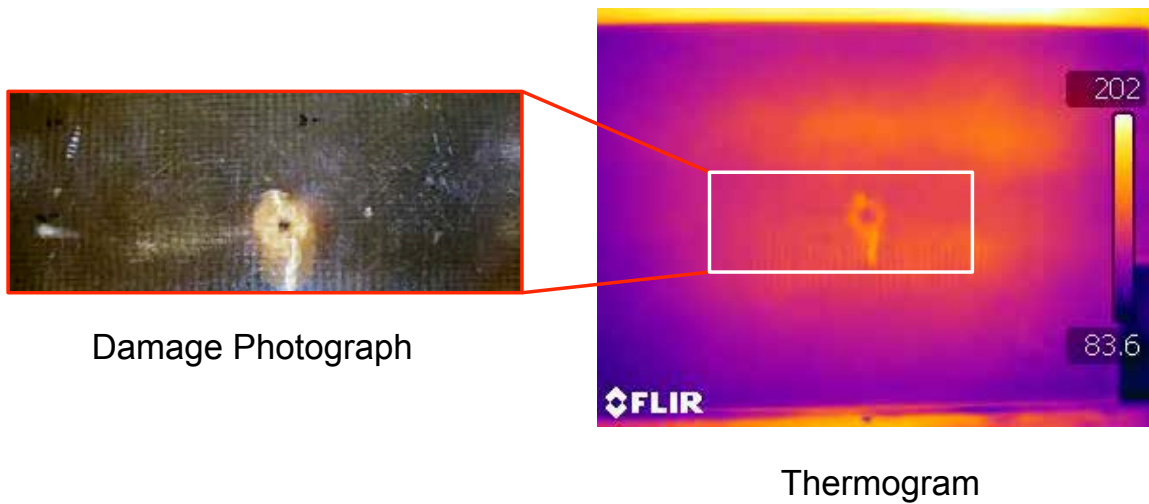
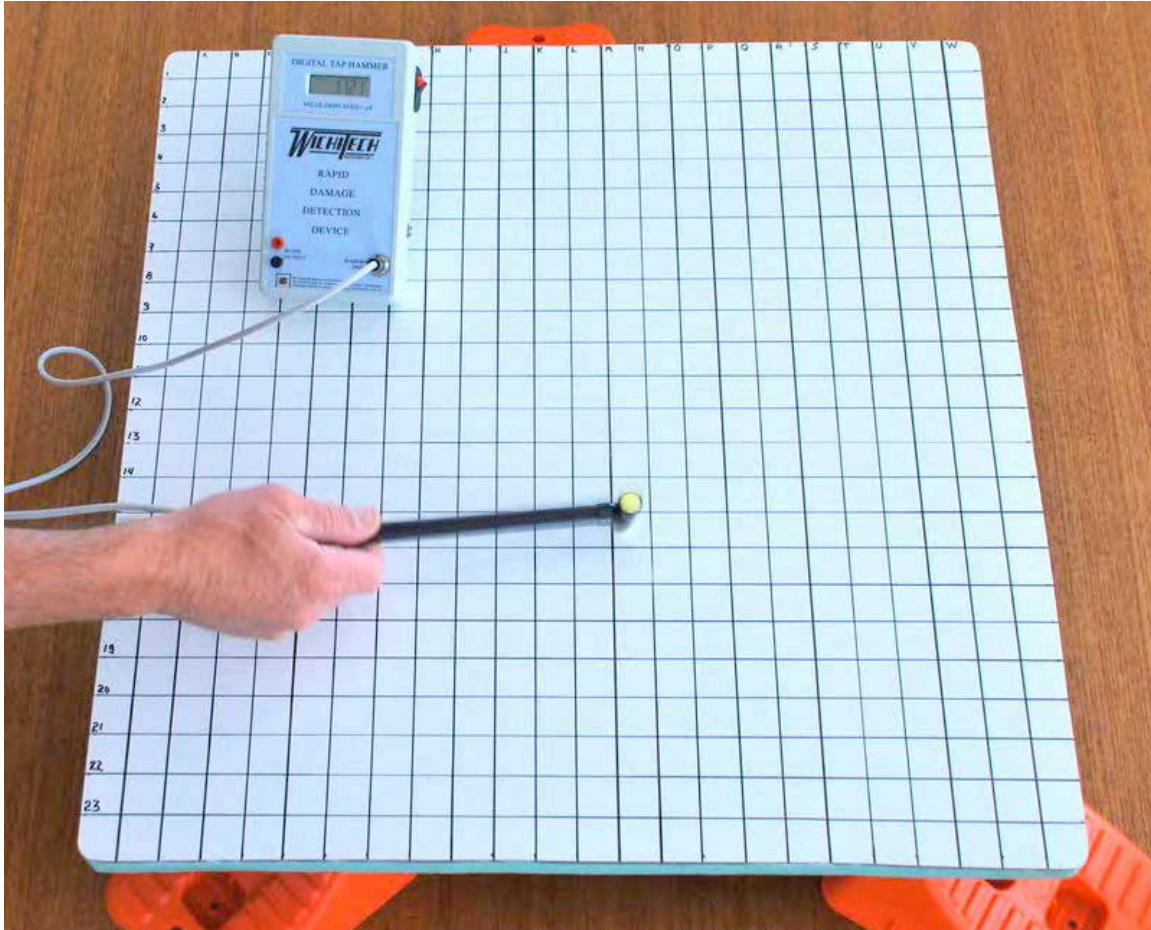


Figure 114. Panel "USNA 6" with impact damage and thermogram

#### 7.4 Digital Tap Hammer

On September 19, 2011 the project test panels were evaluated at Eric Greene Associates, Inc. using a WichiTech RD<sup>3</sup> (Rapid Damage Detection Device) digital tap hammer.

Figure xx shows the digital tap hammer being used to evaluate an Osprey E-glass panel. Note that the panels were supported by plastic stands at three points.



**Figure 115. Digital tap hammer being used to evaluate an Osprey E-glass panel [author photo]**

Table 11 shows the test panels evaluated with the digital tap hammer and anomalies that were detected.

The results observed were similar to experience the author observed in the field. Namely, only delaminations of at least two by two inches are detectable with the device. The digital tap hammer is particularly effective for detecting skin to core separations in sandwich laminates and is certainly an improvement over conventional coin or hammer tapping methods.

**Table 11. Effectiveness of digital tap hammer**

<b>Panel I.D.</b>	<b>Defect or Damage Type</b>	<b>Damage Detected</b>	<b>Comment</b>
Osprey 1	Delamination in E-glass panel	yes	only largest delaminations
Osprey 2	Water Ingress in E-glass panel		
Osprey 3	Core Shear in E-glass panel		
Osprey 4	Impact Damage in E-glass panel	yes	not at impact site
Osprey 5	Delamination in carbon fiber panel		
Osprey 6	Water Ingress in carbon fiber panel	yes	only largest cavity
Osprey 7	Core Shear in carbon fiber panel	no	
Osprey 8	Impact Damage in carbon fiber panel		
Pearson 4	Void simulated by back-face machining	no	
Pearson 5	Void simulated by back-face machining	no	
Pearson 6	Void simulated by back-face machining	no	
Pearson 7	Void simulated by back-face machining	no	
USNA 1	Impact	no	visible damage detected
USNA 2	Impact	no	
USNA 3	Impact	yes	edge delaminations found
USNA 6	Impact	no	
USNA 9	Impact	no	
USNA 10	Impact	yes	only edge delams found

## 8. Case Studies

This section provides case studies of NDE techniques used to evaluate marine composites.

### 8.1 Laser Shearography

Laser Technology, Inc. claims that it has performed Shearography inspection surveys on 70 boats under 250 feet and 12 boats over 250 feet. Shearography NDE during construction serves to validate or corrects process control, reduces risk of loss and lowers builder's liability and warranty costs. Shearography has also been used to determine the extent of damage after an accident.

#### 8.1.1 RNLI Lifeboats

The Royal National Lifeboat Institution (RNLI) in the United Kingdom has a long history of using NDE on composite structures. Laser Shearography has been used for the inspection of new all weather lifeboats since the mid 1990s and has proved to be reliable and effective. Large areas can be inspected quickly making it reasonably cost effective. [Sheppard 2009] Lifeboats are inspected when constructed and as part of life cycle management and monitoring. In these instances the structures are only inspected from the outer surface since due to the construction method this is historically where most defects have occurred.

Where possible a vacuum hood is used to induce stress into the test surface, as shown in Figure 116. This is because the hood anchors firmly to the test surface and prevents de-correlation of the image caused by any movement of the test subject relative to the inspection head. A free-standing camera and stressing by heat is used on the smaller hulls and where the highly curved geometry limits the use of a vacuum hood.



**Figure 116. Vacuum hood used to test flat panel portions of RNLI lifeboat hulls [Laser Technology, Inc.]**

The builder of the RNLI Severn class lifeboat, Green Marine, has found that it is cost effective to find and repair faults immediately after joining of the hull sides before internal bulkheads and equipment are fitted. Figure 117 shows laser shearography

images for bonded and disbonded portions of the topside laminate, also shown in the figure. Figure 118 illustrates how NDE can be used as a Quality Assurance tool during fabrication.

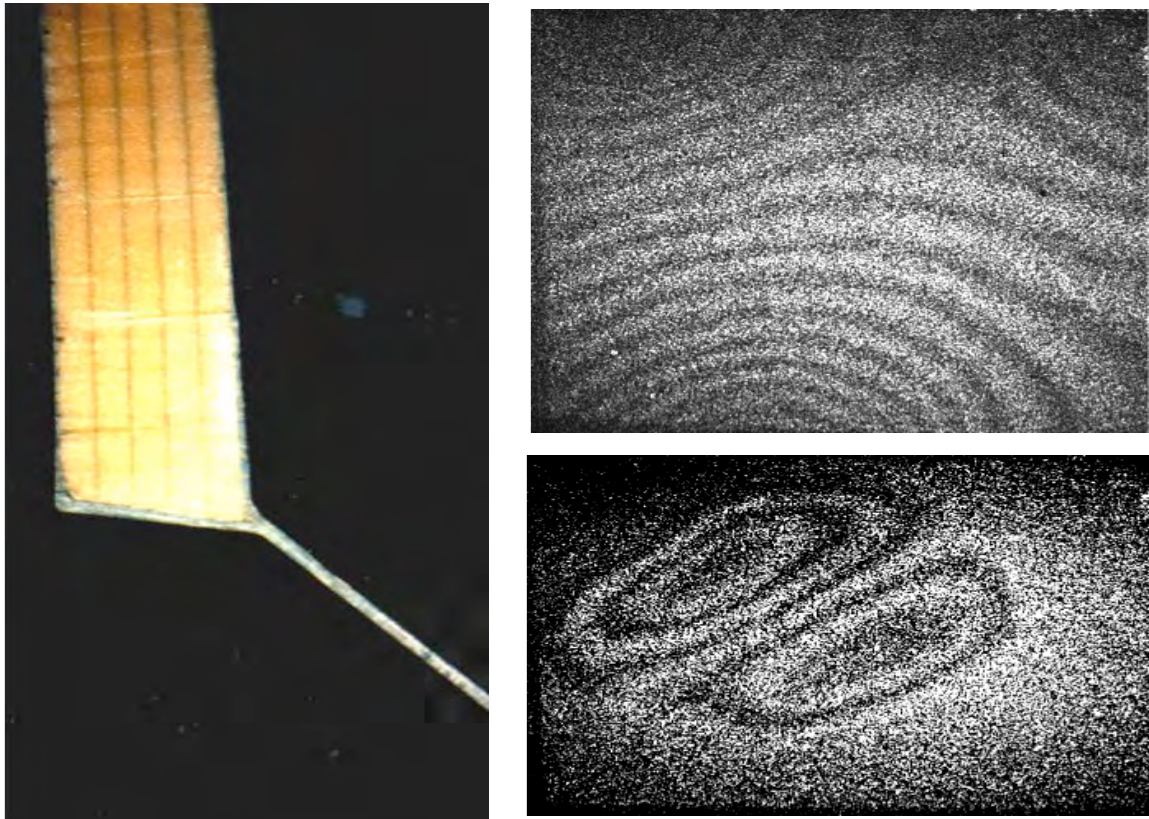


**Figure 117.** RNLi Severn class topside hull section (left) along with bonded (top) and disbonded (bottom) shearography images [Laser Technology, Inc.]

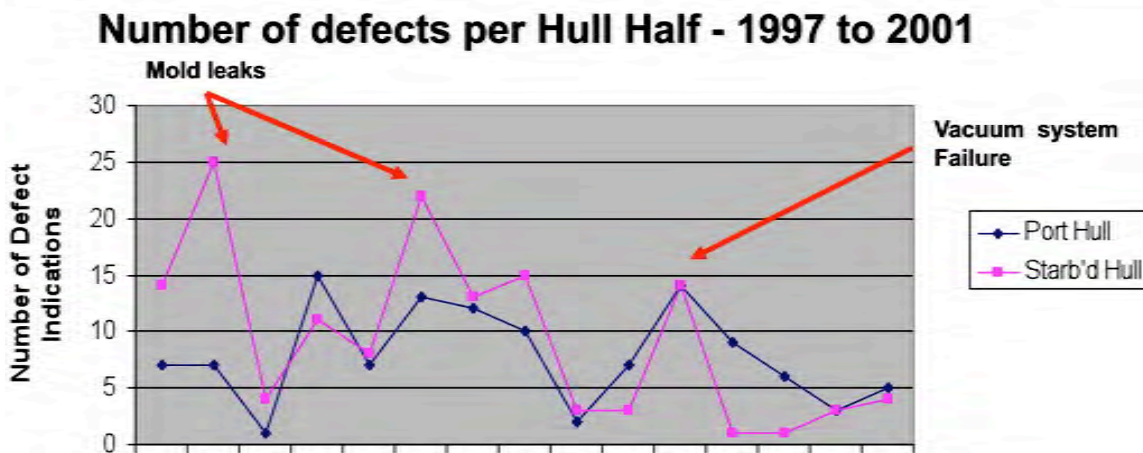


**Figure 118.** RNLi Severn class detected hull defects over time highlights systematic process failures during fabrication [Laser Technology, Inc.]

### 8.1.2 Damaged Yacht Hull

A maxi sailing yacht was severely damaged during a storm while being transported as deck cargo. Laser shearography was used to help determine the extent of damage in order to develop a repair plan. While there was clearly visible damage to the exterior of the sandwich hull laminate, shearography NDE revealed that the extent of damage was much greater than originally anticipated. Figure 119 shows the visible damage and the extent of damage discovered using shearography.



**Figure 119. Full extent of internal damage to hull sandwich construction [Laser Technology, Inc.]**

The deck area in way of the damage was also inspected using shearography after the teak overlay was removed. Although the deck was only inspected from above, it was possible to determine which bulkheads were attached to the underside of the deck.

### 8.2 Infrared Thermography

Thermal Infrared Technology is often used to inspect composite vessels for moisture ingress, delamination, disbonding, fractures and other defects from vessel construction or in-service damage. As the cost of infrared cameras has come down, a number of marine surveyors across the country have adopted this NDE tool. Racing boats that use lightweight, sandwich construction are good candidates for IR inspection to determine the extent of moisture ingress, which can compromise structural integrity or as a minimum, reduce the competitiveness of the hull because of weight gain.

### 8.2.1 Void Detection

Thermography can be used as part of a Quality Control program to quickly and effectively locate and document voids in Fiberglass Reinforced Plastic laminates. The surface temperature of the FRP is artificially raised in discrete sections with a gentle stream of warm air (approximately 45°C) supplied by an electric hot air heat gun, while the surface is simultaneously scanned with an infrared camera that is capable of capturing radiometric images either as single images or in burst recording mode. As each section of the hull surface is “painted” with a gentle, rhythmic sweeping motion of warm air, the “real time” differences in the surface temperature of the laminate is visually observed on the infrared camera’s LCD screen. Areas where voids are present in the FRP laminate warm quickly while the homogeneous and “void free” laminate surrounding the void remain cooler due to its ability to act as a more effective heat sink. [Allinson, 2007] Figures 120 and 121 show examples of thermography used to find voids in a newly constructed yacht.

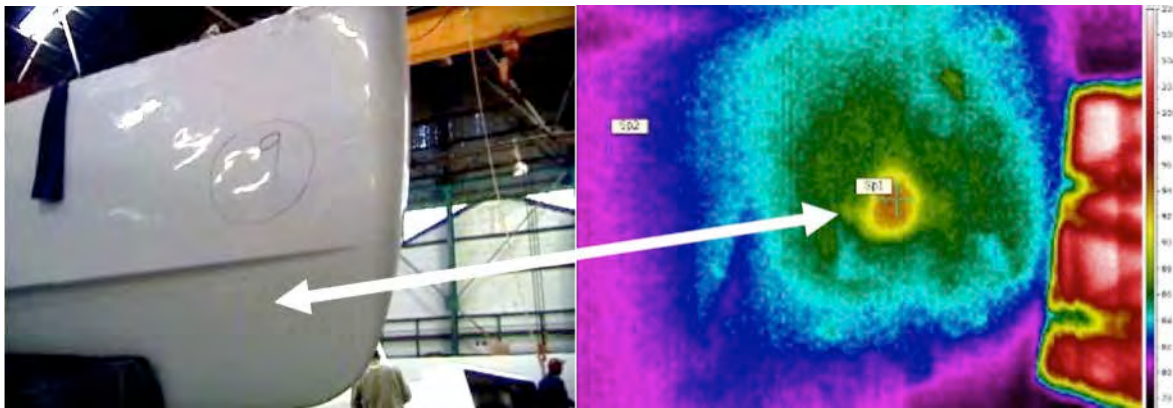


**Figure 120. The surface looks free of defects using visible NDE (left) but thermal pattern shows anomaly when the hull is gently warmed by an electric hot air gun [J.N. Allinson Associates, Inc.]**

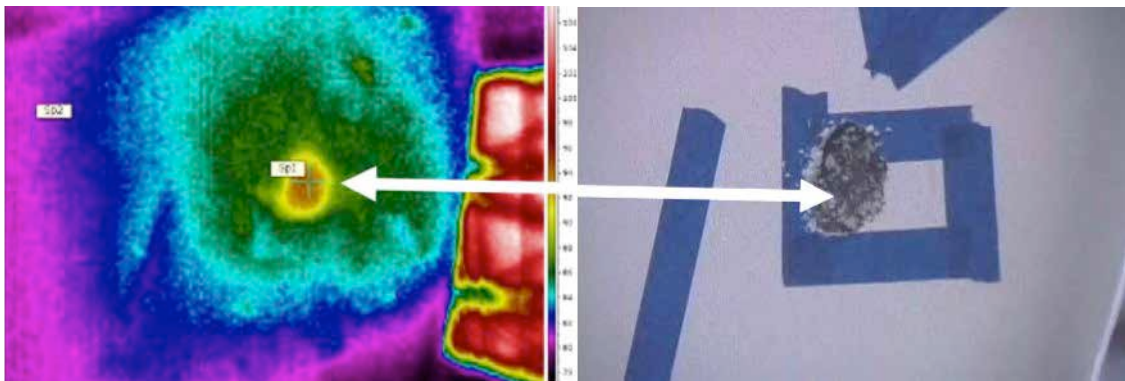


**Figure 121. Thermographic image of void in gel coat confirmed by percussion sounding followed by grinding it out for repair [J.N. Allinson Associates, Inc.]**

### 8.2.2 Extent of Damage

Thermography can also be an effective NDE tool for determining the extent of damage to a composite boat hull prior to repair. In the following example, hull shell laminate failures were noted in areas near the engine girders. The vessel was undergoing a total rebuild of the engine girder support system and the extent of the hull damage needed documentation in order to develop a repair plan. The infrared imaging conducted on the boat revealed subsurface anomalies consistent with delamination of the core from the hull outer skin or intra-laminate delamination due to excessive hull flexure. The IR survey also showed areas of good laminate that were previously marked as suspect based on percussion sounding. Figures 122 and 123 show IR and visual images of the hull laminate.

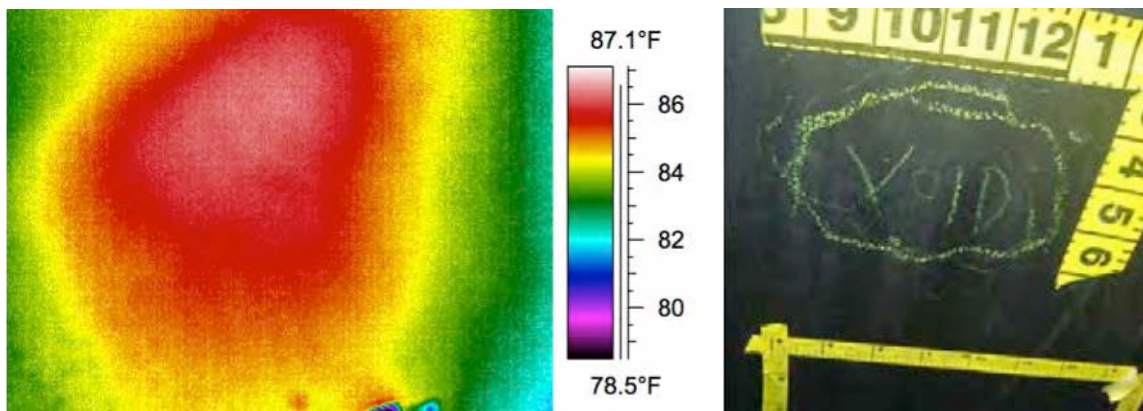


**Figure 122. Red and white areas indicate anomalies consistent with warm air trapped between hull skin and core or between layers of the laminate [Todd Associates, Inc.]**

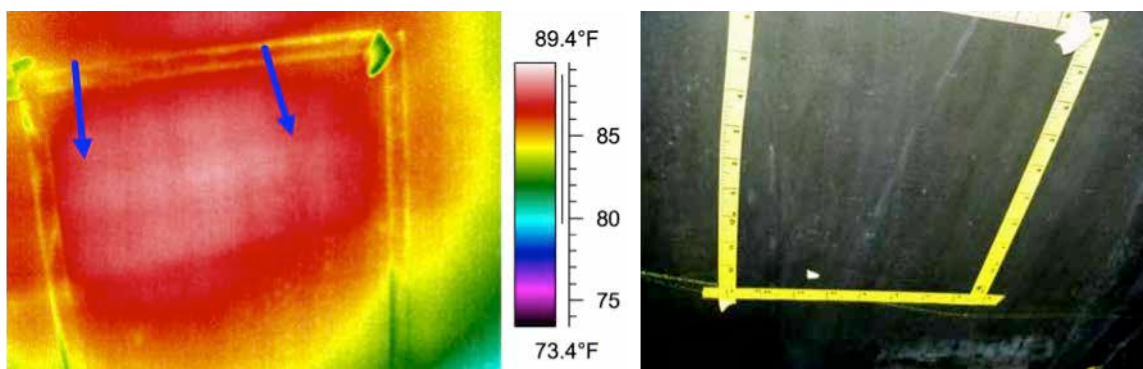


**Figure 123. Infrared image above indicates good contact between outer skin and core as indicated by clearly visible nondestructive kerf lines. [Todd Associates, Inc.]**

### 8.2.3 Water Ingress

The majority of composite boats are now built using sandwich construction to minimize weight. All penetrations of the sandwich skins are potential areas for water ingress, making this a major defect of concern to vessel owners. Numerous yachts have been examined by Independent Marine Systems of Newport, RI with a Raytheon Pro 400D digital thermal infrared camera to determine the extent of water ingress in hull laminates. Figures 124 through 126 show thermographic images that indicate the extent of water ingress for a variety of yachts. In many instances, water ingress was confirmed by either destructive testing (hole saw samples) or during the course of repair.



**Figure 124.** This IR image shows that moisture ingress on the starboard side of the keel box has not migrated further than the local area. The red arrows show laminate anomalies that were confirmed to be “resin starved” areas. [Independent Marine Systems]

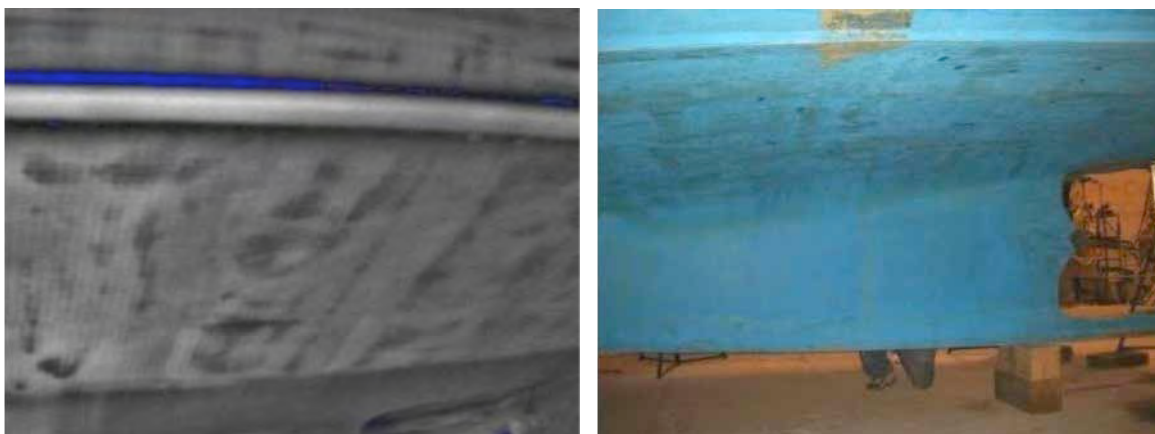


**Figure 125.** This vessel had anomalies on the entire port side of the hull bottom that were characteristic of moisture ingress. Two hole saw samples were taken and both sampled areas produced water when drilled into. [Independent Marine Systems]

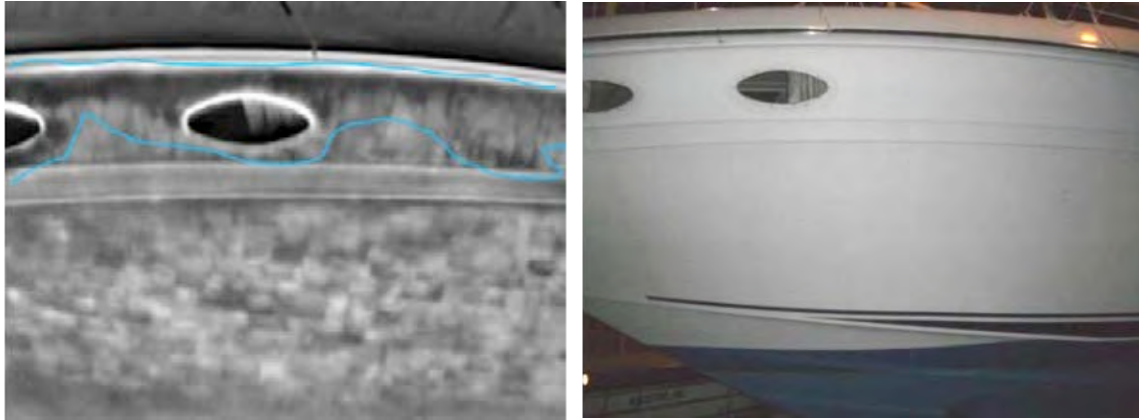


**Figure 126. The dark colored anomaly noted with the blue lines is characteristic of moisture (moisture ingress was first found when the hull ports were removed).  
[Independent Marine Systems]**

### 8.3 Ultrasonics

Ultrasonic inspection of marine laminates is often not appropriate unless there is prior knowledge of suspected damage. That is because survey probes measure about one inch, which would make survey of an entire hull very time consuming. Ultrasonic inspection also requires a good calibration block as a reference, so laminates that vary in thickness can be problematic. With that said, carbon fiber masts built with autoclave-cured prepregs are very high-value components that warrant ultrasonic inspection. They typically have uniform wall thickness (except in reinforcement areas), which facilitates instrument calibration. Ultrasonic NDE inspection of masts is particularly appropriate after a lightning strike, as this case history will illustrate.

A 70-foot racing sailboat was struck by lightning, as evidenced by charring noticed around the VHF antenna, at the chainplate grounding strap and in an area at the keel. An ultrasonic inspection was conducted on 100% of the mast except where fittings or attachments precluded placement of the transducer on composite. An ultrasonic flaw detector in conjunction with a 0.5 MHz, 1-inch diameter probe was utilized to accomplish the inspection. A secondary probe (2.25 MHz, ½ inch diameter ZIP variety) was also utilized to inspect the masthead spinnaker halyard sheave box. Velocity calibration was accomplished on a free edge at the base of the mast (where there was an inspection/access port).

Two areas were determined to contain delaminations. The first area was located at the attachment point of the second spreader bar on the starboard side. It was determined that delamination occurred between the mast and the internal sleeve directly below the external reinforcement, as shown in Figure 127. The second area containing delamination was the secondary reinforcement at the masthead spinnaker halyard sheave box, shown in Figure 128. [Bandos, 2002]

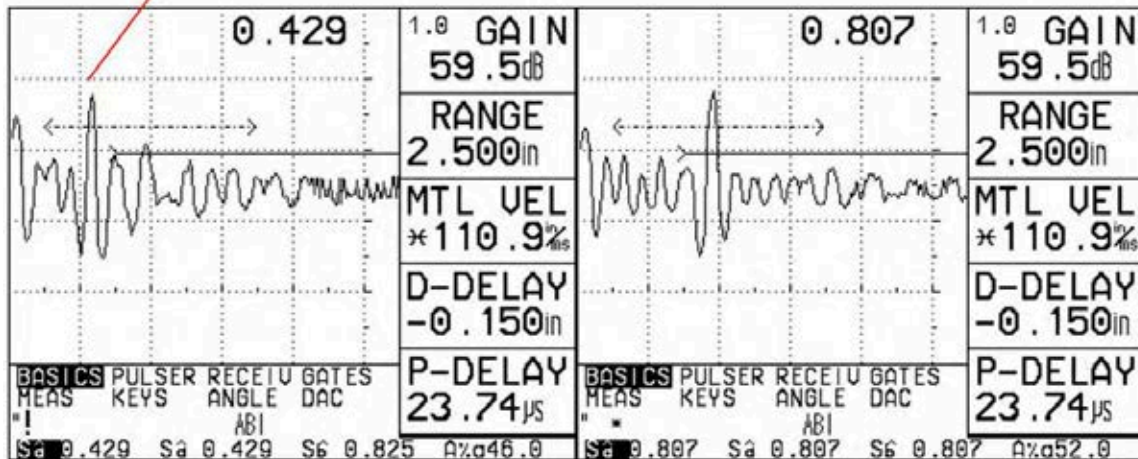


**Figure 127. The captured UT waveform from directly beneath the second starboard spreader (left) indicates the delamination is 0.429 inch from the surface, which is between the mast and the internal sleeve. The waveform from the port spreader (right) shows no ultrasonic reflections from any interfaces [Bandos, 2002]**

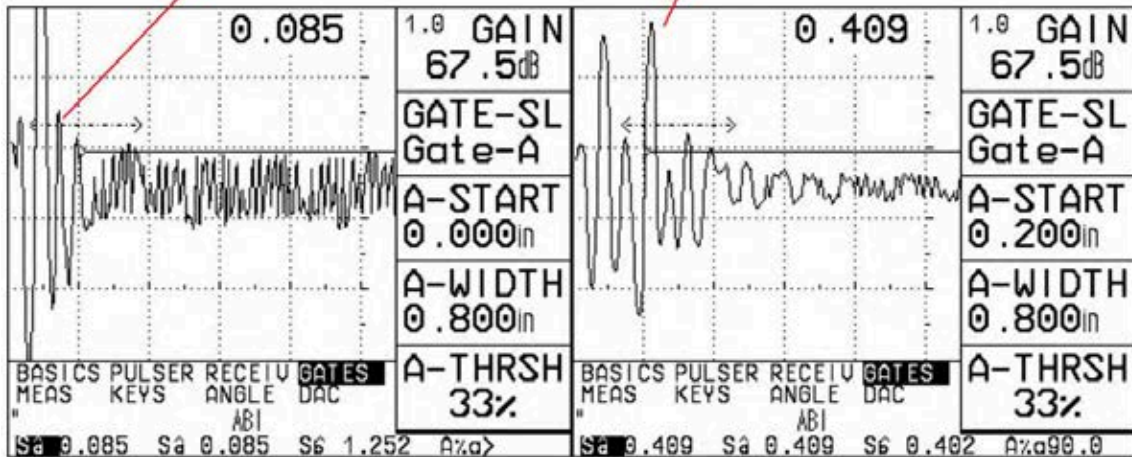
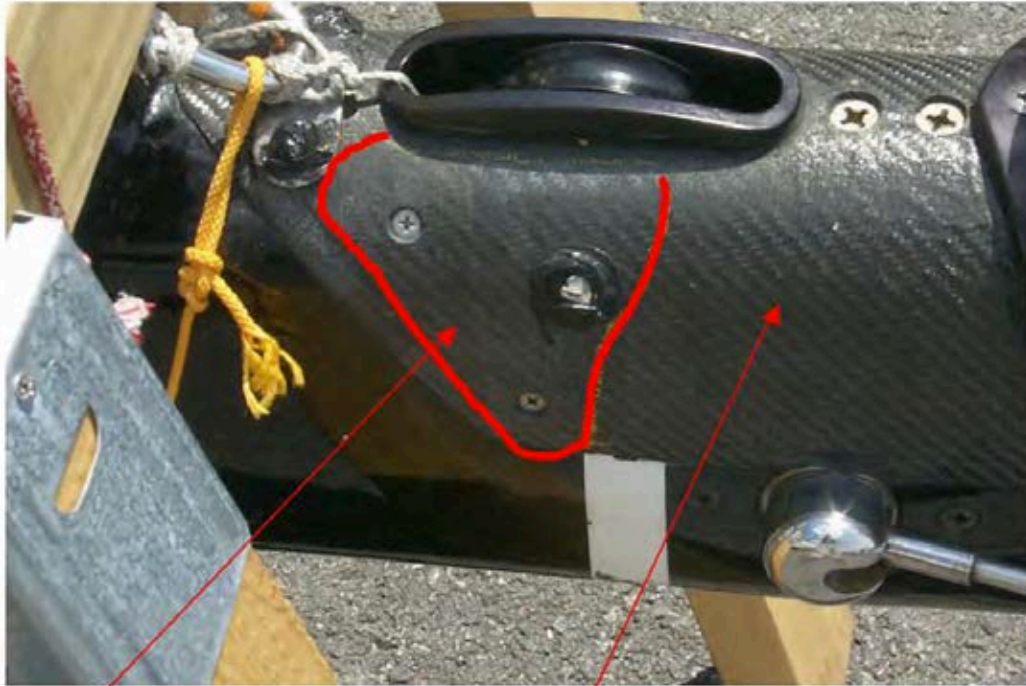


**Figure 128. The top reinforcement layer in this area is delaminated (left), which precluded NDE of the underlying laminate. The second UT scan (right) showed full penetration through the reinforcement and primary mast with no detected anomalies. [Bandos, 2002]**

## **9. Summary**

The goal of this project was to conduct an assessment of current Non-Destructive Evaluation (NDE) methods for large, marine composite structures. The assessment surveyed the military, commercial and recreational maritime industries. Developments in the aerospace and wind energy industries were also investigated. Informational sources included marine surveyors, NDE equipment manufacturers, shipbuilders, platform owners and academia. An operational overview of NDE techniques was developed.

Project resources were also focused on classifying and characterizing defects that are typically found in marine composite construction. Descriptions, schematics, photographs and micrographs were assembled to provide the most comprehensive catalog to date of marine composite defects. Concurrently, a separate assessment of flaw criticality was conducted to determine the lower limit size of as-built flaws or in-service damage that needs to be detected in order to ensure structural integrity. The critical flaw size for a variety of defects formed the basis for NDE detectability thresholds.

The defect characterization exercise highlighted marine composite damage that is not always visible with the naked eye and can thus be best detected with advanced NDE methods. Test panels were built or damaged to represent delaminations, voids, water ingress, core shear and impact damage. These panels were then evaluated using the most promising marine composite NDE methods, which were laser shearography, infrared thermography, ultrasonic testing and digital tap hammer sounding.

Large voids were simulated in solid laminates by machining 1-4 inch diameter cavities from 20% to 80% of panel thickness. Delaminations (or kissing bonds) were simulated in sandwich laminates by placing peel-ply material in between the reinforcement plies. The defects ranged from 0.5 to 4.0 inches in diameter. Water ingress was simulated by embedding pockets of water 1-4 inches in diameter into the core just below the top skin. Core shear was simulated in sandwich panels by slitting the core prior to lamination and inserting peel ply into the slot during fabrication. Impact damage was induced with impact energies between 25 and 250 foot-pounds using a drop weight impactor.

The NDE inspection of the damaged test panels took place in controlled, laboratory environments. The inspections were conducted primarily by the NDE equipment manufacturers identified by this project as developers of leading edge technology. An experienced marine thermographer evaluated our test panels with an IR camera and the digital tap hammer was evaluated in-house.

Case studies of marine composites NDE are also included in this report to illustrate the effectiveness of various NDE tools for boat surveys. Applications included quality assurance NDE used by builders, condition surveys, and NDE used to determine the extent of damage after a known accident.

Finally, a glossary and extended reference list is provided the help the reader understand marine composites NDE terms and to further study research by other investigators.

**9.1 Summary of NDE Techniques Examined**

Appendix B provides “effectiveness tables” of various NDE techniques as applied to the defects described in Section 2. The tables are based on assessments from other investigators and the research done for this project. Table 12 provides a more detailed overview of the four NDE techniques evaluated under the experimental portion of this project.

**Table 12. Summary results from panel testing program**

	<b>Defect</b>	<b>Laser Shearography</b>	<b>Ultrasonic Inspection</b>	<b>Infrared Thermography</b>	<b>Digital Tap Hammer</b>
<b>Delamination</b>	Min. Size Detected	2 inches	2 inches	3 inches	3 inches
	Max. Depth Detected	1- 2 plies	1 ply	2 – 3 plies	2 – 3 plies
	Overall Effectiveness	good esp. for kissing bonds	can’t detect kissing bonds	can’t detect kissing bonds	can’t detect kissing bonds
<b>Water Ingress</b>	Min. Size Detected	2 inches	4 inches	2 inches	4 inches
	Max. Depth Detected	skin/core interface	skin/core interface	skin/core interface	skin/core interface
	Overall Effectiveness	good	use higher frequency transducer	very good	fair
<b>Impact Damage</b>	Min. Size Detected	1 inch	2 inches	1 inch	3 inches
	Max. Depth Detected	skin/core interface	1- 2 plies	skin/core interface	skin/core interface
	Overall Effectiveness	very good	good	good	only edge delaminations found
<b>Void</b>	Min. Size Detected	2 inches	2 inches	1 inch	defect not detected
	Max. Depth Detected	¼ inch	½ inch	¾ inch	
	Overall Effectiveness	fair with thick laminates	good for uniform laminates	very good	not effective
System limitations:		Requires good reflective surface – not good with matt finish black parts or clear gel coat; not good with thick or highly curved parts	Requires good calibration sample and uniform laminate; small probe area	Known good laminate required for baseline data; defect must produce a thermal gradient	Only effective with larger defects
Equipment cost:		≈ \$100,000	≈ \$40,000	≈ \$10,000	≈ \$1,500

## 9.2 Flaw Detection in Marine Composites

Here we revisit the defects described in Section 2 and Appendix A to suggest the best NDE technique for detection and the limits of detectability. Appendix A set allowable and detectable defect sizes. These thresholds were generally based on criteria established for other industries as a standard series of flaw criticality studies has not been done for marine composite structures. In general, the values stated in Appendix A were shown to be more conservative than standard practice for composite yachts and ships and should be viewed as a working document to be refined using additional data and input from other researchers.

### Adhesive bond failures

Laser shearography is the best NDE technique for detecting adhesive bond failure, especially with kissing bonds with very little void space. The minimum practical size that can be detected is about one square inch. If the failure area is larger and there is a sufficient distance between the bonded plies, all of the NDE methods considered should be able to detect the defect.

### Air bubbles

Air bubbles are not easily detected by any of the NDE methods evaluated, unless the bubbles are ¼ inch or greater. Thermography may be effective if bubbles are near the surface. Air bubbles at the surface are best detected using visual inspection methods.

### Blisters

By definition, blisters are a surface phenomenon, which can best be detected with visual inspection. However, infrared thermography may be effective for determining the extent of blister damage in situations where incomplete repairs and coatings hide the underlying defects. Again, expect ¼ inch to be the smallest sub-surface blister that can be detected, while smaller defects on the surface can be identified with visual inspection.

### Core crushing

Core crushing is usually accompanied with surface damage that is detectable with visual inspection. If the surface shows no sign of indentation (i.e. has recovered) then some skin-to-core debond will be associated with core crushing and laser shearography will be the most effective NDE tool that should detect crushing of 1/8 inch.

### Core shear failure

Core shear failure was easily detected by laser shearography, especially with PVC core. Shear failures down to ½ inch in length were detected.

### Crazing

Crazing is best assessed with visual inspection, sometimes enhanced with dye penetrant .

### Delaminations

Delaminations down to 1/8 inch in length are easily detected with laser shearography if the defect is near the surface of a thin laminate. Ultrasonic testing is also useful if the area of suspected damage is known first.

Fiber failure

Unless fiber failure is accompanied by surface damage, laser shearography would be the only NDE method suitable for detecting damage down to about 1/4 inch.

Kissing bonds

Laser shearography can detect kissing bonds, perhaps as small as 1/4 inch diameter provided they are near the surface of the laminate. The resolution of the system diminishes by the depth of the defect to the second power. All other NDE methods surveyed have trouble detecting this type of failure.

Local impact damage

Laser shearography and infrared thermography both worked well to detect impact damage down to about one inch in diameter, with the former a bit more sensitive to damage from lower impact energies.

Matrix cracking

Laser shearography will offer the highest resolution for detecting matrix cracking, as this is the only NDE method that stresses the part. Surface cracks are still best detected with visual inspection. Cracks down to 1/8 inch should be detectable with laser shearography and significantly larger cracks may be detected with infrared thermography.

Moisture ingress

Infrared thermography is the most effective NDE technique for detecting moisture in laminates. It is especially useful for water that has migrated into scored core material. Detection threshold is about one cell length (one inch) by the width of the kerf cut (1/8 inch). Tests on honeycomb material have detected moisture on a single 3/8 inch cell.

Ply waviness

None of the NDE techniques evaluated is suitable for detecting ply waviness except in extreme cases where the structural response of the part was degraded. In this case, laser shearography would detect anomalies when the part was stressed.

Pit (or pinhole)

Although best detected with visual inspection, pits down to 1/8 inch in diameter may be detectable with infrared thermography.

Porosity

Laser shearography and infrared thermography would both be effective NDE techniques for detecting porosity. Thermography may provide the best resolution provided an optimal heating procedure is established. Expect detection threshold to be around ten pits per ten square inch area

Resin rich areas

Infrared thermography would be effective for detecting resin rich areas and was used by the author with early thermography equipment to monitor exotherm during construction,

where resin rich areas were quite noticeable. Expect detection threshold to be around two inches in diameter.

Resin starved areas

Laser shearography and infrared thermography would both be effective NDE techniques for detecting resin starved areas where structural adequacy is compromised. Expect detection threshold to be around two inches in diameter.

Skin-to-core disbond

All of the NDE techniques evaluated were able to detect large skin-to-core disbonds. Laser shearography worked well with thinner skin laminates and one could expect detectable defects down to ½ inch diameter. Thermography would be preferred for sandwich laminates with thicker skins, although resolution may only be to one inch diameter.

Surface cracking

Surface cracking is best detected with visual inspection. Artificial light, magnification and digital photography can help render small details. Other NDE techniques evaluated for this project offer no improvement.

Thermal damage (including lightning)

Thermal damage from lightning is often difficult to detect if the path of the strike is not visually apparent on the surface of the laminate. Ultrasonic inspection has been useful to survey carbon fiber masts that have relatively uniform skin thicknesses and can be 100% inspected with a one-inch probe in a reasonable period of time. Defects as small as ¼ inch should be detectable provided they are not too far beneath the surface.

Voids

Voids are detectable using any of the NDE techniques surveyed in this report. However, laser shearography will detect the smallest voids (down to ¼ inch, if they are near the surface) and ultrasonic inspection will require that the surrounding laminate be uniform.

**10. Conclusion**

By far and away, the best NDE tool for marine composites is still the human eye. Coupled with an experienced surveyor who understands how composite structures resist loads in a marine environment, damage is most often first detected through visual inspection. However, visual inspection cannot reveal the extent of damage with certainty. Defects or damage can exist deep within layers of a laminate, which may not be detected by looking at the surface. Sandwich laminates have additional failure modes that require advanced NDE methods, such as core failures and bondline deficiencies.

The initial assessment of NDE technologies revealed laser shearography, thermography, ultrasonic testing and digital tap hammers to be the most promising for marine composites inspection.

Laser shearography proved to be the most effective NDE technique for discovering the widest variety and smallest defects, perhaps because this is the only NDE method that stresses the part during inspection. It is also the most recently developed technology, and thus the most expensive. Defects very deep in solid laminates were more difficult to detect.

Thermography worked very well to detect water ingress and irregularities in sandwich construction, especially with cores that have kerfs. Voids, even  $\frac{3}{4}$  of an inch deep in solid laminates were readily detected. “Kissing bonds” were not readily identified and internal impact damage was hard to distinguish.

Ultrasonic inspection worked well to document the location and depth of delaminations but small survey probes limit the effectiveness to instances where damage sites are known or suspected. It is also critical to know the thickness of the “skin” being measured to recognize good back wall return signals.

The digital tap hammer proved to be effective only for larger delamination sites. However, it was more accurate than traditional percussion sounding methods.

Using marine composites to build lighter ships is an attractive approach to minimize fuel consumption and reduce life-cycle costs. This field represents a tremendous opportunity for U.S. manufacturing. However, to fully optimize composite construction we need to be able to inspect entire composite ship structure while the vessel is in service in order to avoid failures or “overbuilt” designs.

Advanced integrated circuit development and digital signal processing have made IR cameras and ultrasonic testers smaller and more affordable for a wide variety of applications. Development of a low-cost, lightweight laser shearography system would make this technology affordable for a wider range of structures.

## **11. Recommendations for Future Research**

As marine composite construction migrates from solely the recreational boating industry to more commercial and military applications, shipbuilders and owners will want to see methods to “standardize” the design, fabrication, inspection and repair of composite structure to reduce life-cycle costs. Several areas of recommended research will help establish a baseline of “best practices” for the marine composites industry.

### **11.1 Develop Standardized Structural Details**

A good number of failures in marine composite construction occur at structural details, such as stiffener and bulkhead attachment points. These defects are not covered in this report because they are typically best discovered using visual inspection. Steel and aluminum shipbuilding has benefitted from research on structural details (see SSC-379, Improved Structural Details Relative to Fatigue and SSC 447, In-Service Performance of Aluminum Structural Details). Recreational composite boat builders distinguish themselves by claims of “inventing a better mousetrap,” a case in point being the plethora of hull-to-deck joint configurations. Unique designs must be more conservative (heavier

and more costly) because we have a limited empirical database to show how a particular structural detail will perform over time at sea. Standardized structural details will also be easier to inspect and repair.

### **11.2 Develop Standardized Inspection and Repair Procedures**

Today, every marine surveyor has his or hers own approach to inspection of yachts and ships built with composite materials. Appropriately, the majority of time is spent on visual inspection. However, more subjective techniques, such as tap testing or the use of moisture meters on structure below the waterline, can often produce results that would not be repeatable if performed by a different surveyor. When defects are found, we do not have a set of standard repair procedures to ensure that the entire damaged area is repaired to its original condition, although composite materials are well suited to this task. Research to produce a report on “best practices” for inspection and repair will increase the use of composite materials for commercial and naval applications.

### **11.3 Reduce the Cost of Laser Shearography NDE Equipment**

The laser shearography system evaluated in this report was shown to be the most capable marine composites NDE tool overall. However, because this specialized device is produced in limited quantities on a custom basis, equipment cost is quite high. The development of a lightweight, consumer-based laser shearography system would make this technology more viable for the marine composites industry.

### **11.4 Develop a Method to Electronically Code the Location of NDE Equipment**

One of the most time-consuming activities when surveying a large marine structure is correlating the NDE record to the location on the structure. Surveyors typically use markers or tape to note anomalies as they proceed. However, today’s NDE devices have the ability to store data recorded for an entire ship and there almost always exists a digital 3-D model of the surface being inspected so the next logical step would be to merge these two datasets. This would give the surveyor more complete knowledge of the structure as he is surveying it and could help feed into flaw-criticality models.

Allowable and Detectable Defect Thresholds

Defects	Reinforcement	E-Glass		Carbon Fiber	
	Structure	Solid, Foam or Balsa Core		Sandwich incl. Honeycomb	
	Manufacturing Method	Hand Layup, Infusion		Infusion, Prepreg	
	Description	Allowable	Detectable	Allowable	Detectable
Adhesive bond failure	Failure of bonded joints either by Cohesion (fracture of the adhesive or Adhesion (failure of the interface).	Debond area less than 30% of total bond area. Axial length of debond less than 20% of total axial bond length. <sup>2</sup>	Discontinuities 12 mm (1/2 in.) or larger. <sup>5</sup>	Debond area less than 15% of total bond area. Axial length of debond less than 10% of total axial bond length.	Discontinuities 6 mm (1/4 in.) or larger.
Air bubble	Air entrapment within and between the plies of reinforcement, usually spherical in shape.	Maximum diameter, 3.0 mm (1/8 in.); 4/in <sup>2</sup> . <sup>3</sup>	Any porosity area of 64 mm <sup>2</sup> (0.1 in. <sup>2</sup> )	Maximum diameter, 1.5 mm (1/16 in.); 2/in <sup>2</sup> . <sup>3</sup>	Any porosity area of 32 mm <sup>2</sup> (0.05 in. <sup>2</sup> )
Blister	Rounded elevation of the surface of a laminate, with boundaries that may be more or less sharply defined, somewhat resembling in shape a blister on the human skin.	Maximum diameter, 6.5 mm (1/4 in.); height from surface not to be outside drawing tolerance. <sup>3</sup>	Minimum diameter, 1.5 mm (1/16 in.)	Maximum diameter, 3.0 mm (1/8 in.); height from surface not to be outside drawing tolerance	Minimum diameter, 1.5 mm (1/16 in.)
Core crushing	The distortion or collapse of core material due to pressure or local compression.	Maximum allowable core deformation less than 10% of core thickness	Minimum diameter 9 mm (3/8 in.)	None	Minimum diameter 6 mm (1/4 in.)
Core shear failure	Separation of core that extends between face skins.	Maximum allowable shear cracking less than 5% of core thickness	127 mm disbond 32 mm beneath a 10 to 12 ply (3 mm) skin. <sup>5</sup>	None	
Crazing	Pattern of fine cracks on or beneath the surface.	Maximum crack length less than 25 mm (1 in.). <sup>2</sup> or max. 50 mm (2 in.) long by 0.4 mm (1/64 in.) deep, max density 5 in any 0.1 m <sup>2</sup> (sq. ft.). <sup>4</sup>	Minimum length, 1.5 mm (1/16 in.)	Maximum crack length less than 12 mm (0.5 in.). <sup>2</sup> or max. 25 mm (1 in.) long by 0.4 mm (1/64 in.) deep, max density 3 in any 0.1 m <sup>2</sup> (sq. ft.).	Minimum length, 1.5 mm (1/16 in.)
Delaminations	Separation of laminate plies.	Maximum diameter, 14 mm (9/16 in.). <sup>3</sup>	Any delamination with a length of 6.5 mm (1/4 in) or area of 32 mm <sup>2</sup> (0.05 in. <sup>2</sup> ). <sup>6</sup>	Maximum dimension, 6.5 mm (1/4 in.). <sup>13</sup>	Any delamination with a length of 6.5 mm (1/4 in) or area of 32 mm <sup>2</sup> (0.05 in. <sup>2</sup> ). <sup>6</sup>
Fiber failure	Tensile or compressive failure of individual fibers with dominant strain parallel to the fiber direction.	Less than 1% by volume not to exceed 10 mm (0.4 in.) <sup>2</sup>	none visible	None	none visible
Kissing bond	A void between laminated or bonded skins where surfaces may be touching.	Debond area less than 30% of total bond area. Axial length of debond less than 20% of total axial bond length. <sup>2</sup>	127 mm beneath a 10 to 12 ply (3 mm) skin. <sup>5</sup>	Debond area less than 15% of total bond area. Axial length of debond less than 10% of total axial bond length.	Any kissing bond with a length of 6.5 mm (1/4 in) or area of 32 mm <sup>2</sup> (0.05 in. <sup>2</sup> ). <sup>6</sup>
Local impact damage	Separation of material through entire thickness and visible on the surface.	Circular or ellipsoidal "bright solid" areas with diameter less than 10 mm (0.4 in.). <sup>2</sup>	Minimum diameter 9 mm (3/8 in.)	Circular or ellipsoidal "bright solid" areas with diameter less than 5 mm (0.2 in.).	Minimum diameter 6 mm (1/4 in.)
Matrix cracking	Resin cracking between plies or at the fiber interface caused by excessive shear force, low elongation resins, or exotherm during cure.	Maximum length, 6.5 mm (1/4 in.). <sup>3</sup>	Minimum length, 1.5 mm (1/16 in.)	Maximum length, 3.0 mm (1/8 in.). <sup>3</sup>	Minimum length, 1.5 mm (1/16 in.)

Defects	Reinforcement	E-Glass		Carbon Fiber	
	Structure	Solid, Foam or Balsa Core		Sandwich incl. Honeycomb	
	Manufacturing Method	Hand Layup, Infusion		Infusion, Prepreg	
	Description	Allowable	Detectable	Allowable	Detectable
Moisture ingress	Areas where water has migrated into the laminate or core.	10% by volume maximum allowable core moisture content.	2% - 3%	None	1% - 3%
Ply waviness	Areas where reinforcement plies are wrinkled, often caused by vacuum bag consolidation.	There are to be no wrinkles in the reinforcement and no voids greater than 12 mm (1/2 in.) <sup>1</sup> ; maximum length surface side, 25 mm (1	3%	Maximum length surface side, 6.5 mm (1/4 in.); maximum length opposite side, 13 mm (1/2 in.); depth less than 10% laminate thickness. <sup>3</sup>	1%
Pit (or pinhole)	Small crater in the inner surface of the laminate, with width (max. diameter) similar to or smaller than depth.	Maximum diameter, 0.8 mm (1/32 in.); depth less than 20% of wall thickness, frequency & location TBD. <sup>3</sup>	Pits greater than 3 mm (1/8 in.) in diameter and under 0.75 mm (1/32 in.) deep	Diameter less than 0.4 mm (1/64 in.), and depth less than ply thickness or 10% of laminate thickness, and no damaged fibers. <sup>2</sup>	Pits greater than 3 mm (1/8 in.) in diameter and under 0.75 mm (1/32 in.) deep
Porosity	Presence of numerous visible tiny pits (pinholes) approximate dimension 0.005 inches (for example, 5 in any sq. inch).	Porosity features less than 0.8mm (1/32 in.) diameter. Maximum of ten pits per 64.5 cm <sup>2</sup> (10 in <sup>2</sup> ) of area and no more than one such area per 0.3 m (lineal foot) <sup>7</sup>	Any porosity area of 65 mm <sup>2</sup> (0.1 in. <sup>2</sup> )	Porosity features less than 0.8mm (1/32 in.) diameter. Maximum of ten pits per 64.5 cm <sup>2</sup> (10 in <sup>2</sup> ) of area and no more than one such area per 0.3 m (lineal foot) <sup>7</sup>	Any porosity area of 32 mm <sup>2</sup> (0.05 in. <sup>2</sup> )
Resin rich area	Portion of a laminate with resin pockets or poor consolidation that results in low fiber volume.	Maximum diameter, 14 mm (9/16 in.) <sup>3</sup>	Minimum diameter 9 mm (3/8 in.)	Maximum diameter, 9.5 mm (3/8 in.) <sup>3</sup>	Minimum diameter 6 mm (1/4 in.)
Resin starved area	Area of laminate that was not thoroughly wetted with resin.	Maximum diameter, 14 mm (9/16 in.) <sup>3</sup>	Minimum diameter 9 mm (3/8 in.)	Maximum diameter, 9.5 mm (3/8 in.) <sup>3</sup>	Minimum diameter 6 mm (1/4 in.)
Skin-to-core disbond	Delamination at the skin-to-core bondline.	Maximum diameter, 14 mm (9/16 in.)	50 mm under a 10 to 12 ply (3 mm) skin; 127 mm under 20 to 24 ply (6 mm) skin. <sup>5</sup>	Maximum dimension, 6.5 mm (1/4 in.)	A skin-to-core disbond with a length of 25 mm (1 in) or area of 500 mm <sup>2</sup> (0.785 in. <sup>2</sup> ) <sup>6</sup>
Surface cracking	Fine cracks at the surface of the laminate.	Maximum length, 6.5 mm (1/4 in.) <sup>3</sup>	Minimum length, 1.5 mm (1/16 in.)	Maximum length, 3.0 mm (1/8 in.) <sup>3</sup>	Minimum diameter 6 mm (1/4 in.)
Thermal damage (including lightning)	Heat damage that diminishes matrix properties and is maximum at the surface of a laminate.	Never in more than one ply and not to exceed 0.01 m <sup>2</sup> (16 sq. in.) in any panel. <sup>4</sup>	Minimum diameter 6 mm (1/4 in.)	No distortion and/or burn deeper than surface resin layer. <sup>2</sup>	Minimum diameter 6 mm (1/4 in.)
Voids	An air pocket within a laminate characterized by its thickness and area.	i) There are to be no voids extending through more than one ply of laminate. ii) There are to be no voids larger than 12 mm (0.50 in.) in their greatest dimension. iii) There are to be no voids larger than 3 mm (0.125 in.) on each ply in any 150 mm x 150 mm (6 in. x 6 in.) area, with a maximum of six (6) total voids in this area. iv) There are to be no more than three (3) voids larger than 3 mm (0.125 in.) on each ply in any 300 mm x 300 mm (12 in. x 12 in.) area, with a maximum of twenty (20) total voids in this area. The void content is not to exceed 4%. Where the void content is in excess of 2%, additional testing may be required <sup>1</sup>	Any void with a length of 12 mm (1/2 in) or area of 65 mm <sup>2</sup> (0.1 in. <sup>2</sup> ) <sup>6</sup>	i) There are to be no voids extending through more than one ply of laminate. ii) There are to be no voids larger than 6 mm (0.25 in.) in their greatest dimension. iii) There are to be no voids larger than 1.5 mm (0.0625 in.) on each ply in any 150 mm x 150 mm (6 in. x 6 in.) area, with a maximum of three (3) total voids in this area. iv) There are to be no more than two (2) voids larger than 1.5 mm (0.0625 in.) on each ply in any 300 mm x 300 mm (12 in. x 12 in.) area, with a maximum of ten (10) total voids in this area. The void content is not to exceed 2%. Where the void content is in excess of 1%, additional testing may be required <sup>1</sup>	Any void with a length of 6.5 mm (1/4 in) or area of 32 mm <sup>2</sup> (0.05 in. <sup>2</sup> ) <sup>6</sup>

Notes:

1. American Bureau of Shipping Materials and Welding 2006, Part 2 Aluminum and Fiber Reinforced Plastic (FRP) (Chapters 5-6)
2. ISO Standard 14692-4 Petroleum and natural gas industries — Glass-reinforced plastics (GRP) piping, Part 4: Fabrication, installation and maintenance, Annex A (normative) Defect types — Acceptance criteria and corrective actions, Second edition 2010-04-06
3. ASME SD-2563 Standard Practice for Classifying Visual Defects in Glass-Reinforced Plastic
4. ASME/ANSI RTP-1-1989: Reinforced thermoplastic corrosion resistant equipment
5. Eugene T. Camponeschi, Jr., Roger Crane, Kirsten Lipetzky and Bruce Bandos, "The Role and Use of Nondestructive Testing for US Navy Composite Ship Structures," Materials Evaluation/July 2007.
6. National Aeronautics and Space Administration, Lyndon B. Johnson Space Center, "Process Specification for Ultrasonic Inspection of Composites," May 2003.
7. Creative Pultrusions, Inc., "Standard Practice for Classifying Visual Defects," CPQ008-1206.1C, Revised 3-13-07

Effectiveness of Various NDE Techniques

from SSC Project 1464 Test Panel Program

Defects	Visual	Ultrasonics		Thermography		Laser Shearography		Tap Hammer	
		A-Scan	C-Scan	Steady	Pulsed	Vacuum	Heat	Manual	Digital
Adhesive bond failure	0	A	A	B	A	A	B	B	A
Air bubble	C	C	C	C	B	C	B	0	0
Blister	A	C	C	C	B	C	C	0	0
Core crushing	C	B	B	B	A	B	C	B	B
Core shear failure	0	C	C	B	A	A	B	C	B
Crazing	A	0	0	C	C	C	C	0	0
Delaminations	C	B	A	C	B	A	B	B	B
Fiber failure	C	B	B	0	C	A	A	C	C
Kissing bond	0	B	A	B	A	A	B	C	B
Local impact damage	B	C	B	B	B	A	B	C	B
Matrix cracking	A	C	B	C	C	B	C	0	C
Moisture ingress	C	C	B	A	A	B	A	C	C
Ply waviness	B	0	0	0	C	C	C	0	0
Pit (or pinhole)	A	0	C	0	0	0	C	0	0
Porosity	B	0	C	C	B	0	C	0	0
Resin rich area	0	C	B	B	A	0	C	C	C
Resin starved area	0	C	B	B	A	0	C	C	C
Skin-to-core disbond	0	C	B	B	A	A	B	B	A
Surface cracking	A	0	0	C	C	C	C	0	0
Thermal damage	B	C	B	B	B	C	B	C	C
Voids	C	C	B	C	B	C	C	C	C

- A = High  
(best/optimal)
- B = Average  
(works generally well)
- C = Limited  
(may be used under certain conditions only)
- 0 = Not applicable  
(will not detect the defect)

Roby Scalvini of Marine Survey Bureau

Defects	Ultrasound Flaw Detection			Infrared Thermography		Laser Shearography		
	A-scan Pulse-Echo	C-scan Phased Array	Bond Tester Pitch-Catch	Manual	Pulse-Phase	Vacuum Load	Heat Load	Dynamic Excitation
Crack	C <sup>1</sup>	C <sup>1</sup>	Ø	Ø	C	B	B	A
Delamination (shallow)	C	A	A	A	A	A	A	B
Delamination (deep)	A	C	C	Ø <sup>2</sup>	C <sup>2</sup>	C <sup>3</sup>	Ø	A
Disbond (solid-to-solid)	A	A	A	B	A	Ø <sup>3</sup>	C	A
Voids/lack of resin infusion	C	B	Ø	B	A	A	B	C
Porosity	C	B	Ø	Ø	C	C	C	B
Matrix cracking	C <sup>5</sup>	C	Ø	Ø	Ø	Ø	Ø	B
Core disbond (foam/balsa)	C <sup>6</sup>	B	A	A	A	A	B	A
Core disbond (honeycomb)	Ø	B	A	C	A	A	B	A
Water in core	Ø	C	Ø	A	A	Ø	Ø	C
Scarf repair validation	Ø	C	Ø	Ø	C	C	A	C

A = High (best/optimal)
B = Average (works generally well)
C = Limited (may be used under certain conditions only)
Ø = Not applicable (will not detect the defect)

Notes:

- Cracks in line with the beam of ultrasounds can be detected only if there is a small planar delamination associated with the crack (as is mostly the case in composites laminates).
- Detectability with infrared thermography of delaminations set deep into a laminate is a direct function of the ratio between the flaw's diameter (D) and its depth (d) in the laminate (expressed as D:d). For FRP laminates the limit is normally in the range of a ratio 2:3; for CFRP laminates the ratio can be as low as 5:8.
- Detectability with laser shearography (vacuum load) of delamination set deep into a laminate is a direct function of both the ratio between the flaw's diameter (D) and its depth (d) in the laminate and the stiffness of the material.
- Normally not inspectable due to geometry of secondary bonded part (stiffeners, bulkheads tabbings, etc)
- Detection of matrix cracking with ultrasound A-scan is possible only if there is a known gain setting to use as reference. Results so obtained are to be considered purely indicative of a flaw and not conclusive.
- Assessment of skin bondline with ultrasound A-scan is possible only with extremely high density cores (whose density is not too dissimilar to the skin's density).

Scalvini, Roby, Marine Survey Bureau, "Carbon and Lightning," Professional Boatbuilder, Number 128, Dec/Jan 2011, Brooklin, ME.

from Data on www.NetComposites.com Web Site

Defects	Acoustic Emission	Acoustic Impact	Coin Testing	Laser Shearography	Mechanical Impedance	Membrane Resonance	Thermography	Ultrasonic Amplitude C-Scan	Ultrasonic Thickness A-Scan	Ultrasonic 0 deg PE B-Scan	Ultrasonic Depth Scan	Visual	X-Radiography
Core crushing	B	A	A	B	A	A	B	B	B	B	0	C	B
Core disbond	C	A	A	A	A	A	A	A	A	A	B	0	B
Core splice	0	B	B	B	B	B	C	B	C	C	0	C	B
Crack	B	0	0	A	0	0	C	0	0	0	0	B	B
Delamination small (<10 mm)	B	C	C	A	C	C	B	A	B	B	A	0	B
Delamination (>10 mm)	B	B	C	A	B	B	A	A	A	A	A	0	B
Disbond	C	B	C	A	B	B	A	A	B	A	A	0	B
Environment ingress	0	0	0	C	0	0	A	B	C	B	0	C	B
Erosion	0	0	0	B	0	0	B	B	A	A	A	C	C
Excess fiber	0	0	0	B	0	0	B	B	0	B	B	C	C
Excess resin	0	0	0	B	0	0	B	B	0	B	B	C	C
Fiber and ply misalignment	0	0	0	C	0	0	C	A	0	C	0	C	B
Fiber breakage	A	C	C	B	C	C	0	0	0	0	0	C	B
Fiber wrinkling/waviness	0	0	0	C	0	0	C	A	C	B	0	C	C
Impact	B	B	C	A	B	B	B	A	A	A	A	B	C
Inclusion	0	C	C	B	C	C	B	A	B	B	B	0	B
Incorrect cure	0	0	0	0	0	0	0	C	0	B	B	0	0
Kissing bond	0	C	C	B	C	C	C	C	0	0	0	0	0
Matrix cracking	A	0	0	0	0	0	0	0	0	0	0	0	B
Porosity	0	0	0	B	0	0	B	A	B	B	C	0	A
Void	0	C	C	B	C	C	B	A	B	B	B	0	A

- A = High (best/optimal)
- B = Average (works generally well)
- C = Limited (may be used under certain conditions only)
- 0 = Not applicable (will not detect the defect)

based on data from www.NetComposites.com

from NDE Methods for Infrastructure Composites

Defects	Acoustic Emission	Acoustic Impact Testing	Eddy Current Testing	Modal Analysis	Optical Methods (Shearography)	Penetrant Testing	Radiographic Testing	Rapid Load Testing	Strain Measurement Techniques (Optical Fibers)	Thermographic Testing	Ultrasonics	Visual Testing
Delamination	C	A	0	?	A	0	A	?	C	A	A	C
Fiber Breakage	B	C	B	?	A	C	A	?	0	?	?	0
Fiber Waviness	0	C	B	0	A	0	A	?	C	?	?	C
Matrix Cracking	B	0	0	0	?	C	A	0	0	0	0	0
Moisture	0	0	?	?	?	0	C	?	0	C	C	0
Porosity	0	0	0	0	?	0	A	0	0	?	?	0
Resin Thickness Irregularities	0	0	0	0	?	0	A	0	C	?	?	0
Voids	0	C	0	?	A	0	A	?	0	C	C	0

- A = High  
(allows localization or accurate sizing)
- B = Generally Detectable  
(works generally well)
- C = Limited Detectability  
(may be used under certain conditions only)
- 0 = Not applicable  
(will not detect the defect)

Karbhari, V.M., Kaiser, H., Navada, R., Ghosh, K. and Lee, L., "Methods for Detecting Defects in Composite Rehabilitated Concrete Structures," Federal Highway Administration report FHWA-OR-RD-05-09, April 2005.

from Abaris Composites Training Program

Defects	Visual	Tap Test	Ultrasonic		X-Rays	Thermal	Dye Penetrant
			A-Scan	C-Scan			
Surface Delaminations	B	A	B	A	B	A	0
Deep Delaminations	0	C	A	A	B	B	0
Full Disbond	B	B	A	A	B	A	0
Kissing Disbond	0	C	C	C	0	0	0
Core Damage	B	B	C	A	A	B	0
Inclusions	B	B	A	A	A	A	0
Porosity	B	0	B	A	0	0	B
Voids	B	B	B	B	B	B	B
Backing Film	0	B	B	B	B	B	0
Edge Damage	A	B	B	A	A	B	A
Heat Damage	B	B	B	B	0	B	0
Severe Impact	A	A	A	A	C	A	A
Medium Impact	A	A	A	A	0	C	C
Minor Impact	C	C	C	C	0	C	0
Uneven Bondline	C	0	C	C	C	C	0
Weak Bond	0	0	0	0	0	0	0
Water in Core	0	B	C	A	B	A	0

A = High  
(best/optimal)

B = Average  
(works generally well)

C = Limited  
(may be used under certain conditions only)

0 = Not applicable  
(will not detect the defect)

from [www.abarisonline.com/Topicdisplay.asp?TPCID=3](http://www.abarisonline.com/Topicdisplay.asp?TPCID=3)

## Glossary of Marine Composites Damage and NDE Terms

### A

**Acoustic Emission (AE)** The class of phenomena whereby transient elastic waves are generated by the rapid release of energy from localized sources within a material or from the transient elastic waves so generated. (Acoustic emission is the recommended term for general use. Other terms that have been used in AE literature include (1) stress wave emission, (2) microseismic activity, and (3) emission or acoustic emission with other qualifying modifiers.)

**Acousto-Ultrasonic** A technique that combines highly pulsed ultrasonic transducers with an acoustic emission system to detect subtle defects in composites and bonded joints.

**Active Thermography** Active thermography involves using an excitation source to induce thermal contrast into the material and an IR camera to measure the stationary or transient response. **Pulsed thermography**, in which the specimen is heated for few seconds and the thermal decay response at the surface is measured by the infrared camera, is one of the most common thermal stimulation methods.

**Adherent** A body that is held to another body usually by an adhesive.

**Adhesive** Substance capable of holding two materials together by surface attachment. Can be a film, paste or liquid.

**Adhesive Bond Failure** Failure of bonded joints either by Cohesion

(fracture of the adhesive or Adhesion (failure of the interface).

**Air Bubble** Air entrapment within and between the plies of reinforcement, usually spherical in shape.

**Air Inhibition** Undercuring of exposed resin surface leaving sticky finish.

**Aramid** A manufactured fiber in which the fiber-forming substance consisting of a long-chain synthetic aromatic polyamide in which at least 85% of the amide (-CONH-) linkages are attached directly to two aromatic rings.

**A-Scan** A method of data presentation on a cathode-ray tube (CRT) using a horizontal baseline that indicates distance, or time, and a vertical deflection from the baseline, which indicates amplitude.

**Attenuation** Factor representing a decrease in signal intensity with distance. Expressed in decibels (dB) per unit distance.

### B

**B-Scan** A B-scan is an image showing a cross-sectional profile through one vertical slice of the test piece, showing the depth of reflectors with respect to their linear position.

**Blister** Rounded elevation of the surface of a laminate, with boundaries that may be more or less sharply defined, somewhat resembling in shape a blister on the human skin.

**Bond Strength** The amount of adhesion between two surfaces.

**Bond Testers** This NDI uses instruments based on mechanical impedance measurements. Bond testers are typically used to detect composite delaminations and adhesive debonds.

**Boroscope** Industrial scope that transmits images from inaccessible regions for visual inspection. They can be flexible or rigid in nature.

**Bubbler** A device using a liquid stream to couple an ultrasonic beam to the test piece.

## C

**Carbon Fibers** Fibers produced by the pyrolysis of organic precursor fibers such as rayon, polyacrylonitrile (PAN), and pitch in an inert atmosphere. The term is often used interchangeably with "graphite"; however, carbon fibers and graphite fibers differ in the temperature at which the fibers are made and heat-treated, and the amount of carbon produced. Carbon fibers typically are carbonized at about 2400° F (1300 °C) and assay at 93 to 95% carbon, while graphite fibers are graphitized at 3450° to 5450 °F (1900° to 3000° C) and assay at more than 99% elemental carbon.

**Catalyst** A substance that changes the rate of chemical reaction without itself undergoing permanent change in composition.

**Caul Plates** Smooth metal plates, free of surface defects, the same size and shape as a composite layup, used immediately in contact with the lay-up during the curing process to transmit

normal pressure and to provide a smooth surface on the finished laminate.

**Chopped Strand Mat (CSM)** A lightly compressed and bound mat formed from filaments of glass that have been chopped to short lengths and bound together.

**Composite Material** Composites are considered to be combinations of materials differing in composition or form on a macroscale. The constituents retain their identities in the composite; that is, they do not dissolve or otherwise merge completely into each other although they act in concert. Normally, the components can be physically identified and exhibit an interface between one another.

**Contact Testing** A technique in which the search unit makes contact directly with the test piece through a thin layer of couplant.

**Core** Foam, wood or other material between the skins of a sandwich laminate.

**Core Crushing** The distortion or collapse of core material due to pressure or local compression.

**Core Shear Failure** Separation of core that extends between face skins.

**Couplant** A material used at the structure-to-sensor interface to improve the transmission of acoustic energy across the interface during acoustic emission monitoring. (From ASTM E610)

**Crazing** Apparent fine cracks at or under the surface of an organic matrix.

SSC-463

**Creep** The time dependent part of strain resulting from an applied stress.

**Crimp** The undulations induced into a braided fabric via the braiding process.

**C-Scan** A means of data presentation that provides a plane view of the material and discontinuities therein.

**Cure** To change the properties of a thermosetting resin irreversibly by chemical reaction, i.e., condensation, ring closure, or addition. Cure may be accomplished by addition of curing (cross-linking) agents, with or without catalyst, and with or without heat. Cure may occur also by addition, such as occurs with anhydride cures for epoxy resin systems.

## D

**Debond** An initially unbonded or nonadhered region between two adherents. Also used to describe a separation at the fiber-matrix interface. In the construction industry, debond and delamination are sometimes used interchangeably when referring to separations at the concrete-composite interface.

**Decibel (dB)** Logarithmic scale expressing relative amplitude or intensity of ultrasonic signals.

**Degradation** Deleterious change in physical properties or appearance.

**Delamination** Separation of the layers of material in a laminate, either local or covering a wide area.

**Disbond** An area within an initially bonded interface between two adherents

in which adhesion failure or separation has occurred.

**Dry Laminate** Resin to fiber ratio below specification.

**Dual Search Unit (Twin Probe)** A probe or search unit containing two elements—one a transmitter, the other a receiver.

**Dye Penetrant** Visible or fluorescent solution that seeps into porous surfaces.

## E

**Eddy Current** Typically an electromagnetic coil or arrays of coils are passed over the surface. This induces local currents, eddy currents, below the coil, which are sensed by detection coils. The presence of a defect will affect the flow of eddy-currents.

**Emissivity** Ability to radiate energy relative to a perfect radiator (blackbody) with values ranging from zero to one.

**Epoxy Resin** Resins that may be of widely different structures but are characterized by the presence of the epoxy group. (The epoxy or epoxide group is usually present as a glycidyl ether, glycidyl amine, or as part of an aliphatic ring system. The aromatic type epoxy resins are normally used in composites.)

**Exotherm** Heat generated during curing process.

## F

**Fiber** A general term used to refer to filamentary materials. Often, fiber is used synonymously with filament. It is a

general term for a filament of finite length. A unit of matter, either natural or manmade, which forms the basic element of fabrics and other textile structures.

**Fiber Content** The amount of fiber present in a composite. This is usually expressed as a percentage volume fraction or weight fraction of the composite.

**Fiber Failure** Tensile or compressive failure of individual fibers with dominant strain parallel to the fiber direction.

**Filament Winding** A reinforced-plastics process that employs a series of continuous, resin-impregnated fibers applied to a mandrel in a predetermined geometrical relationship under controlled tension.

**Finish (or Size System)** A material, with which filaments are treated, which contains a coupling agent to improve the bond between the filament surface and the resin matrix in a composite material. In addition, finishes often contain ingredients which provide lubricity to the filament surface, preventing abrasive damage during handling, and a binder which promotes strand integrity and facilitates packing of the filaments.

**Fluoroscope** Real-time viewing of X-ray radiography.

**Foreign Material** Any object contained within the laminated composite, bonded laminate or adhesively bonded honeycomb composite that is not specified on the engineering drawing.

## G

**Galvanic Corrosion** Galvanic reaction between metals and conductive carbon fibers, resulting in degradation of matrix and metal.

**Gel Coat** A quick-setting resin used in molding processes to provide an improved surface for the composite; it is the first resin applied to the mold after the mold-release agent.

**Glass Fibers** A fiber spun from an inorganic product of fusion that has cooled to a rigid condition without crystallizing.

## H

**Hand Lay-up** A process in which components are applied either to a mold or a working surface, and the successive plies are built up and worked by hand.

**Holography (Acoustic)** A data presentation system using acoustic waves; analogous to optical holography.

**Holography (Optical)** A data presentation system using light waves to form an image.

**Holography (Thermal)** A data presentation system using temperature gradients; analogous to optical holography.

**Hydrolysis** Process of degradation that generically includes the splitting of chemical bonds and the addition of water.

## I

**Immersion Testing** An examination method during which the search unit and the material are submerged in water.

**Impedance (Acoustic)** A mathematical quantity used in commutation of reflection characteristics at boundaries, i.e., product of wave velocity and material density.

**Inclusion** Mechanical discontinuity occurring within a material, consisting of a solid, encapsulated material.

**Infusion** Manufacturing process whereby resin is drawn into dry reinforcement with vacuum assistance.

**Interface** The boundary between two materials.

**Interlaminar** Descriptive term pertaining to some object (e.g., voids), event (e.g., fracture), or potential field (e.g., shear stress) referenced as existing or occurring between two or more adjacent laminae.

## K

**Kink Bands** A phenomenon visible in fiber composite structures that have failed in compression. Kink bands are formed by fibers buckling before failure occurs and can be seen as cracks in the matrix.

**Kissing Bond** A void between laminated or bonded skins where surfaces may be touching.

## L

**Lamina** A single ply or layer in a laminate made up of a series of layers.

**Laminae** Plural of lamina.

**Laminate** A product made by stacking of multiple layers of unidirectional fibers or oriented fiber configurations embedded in a resin matrix.

**Laser Shearography** Laser shearography determines the surface strain fields from the difference in displacements between unloaded and loaded states using a scanning laser system.

**Lay-up** A process of fabrication involving the assembly of successive layers of resin-impregnated material.

**Local Impact Damage** Separation of material through entire thickness and visible on the surface.

## M

**Mat** A fibrous material consisting of randomly oriented chopped or swirled filaments loosely held together with a binder.

**Matrix** The essentially homogeneous material in which the fiber system of a composite is embedded.

**Matrix Cracking** Resin cracking between plies or at the fiber interface caused by excessive shear force, low elongation resins, or exotherm during cure.

**Mechanical Impedance** A technique that uses low frequency mechanical vibrations to locate defects.

**Modal Methods** Modal analysis refers to the identification of the modal parameters of a structure in order to characterize its dynamic behavior. These modal parameters are the resonant frequencies, damping ratios and mode shapes.

**Modulus, Young's** The ratio of change in stress to change in strain below the elastic limit of a material. (Applicable to tension and compression).

**Moisture Content** The amount of moisture in a material determined under prescribed condition and expressed as a percentage of the mass of the moist specimen, i.e., the mass of the dry substance plus the moisture present.

**Moisture Ingress** Areas where water has migrated into the laminate or core.

**Moisture Meter** Most moisture meters rely on radio frequency dielectric power loss to detect moisture, which is attributed to an increase in the conductivity of the composite due to moisture absorption.

## N

**NDE** Nondestructive evaluation. Broadly considered synonymous with NDI.

**NDI** Nondestructive inspection. A process or procedure for determining the quality or characteristics of a material, part, or assembly without permanently altering the subject or its properties.

**NDT** Nondestructive testing. Broadly considered synonymous with NDI.

**Neutron Radiography** A process of making an image of the internal details of an object by the selective attenuation of a neutron beam by the object.

## P

**Peel Ply** A layer of resin free material used to protect a laminate for later secondary bonding.

**Phased Array Systems** Conventional ultrasonic transducers for NDT commonly consist of either a single active element that both generates and receives high frequency sound waves, or two paired elements, one for transmitting and one for receiving. Phased array probes typically consist of a transducer assembly with from 16 to as many as 256 small individual elements that can each be pulsed separately

**Pit (or pinhole)** Small crater in the inner surface of the laminate, with width (max. diameter) similar to or smaller than depth.

**Ply Waviness** Areas where reinforcement plies are wrinkled, often caused by vacuum bag consolidation.

**Porosity** Trapped pockets of air, gas or vacuum within a solid material, typically less than 10µm in diameter.

**Prepreg** Ready-to-mold material in sheet form impregnated with resin and stored for use. The resin is partially cured to a B-stage.

**Probe** See Search Unit.

**Pulse-Echo Method** An inspection method in which the ultrasonic pulse is emitted and received by a single transducer. The presence and position of a flaw are indicated by the amplitude and time-of-flight of the ultrasonic energy reflected from the flaw.

## **R**

**Resin** An organic polymer or prepolymer used as a matrix to contain the fibrous reinforcement in a composite material or as an adhesive. This organic matrix may be a thermoset or a thermoplastic, and may contain a wide variety of components or additives to influence; handleability, processing behavior and ultimate properties.

**Resin Content** The amount of matrix present in a composite either by percent weight or percent volume.

**Resin Rich Area** Resin to fiber ratio higher than specification.

**Resin Starved Area** Area of composite part where the resin has a non-continuous smooth coverage of the fiber.

## **S**

**Search Unit** A device incorporating one or more transducers.

**Secondary Bonding** The joining together, by the process of adhesive bonding, of two or more already cured composite parts, during which the only chemical or thermal reaction occurring is the curing of the adhesive itself.

**Sensitivity** Measure of the smallest feature inside a material that produces a discernible signal.

**Sizing** A generic term for compounds that are applied to yarns to bind the fiber together and stiffen the yarn to provide abrasion-resistance during weaving. Starch, gelatin, oil, wax, and man-made polymers such as polyvinyl alcohol, polystyrene, polyacrylic acid, and polyacetates are employed.

**Skin-to-Core Disbond** Delamination at the skin-to-core bondline.

**S-Scan Displays** An S-scan or sectorial scan image represents a two-dimensional cross-sectional view derived from a series of A-scans that have been plotted with respect to time delay and refracted angle.

**Stringer** Thin structural member that runs down the length of a hull between frames, providing rigidity and as attachment points.

**Surface Cracking** Fine cracks at the surface of the laminate.

## **T**

**Tap Testing** There are many different tap-testing devices ranging from a simple coin tap, where the human ear is used to audibly sense damaged structure, to automated methods that make a recording of changes in the sound.

**Thermal Conductivity** Rate at which heat flows through a body.

**Thermal damage (including lightning)** Heat damage that diminishes matrix properties and is maximum at the surface of a laminate.

**Thermography** Infrared thermography is the science of detecting and measuring

SSC-463

variations in heat emitted by an object and transforming them into visible images.

**Thermoplastic** A plastic that repeatedly can be softened by heating and hardened by cooling through a temperature range characteristic of the plastic, and when in the softened stage, can be shaped by flow into articles by molding or extrusion.

**Thermoset** A plastic that is substantially infusible and insoluble after having been cured by heat or other means.

**Through Transmission** A test procedure during which ultrasonic vibrations are emitted by one search unit and received by another at the opposite surface of the material examined.

**Toughness** A measure of a material's ability to absorb work, or the actual work per unit volume or unit mass of material that is required to rupture it. Toughness is proportional to the area under the load-elongation curve from the origin to the breaking point.

**Transducer** An electro-acoustical device for converting electrical energy to acoustical energy and vice versa.

## U

**Ultrasonic Inspection** Ultrasonic Testing (UT) is a nondestructive testing technique, which uses high frequency sound energy to conduct examination and make measurements. When there is a discontinuity such as cracks or at material interfaces in the wave path, part of the energy will be reflected back from the flaw surface

**Undercure** A condition resulting from the allowance of too little time and/or temperature for adequate hardening.

## V

**Vibrothermography** A system that uses the heat developed by a defect under vibration to locate the defect.

**Visual Inspection** Visual inspection is the most common form of inspection for composites and other material systems. This may be termed enhanced or close visual inspection if assisted by magnifying glasses, lighting or other tools.

**Void** Air or gas that has been cured into a laminate or an interface between two adherents. Porosity is an aggregation of microvoids.

**Volatiles** Materials, such as water or alcohol, in a resin formulation that are capable of being driven off as vapor at room temperature or at a slightly elevated temperature.

## W

**Wet Lay-up** A method of making a reinforced product by applying a liquid resin system while or after the reinforcement is put in place.

## X

**X-Radiography (X-Ray)** Radiography uses localized differences in attenuation under X-ray illumination to provide a cross-sectional picture of the density of a materials system.

**Glossary References**

ASM Society of Materials, ASM Handbook of Composites, Part 1, Materials Park, OH, ASM International, 2000.

ASTM International, ASTM E1316 - 10c Standard Terminology for Nondestructive Examinations, ASTM International, West Conshohocken, PA, DOI: 10.1520/E1316-10C.

Coackley, N., "Fishing boat construction: Building a fiberglass fishing boat," FAO Fisheries Technical Paper 321, Food and Agriculture Organization of the United Nations, Rome, 1991.

Karbhari, V.M., Kaiser, H., Navada, R., Ghosh, K. and Lee, L., "Methods for Detecting Defects in Composite Rehabilitated Concrete Structures," Federal Highway Administration report FHWA-OR-RD-05-09, April 2005.

MIL-HDBK-17-3e, Vol 3., Polymer Matrix Composites, Volume 3. Materials Usage, Design and Analysis, Department of Defense, January 1997.

**Text References**

Allin, J.M., "Disbond Detection in Adhesive Joints Using Low-Frequency Ultrasound," University of London, May 2002.

Allinson, J.N., "Infrared Thermography and Void Detection in GRP laminates," J.N. Allinson Associates, Inc., Jacksonville, FL, 2007.

American Bureau of Shipping, Materials and Welding, Part 2 - Aluminum and Fiber Reinforced Plastic (FRP) (Chapters 5-6), 2006.

Anastasi, R.F., "Investigation of Fiber Waviness in a Thick Glass Composite Beam Using THz NDE," Nondestructive Evaluation Sciences Branch, NASA Langley Research Center, 2008.

Arvidson, M.H. and Miller, P.H., "Hull Material Evaluation for Navy 44 Sail Training Craft," *Naval Engineers Journal*, Volume 113, April 2001.

ASME SD-2563 Standard Practice for Classifying Visual Defects in Glass-Reinforced Plastic.

ASME/ANSI RTP-1-1989: Reinforced thermoplastic corrosion resistant equipment, 1989.

Bandos, B., "Mast Ultrasonic Inspection," letter report, June 2002.

Berggreen, C., "Growth of Debonds in Foam Cored Sandwich Structures under Cyclic Loading" (SANTIGUE) funded by the Danish Research Agency (Grant nr. 274-05-0324), August 2008.

Bisle, W., "NDT Toolbox for Honeycomb Sandwich Structures - a comprehensive approach for maintenance inspections," Air Transport Association NDT Forum, Albuquerque, NM, September 2010.

Camponeschi, Jr., E.T., Crane, R., Lipetzky, K. and Bandos, B., "The Role and Use of Nondestructive Testing for US Navy Composite Ship Structures," Materials Evaluation, July 2007.

Cairns, D., "Montana State University Wind Turbine Blade Research," Blade Reliability Workshop, July 2010.

Choqueuse, D., Baizeau, R. and Davies, P., "Experimental studies of Impact on Marine Composites," Marine Materials Laboratory, IFREMER, Centre de Brest, Plouzané, France, April 1999.

SSC-463

Clegg, N., "A Short Guide to Osmosis & its Treatment," Nigel Clegg Associates, Sedgefield, UK, 2009.

Coackley, N., "Fishing boat construction: Building a fiberglass fishing boat," FAO Fisheries Technical Paper 321, Food and Agriculture Organization of the United Nations, Rome, 1991.

Creative Pultrusions, Inc., "Standard Practice for Classifying Visual Defects," CPQ008-1206.1C, March 2007.

Davis, M.J. and Bond, D.A., "The Importance of Failure Mode Identification in Adhesive Bonded Aircraft Structures and Repairs," Aircraft Structural Integrity Section Directorate, Royal Australian Air Force, ICCM 12, Paris, France, September 2008.

Davis, M. J. and McGregor, A., "Assessing Adhesive Bond Failures: Mixed-Mode Bond Failures Explained," ISASI Australian Safety Seminar, Canberra, June 2010.

Det Norske Veritas Offshore Standard DNV-OS-C501, Composite Components, January 2003.

Dow Chemical Company, Fabricating Tips, DERA KANE epoxy vinyl ester resins, Midland MI, Feb 1997.

Ehrhart, B., Valeske, B., Muller, C.-E., and Bockenheimer, C., "Methods for the Quality Assessment of Adhesive Bonded CFRP Structures - A Resumé," 2nd International Symposium on NDT in Aerospace, Hamburg, Germany, November 2010.

Galella, D., "FAA Inspection Research Activities for Composite Materials," The 2006 Composite Damage Tolerance & Maintenance Workshop, July 2006.

Gdoutos, E.E and Daniel, I.M., "Failure Mechanisms of Sandwich Structures," Sep 2004.

Gower, M., Sims, G., Lee, R., Frost, S. and Wall, M., Measurement Good Practice Guide No. 78 "Assessment and Criticality of Defects and Damage In Material Systems," National Physical Laboratory, Teddington, Middlesex, United Kingdom, June 2005.

Greene, E., *Marine Composites*, Eric Greene Associates, ISBN 0-9673692-0-7, Annapolis, MD, December 1999.

Greene, E., "Design Guide for Marine Application of Composites," Ship Structure Committee, Report Number SSC-403, December 1997.

Hartman, R. and Roach, D., FAA Airworthiness Assurance NDI Validation Center (AANC), Presentation to ATA NDT Forum 21 September 2010.

SSC-463

Hart-Smith, L.J., "The Critical Factors Controlling the Durability of Bonded Composite Joints – Surface Preparation and the Presence or Absence of Pre-Bond Moisture," MIL-HDBK-17 & FAA Meeting, Seattle, Washington, June 14-18, 2004.

Herzog, B., Goodella, B. and Lopez-Anidob, R., "Electron microprobe imaging for the characterization of polymer matrix composites," Elsevier, Composites: Part A 35 1075–1080, 2004.

Hildebrand, M., "A comparison of FRP-sandwich penetrating impact test methods," VTT Publication 281, Technical Research Centre of Finland, 1996.

Hildebrand, M., "Local impact strength of various boat-building materials," VTT Publication 317, Technical Research Centre of Finland, 1997.

Hsu, D.K., "Nondestructive Inspection of Composite Structures: Methods and Practices," 17th World Conference on Nondestructive Testing, Shanghai, China, October 2008.

Huang, C.K. and Lin, K.Y., "A Method for Reliability Assessment of Aircraft Structures Subject to Accidental Damage," American Institute of Aeronautics and Astronautics, June 2005.

Ilcewicz, L., Cheng, L., Hafenricher, J. and Seaton, C., "Guidelines for the Development of a Critical Composite Maintenance and Repair Issues Course," DOT/FAA/AR-08/54, U.S. Department of Transportation, Federal Aviation Administration, February 2009.

Ilcewicz, L., "Composite Damage Tolerance and Maintenance Safety Issues," FAA Composite Damage Tolerance & Maintenance Federal Aviation Workshop, July 2006.

ISO Standard 14692-4 Petroleum and natural gas industries — Glass-reinforced plastics (GRP) piping, Part 4: Fabrication, installation and maintenance, Annex A (normative) Defect types — Acceptance criteria and corrective actions, second edition, June 2010.

Karbhari, V.M., Kaiser, H., Navada, R., Ghosh, K. and Lee, L., "Methods for Detecting Defects in Composite Rehabilitated Concrete Structures," Federal Highway Administration report FHWA A-OR-RD-05-09, April 2005.

Kessler, S.S., Spearing, S.M., Atalla, M.J., Cesnika, C.E.S. and Soutis, C., "Structural Health Monitoring in Composite Materials using Frequency Response Methods," October 2001.

Kithil, R., Knight & Carver, "Case Study of Lightning Damage to Wind Turbine Blade," National Lightning Safety Institute (NLSI), June 2008.

Lendze, T., Wojtyra, R., Guillaumat, L., Biateau, C. and Imielińska, K., "Low Velocity Impact Damage in Glass/Polyester Composite Sandwich Panels," Advances in Material Science, Vol. 6, No. 1 (9), June 2006.

Matthews, T.S., "Non-Destructive Inspection of Composite Structures Using Modal Analysis," PhD Thesis, Naval Postgraduate School, Monterey, CA, March 1995.

Miller, P.H., U.S. Naval Academy Naval Architecture and Ocean Engineering Department, project collaboration 2011.

Montanini, R. and Freni, F. "Nondestructive inspection of luxury yacht glass reinforced composite Panels by Means of Transient Thermography," 10th International Conference on Quantitative InfraRed Thermography, Québec, Canada, July 2010.

National Aeronautics and Space Administration, Lyndon B. Johnson Space Center, "Process Specification for Ultrasonic Inspection of Composites," May 2003.

Nelligan, T. and Kass, D. "An Introduction to Ultrasonic Phased Array Technology," Olympus Technologies, <http://www.olympus-ims.com/en/ultrasonics/intro-to-pa/>, 2010.

Olympus Ultrasonic Flaw Detector Epoch 1000 Series product brochure, [www.olympus-ims.com](http://www.olympus-ims.com), 2008.

Paiva, J. M. F., Mayer, S. and Rezende, M. C., "Evaluation of mechanical properties of four different carbon/epoxy composites used in aeronautical field," Mat. Res. [online]. 2005, vol.8, n.1, pp. 91-97.

Pansart, S., Sinapius, S. and Gabbert, U., "A comprehensive explanation of compression strength differences between various CFRP materials: Micro-meso model, predictions, parameter studies," Elsevier, Composites: Part A 40, 2009.

Pasztor, A., "Older Airbus Jets Get High-Tech Rudder Check," *Wall Street Journal*, December 19, 2006.

Rajic, N., Rowlands, D. and Tsoi, K.A., "An Australian Perspective on the Application of Infrared Thermography to the Inspection of Military Aircraft," 2nd International Symposium on NDT in Aerospace, Hamburg, Germany, November 2010.

Rakow, J & Pettinger, A 2006, "Failure Analysis of Composite Structures in Aircraft Accidents," Proceedings of the ISASI 2006 Annual Air Safety Seminar, International Society of Air Safety Investigators (ISASI), Cancun, Mexico, 2006.

Ratcliffe, C.P., Crane, R.M., Heider, D., Yoon, M.K. and Gillespie Jr., J.W., "Structural Integrity and Damage Evaluation and Damage Evaluation Routine (SIDER) for Quality Control and Health Monitoring of Structures," NSWCCD-65-TR-2001/23 Carderock Division, Naval Surface Warfare Center, October 2001.

Roach, D., "Assessing Conventional and Advanced NDI for Composite Aircraft," *High-Performance Composites* July 2008.

Roach, D. and Hartman, R., "FAA Airworthiness Assurance NDI Validation Center (AANC) Operated by Sandia National Laboratories," Presentation to ATA NDT Forum, September 2010.

Roosen, D., "Fatigue Behavior of Sandwich Foam Core Materials – Comparison of Different Core Materials," Degussa. Röhm GmbH & Co., SAMPE 2002

Schnars, U. and Henrich, R., "Applications of NDT Methods on Composite Structures in Aerospace Industry," Airbus, Bremen, Germany, September 2006.

Shepard, S.M., Lhota, J.R., Hou, Y., Ahmed, T. and Wang, D., "Thermographic Characterization of Composite Materials and Structures," SAMPE 2004, May 2004, Long Beach, CA.

Sheppard, P. J. Phillips, H.J. and Cooper, I., "The Practical use of NDE Methods for the Assessment of Damaged Marine Composite Structures," Seventeenth International Conference on Composite Materials, Edinburgh, Scotland, July 2009.

Sheppard, R.E. and Puskar, F.J., "Inspection Guidance for Offshore Wind Turbine Facilities," 2010 Offshore Technology Conference, Houston, Texas, May 2010.

Shyprykevich, P., Tomblin, J., Ilcewicz, L., Vizzini, A.J., Lacy, T.E. and Hwang, Y., "Guidelines for Analysis, Testing, and Nondestructive Inspection of Impact- Damaged Composite Sandwich Structures," DOT/FAA/AR-02/121, U.S. Department of Transportation, Federal Aviation Administration, March 2003.

Snell Jr., J.R. and Robert W. Spring, R.W., "Infrared Thermography Advances," *NDT Magazine*, October 2007.

Sørensen, B.F., Jørgensen, E, Debe, C.P., Jensen, F.M., Jensen, H.M., Jacobsen, T.K. and Halling, K.J., "Improved design of large wind turbine blade of fibre composites based on studies of scale effects (Phase 1) - Summary Report," Risø National Laboratory, Roskilde, Denmark, September 2004.

Tomblin, J., Raju, K.S., J. Liew, J. and Smith, B.L., "Impact Damage Characterization and Damage Tolerance of Composite Sandwich Airframe Structures," DOT/FAA/AR-00/44, Federal Aviation Administration, January 2001.

Tomblin, J.S., Salah, L., Welch, J.M. and Borgman, M.D., "Bonded Repair of Aircraft Composite Sandwich Structures," DOT/FAA/AR-03/74, Federal Aviation Administration, February 2004.

Zenkert, D., Shipsha A., Bull, P. and Hayman, B., "Damage Tolerance Assessment of Composite Sandwich Panels with Localised Damage," Composites Science and Technology 65, Elsevier Ltd., 2005.

Zhang, Z.Y. and Richardson. M.O.W., "Non-destructive testing of barely visible impact damage in polymer matrix composites," *The Chinese Journal of Nonferrous Metals*, Oct 2004.

Zvanik, M., Composotech Structures, personal telephone conversation, Nov 2010.



## SHIP STRUCTURE COMMITTEE LIAISON MEMBERS

### LIAISON MEMBERS

American Society of Naval Engineers	Captain Dennis K. Kruse (USN Ret.)
Bath Iron Works	Mr. Steve Tarpy
Colorado School of Mines	Dr. Stephen Liu
Edison Welding Institute	Mr. Rich Green
International Maritime Organization	Mr. Igor Ponomarev
Int'l Ship and Offshore Structure Congress	Dr. Alaa Mansour
INTERTANKO	Mr. Dragos Rauta
Massachusetts Institute of Technology	
Memorial University of Newfoundland	Dr. M. R. Haddara
National Cargo Bureau	Captain Jim McNamara
National Transportation Safety Board - OMS	Dr. Jack Spencer
Office of Naval Research	Dr. Yapa Rajapaksie
Oil Companies International Maritime Forum	Mr. Phillip Murphy
Samsung Heavy Industries, Inc.	Dr. Satish Kumar
United States Coast Guard Academy	Commander Kurt Colella
United States Merchant Marine Academy	William Caliendo / Peter Web
United States Naval Academy	Dr. Ramswar Bhattacharyya
University of British Columbia	Dr. S. Calisal
University of California Berkeley	Dr. Robert Bea
Univ. of Houston - Composites Eng & Appl.	
University of Maryland	Dr. Bilal Ayyub
University of Michigan	Dr. Michael Bernitsas
Virginia Polytechnic and State Institute	Dr. Alan Brown
Webb Institute	Prof. Roger Compton

## RECENT SHIP STRUCTURE COMMITTEE PUBLICATIONS

Ship Structure Committee Publications on the Web - All reports from SSC 1 to current are available to be downloaded from the Ship Structure Committee Web Site at URL:

<http://www.shipstructure.org>

SSC 445 – SSC 393 are available on the SSC CD-ROM Library. Visit the National Technical Information Service (NTIS) Web Site for ordering hard copies of all SSC research reports at

URL: <http://www.ntis.gov>

SSC Report Number	Report Bibliography
SSC 462	Review of Current Practices of Fracture Repair Procedures for Ship Structures Wang, G, Khoo, E., ABS Corporate Technology 2012
SSC 461	Structural Challenges Faced By Arctic Ships, Kendrick A., Daley C. 2011
SSC 460	Effect of Welded Properties on Aluminum Structures, Sensharma P., Collette M., Harrington J. 2011
SSC 459	Reliability-Based Performance Assessment of Damaged Ships, Sun F., Pu Y., Chan H., Dow R.S., Shahid M., Das P.K. 2011
SSC 458	Exact Mapping of Residual Stress in Ship Hull Structures by Use of Neutron Diffraction Das. S. Kenno S. 2009
SSC 457	Investigation of Plastic Limit States for Design of Ship Hull Structures, Daley C., Hermanski G. 2009
SSC 456	Buckling Collapse Testing on Friction Stir Welded Aluminum Stiffened Plate Structures, Paik J.K. 2009
SSC 455	Feasibility, Conceptual Design and Optimization of a Large Composite Hybrid Hull, Braun D., Pejicic M. 2008
SSC 454	Ultimate Strength and Optimization of Aluminum Extrusions, Collette M., Wang C. 2008
SSC 453	Welding Distortion Analysis Of Hull Blocks Using Equivalent Load Method Based On Inherent Strain, Jang C.D. 2008
SSC 452	Aluminum Structure Design and Fabrication Guide, Sielski R.A. 2007
SSC 451	Mechanical Collapse Testing on Aluminum Stiffened Panels for Marine Applications, Paik J.K. 2007
SSC 450	Ship Structure Committee: Effectiveness Survey, Phillips M.L., Buck R., Jones L.M. 2007
SSC 449	Hydrodynamic Pressures and Impact Loads for High Speed Catamaran / SES, Vorus W. 2007